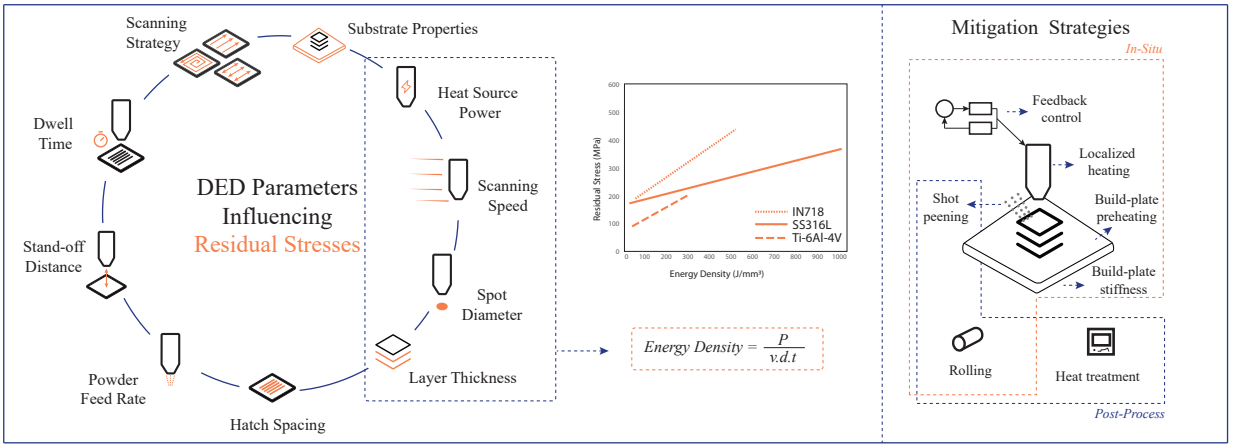
Graphical Abstract

Decoding Residual Stresses in Directed Energy Deposition: A Comprehensive Review from Parameters to Final Stress State

Sukayna Fakher, Bey Vrancken, Roland Logé, Houda Houban, Zoé Jardon, Antoine Devroe, Michaël Hinderdael[‡], Dieter De Baere [‡]



Highlights

Decoding Residual Stresses in Directed Energy Deposition: A Comprehensive Review from Parameters to Final Stress State

Sukayna Fakher, Bey Vrancken, Roland Logé, Houda Houban, Zoé Jardon, Antoine Devroe, Michaël Hinderdael[‡], Dieter De Baere [‡]

- Higher scanning speed generally favours lower residual stress, but the effect of laser power depends on beam diameter and layer thickness.
- Segmented scan patterns with rotation between layers produce less residual stress.
- Residual stress generally rises as energy density increases in directed energy deposition.
- Normalized enthalpy, rarely applied to residual stress studies, accounts for material properties that energy density leaves out.
- In-situ strategies such as remelting, rolling, and ultrasonic vibration can reduce residual stress, but their effect depends on the mechanism and is not always beneficial.

Decoding Residual Stresses in Directed Energy Deposition: A Comprehensive Review from Parameters to Final Stress State

Sukayna Fakher[a,*], Bey Vrancken[b], Roland Logé[c], Houda Houban[a], Zoé Jardon[a], Antoine Devroe[a], Michaël Hinderdael[‡a] and Dieter De Baere [‡a]

[a]Department of Mechanical Engineering, Vrije Universiteit Brussel (VUB), Belgium
[b]Department of Mechanical Engineering, Katholieke Universiteit Leuven (KUL), Belgium
[c]School of Engineering, Ecole Polytechnique Fédérale de Lausanne (EPFL), Switzerland

ARTICLE INFO

Keywords:
Directed Energy Deposition
Residual Stress
Additive Manufacturing
Energy Density
Heat Input
Normalized Enthalpy

ABSTRACT

Residual stresses (RS) are a critical challenge in metal additive manufacturing (AM). This challenge is especially significant in directed energy deposition (DED), where larger part sizes and melt pools, together with heat accumulation and repeated thermal cycling, promote substantial stress accumulation. Control of RS is further complicated by the many tunable process parameters. Existing reviews either isolate individual parameters or cover RS in AM generally, and rarely address how parameters interact to shape the final stress state. This review addresses that gap with a framework that breaks RS formation into sequential steps: process parameters, intermediate variables, thermal drivers, and RS mechanisms. Using this framework, it analyses how changes in individual parameters propagate through the process to the resulting RS, focusing on experimental studies in DED. It then examines energy density as a unifying metric that captures the combined effect of interacting parameters, collecting published data to correlate calculated energy densities with reported RS levels. Normalised enthalpy is also evaluated as a complementary metric that accounts for intrinsic material properties. Beyond parameter optimisation, the review evaluates the effectiveness of in-situ and post-process mitigation strategies. This work consolidates current knowledge and provides a structured foundation for reducing RS in DED-fabricated parts.

1. Introduction

From the emergence of forging around 4000 BC to the most advanced manufacturing processes today, residual stresses (RS) have been an inherent issue affecting the quality of fabricated parts [1]. RS are self-equilibrating stresses that remain in the material when no external forces or thermal gradients are applied [2, 3]. The origin of these stresses can be non-uniform plastic deformation, thermal cycles or phase transformations [4]. In additive manufacturing (AM), rapid heating and cooling thermal cycles are the leading cause of RS [5].

RS influence various material properties, ranging from part geometry to static and dynamic strength, as well as chemical resistance and even magnetisation [2, 6–8]. These stresses may push or pull on the material, resulting in part deformation. Given that the rapid growth of AM is largely attributed to its ability to produce near-net-shape parts, deviations from the intended design caused by RS poses a significant challenge [9]. In certain materials, RS can also induce cracking within the bulk material, examples of which can be seen in Figure 1 (a) and (c). Cracks can also form between the substrate and the deposited material due to the high tensile RS typically present at the outer edges of the cross-section (Figure 1(b)) [7, 8, 10]. Post-production cracks appear during the service life of a part, as a result of reduced fatigue resistance caused by RS. Under cyclic loading, tensile RS act as a driving force for the initiation and propagation of cracks, which can lead to critical failure during operation and significantly shorten the component life [2, 6, 7, 9]. Corrosion resistance behaviour may also be affected, as RS may accelerate corrosion rates, potentially leading to corrosion cracking [2, 8, 11, 12]. Lastly, RS can also lower the magnetisation in metals [7]. As indicated, RS cause a wide range of issues, which are especially magnified in AM materials due to the repeated thermal cycles involved in the process. Especially in hybrid AM, where deposition and machining are repeated over several steps. Stress redistribution after the machining step can change the part geometry, so RS have to be controlled throughout the

*Corresponding author
‡ These authors contributed equally to this work.
Sukayna.Fakher@vub.be (S. Fakher)
ORCID(s):

process rather than only at the end [13]. Therefore, although it may not be possible to eliminate these stresses entirely, reducing them as much as possible remains essential. An exception to this, however, is when RS are intentionally tailored to be compressive for their beneficial effects. Compressive stresses improve the mechanical properties of near-surface layers and can prevent the origination and propagation of cracks, as well as increase wear and corrosion resistance [2]. Therefore, the ultimate objective is not to eliminate RS entirely, but to engineer the stress state most suitable for the part's intended application [14, 15]. This can be achieved through various approaches, such as inducing compressive RS via careful material selection and interpass temperature control [14, 16], interlayer deformation [15], or post-processing techniques such as shot peening [17, 18].

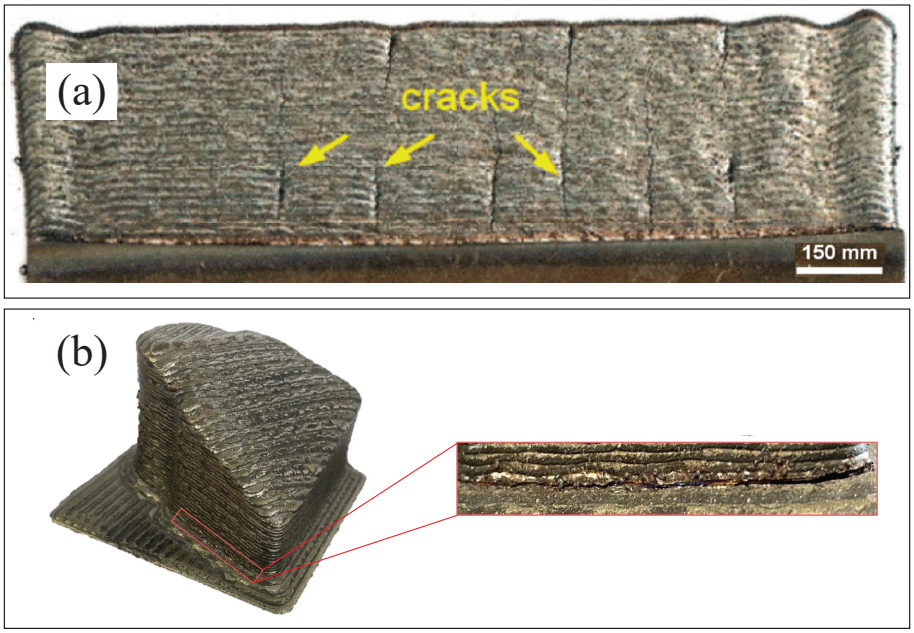


Figure 1: Examples of cracking and deformation due to RS in additively manufactured parts: (a)[19], (b)[20]. Reproduced from [19], [20], with permission from Elsevier and Springer, respectively.

RS are usually categorised into three types based on the length over which they equilibrate [21]. Type I or macro RS are in equilibrium across the entire part. Deformation occurs when this equilibrium is disturbed, such as when the part's constraints or boundary conditions change. [6, 7, 22]. Type II or intergranular RS varies over the grain scale of the material and is caused by different grain orientations and the anisotropy in the material [6, 21]. Type III RS occurs at the nano-scale inside individual grains and is due to the distortion of the crystal lattice caused by dislocations or vacancies [2, 7]. Dimensional accuracy, fatigue life, and fracture behaviour are predominantly governed by Type I RS, as its macroscopic nature means it produces the largest stress magnitudes and affects the part as a whole [5, 21]. Type II and III RS, while locally significant, are of comparatively smaller magnitude and are typically superimposed on the Type I stress field. This makes their independent contribution to part-level mechanical behaviour difficult to isolate. They are also beyond the scope of most current RS measuring methods [5, 21].

While the mitigation of RS has been studied extensively in general and in AM, the Directed Energy Deposition (DED) technique presents unique challenges. In DED, a high-energy source melts the wire or powder feedstock and deposits it on a substrate. The energy source and feedstock move along a predefined scanning path to form a single layer. This process is repeated layer by layer until the full part is built [23, 24]. Although DED offers many advantages, its unique method of continuously feeding material during deposition introduces significant challenges, particularly in the evolution and distribution of RS [5, 25].

Two mechanisms have been proposed to understand the formation of RS in AM: the cool-down phase model and the temperature gradient mechanism (TGM). In the cool-down phase model, illustrated in Figure 2, RS are formed during the solidification of molten material. First, the heat source melts the feedstock material to deposit it on the previous layer. As the deposited material cools down, it contracts. This contraction is restricted by the previously solidified

layers below, leading to tensile RS in the top layers. Since RS must be in equilibrium, compressive RS will appear in the layers below [5, 6, 26].

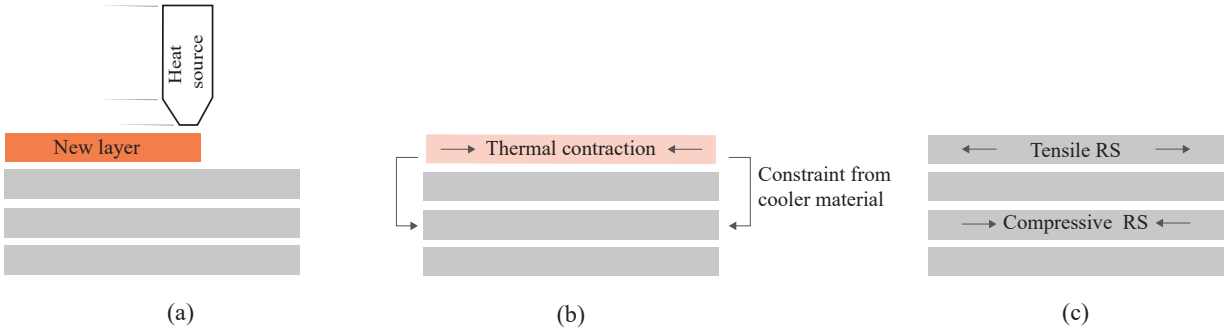


Figure 2: The cool-down phase model for formation of RS (a) Deposition of a new layer, (b) contraction occurs during cooling being restricted by underlying material, (c) After cool-down, tensile and compressive RS are formed in the part.

The TGM model, represented in Figure 3, does not necessarily involve molten material. When the energy source heats the workpiece surface, a steep temperature gradient develops between the top and bottom layers. The hotter top layers attempt to expand, but the cooler bottom material resists this expansion, introducing mechanical restraint on the top layers. This restraint leads to internal compressive stresses in the heated layers. Because yield strength typically decreases with temperature, these compressive stresses can exceed the material's yield strength and cause plastic compression in the hot region. During cooling, the heated surface tends to shrink to its new, compressed size, but this contraction is restrained by the cooler layers below, producing tensile RS in the near-surface region and compensating compressive stresses deeper in the part. [5, 6, 26]. As both of the above mechanisms arise due to non-uniform temperature distributions, thermal gradients play a central role in the formation of RS. The combined effect of these mechanisms typically yields compressive stresses in the core and tensile stresses near the surfaces of manufactured parts [5, 6, 26].

The relative influence and magnitude of these two mechanisms is dependant on the melt pool dimensions and peak thermal cycles. Melt pool size controls the volume and geometry of the material that undergoes a cycle of expansion and contraction and maximum temperature indicates the severity of the temperature the part goes through [27–29]. However, the effect that these variable have on RS is not consistent. A higher peak temperature and a larger melt pool tend to raise RS, but only when the larger pool is accompanied by a steeper gradient and a larger constrained volume [12, 30]. The reverse can occur when the larger pool is the result of a hotter substrate or heat accumulation, which lowers the gradient and cooling rate [31, 32]. Reported trends therefore differ between studies, since pool size and peak temperature correlate with the gradient and cooling rate but do not uniquely determine them.

The TGM and cool-down phase model are the primary contributors to RS formation in AM. However, other more general mechanisms, occurring during thermally-driven manufacturing processes, are also naturally involved. A summary of the most important phenomena contributing to the formation of RS is presented in Table 1. The material-specific mechanisms are discussed in later sections as their behaviour is analysed within the relevant process parameter context. Some mechanisms, such as solidification shrinkage, have not been included due to their minimal effect on Type I RS, being more relevant to other types of RS, which fall outside the focus of this article.

Although the current literature offers a valuable foundation for understanding RS in AM, to the best of our knowledge, a dedicated assessment of its experimental mitigation in DED is still lacking. Reviews like those of Chen et al. [3], Liu et al. [25], and Movahed et al. [33] provide a useful, high-level overview of in-situ strategies across various laser-based processes. Their broad scope, however, combines insights from both DED and Laser Powder Bed Fusion (LPBF). These two manufacturing methods can differ meaningfully in their thermal cycles, scale, and the practical challenges they present. The goal here is to focus specifically on DED. The distinct characteristics of DED, such as its relatively larger melt pools, high deposition rates, and 3D freeform deposition capability create complicated states of RS [25]. Additionally, many of the reviews on this topic include computational and simulation models. These approaches are highly valuable as well as increasingly prominent, but we've prioritised compiling and examining experimental data to clarify the connections between process parameters and RS. We also especially focus

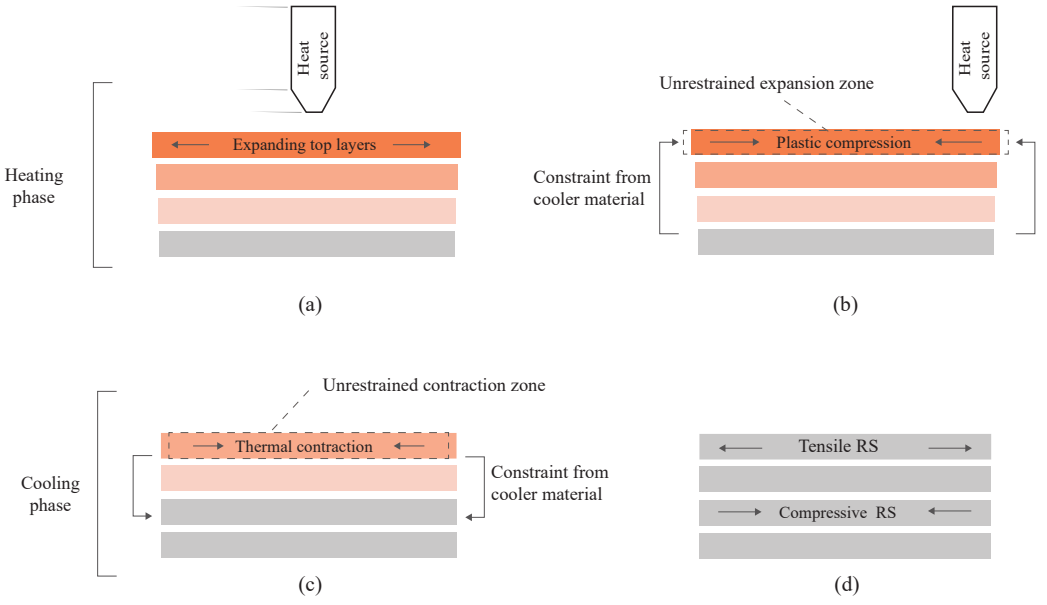


Figure 3: The temperature gradient mechanism (TGM) for formation of RS: (a) The heat source introduces a steep thermal gradient between top and bottom layers. (b) Expansion of the top layers is constrained by the cooler layers below, causing plastic compression in the top layers. (c) Upon cooling, the top layers attempt to deform to a newly compressed size but are restrained by cooler material below. (d) Tensile RS is formed on the surface, balanced by compressive RS below.

Table 1
Overview of mechanisms contributing to Type I residual stress formation.

Mechanism	Process Stage	Primary Physical Driver	Stress Response & Spatial Condition	Alloy Systems
TGM	Heating → final cooldown	Localised thermal expansion restrained by cooler substrate	Heating: top layer yields compressively. Final state: Surface tensile ($+\sigma$), sub-surface compressive ($-\sigma$)	General — all alloys
Cool-Down phase	Cooling (solid)	Thermal contraction ($T_{solidus} \rightarrow T_{room}$) restrained by cooler bulk	Surface & bulk: high tensile ($+\sigma$)	Ti-6Al-4V, IN718, IN625, SW 316L (no significant compensating transformation)
Solid-State Phase Transformation	Cooling (solid)	Lattice expansion on transformation (e.g. $\gamma \rightarrow \alpha'$), below M_s (for steels)	Transformed zone: compressive ($-\sigma$), offsets cool-down contraction	17-4PH, H13, P91
Thermal Relaxation & Stress Relief	Reheating (solid)	Recovery/recrystallization ($T > T_{recry}$ or partial recovery)	HAZ: stress reduction ($\lvert\sigma\rvert \rightarrow 0$)	Ti-6Al-4V , 316L
Global Mechanical Restraint	Continuous	Fixture/substrate stiffness resisting deflection	Base/interface: high shear & tensile; free boundaries: relaxation	All

on energy density as a parameter, as it provides a representation of the combined effects of important DED parameters. This is to assess whether it can serve as a metric for comparing different parameter sets across various experimental setups, and whether there is any correlation between RS and energy density. Furthermore, we explore the potential use of normalized enthalpy as an additional metric that incorporates intrinsic material properties not included in energy density. Finally, we extend the discussion to mitigation techniques; both post process and specialised in-situ techniques such as interlayer rolling and ultrasonic vibration, which show significant promise.

2. Process parameters

Many parameters are involved in the DED process, and modifying each one can significantly affect the RS in the final part. In this section, we review studies that have evaluated the effects of DED parameters individually to understand how each one contributes to the formation of RS. Understanding how these parameters affect RS is more complex than simply reviewing the reported results in isolation. At times, findings across studies appear contradictory, but these apparent contradictions are largely resolved once the underlying physics is considered more broadly, rather than parameter by parameter.

In general, a process parameter does not influence RS directly. Rather, it first modifies a physically measurable process characteristic, such as melt pool size, absorptance, or peak temperature, which in turn governs the primary thermal drivers: thermal gradient (temperature change over distance), cooling rate (temperature change over time), and heat accumulation (build-up of heat in the part over successive layers). These drivers determine the extent to which each RS mechanism is activated in the final part. Specifically, the thermal gradient primarily governs the TGM, the cooling rate controls the cool-down phase mechanism as well as the completeness of Solid-State Phase Transformation, and heat accumulation governs thermal relaxation and stress redistribution [5, 6, 12, 26, 34–36]. A schematic of these relationships is shown in Fig. 4. Throughout the following sections, apparent contradictions between studies are interpreted within this framework, rather than treated as evidence of inconsistency.

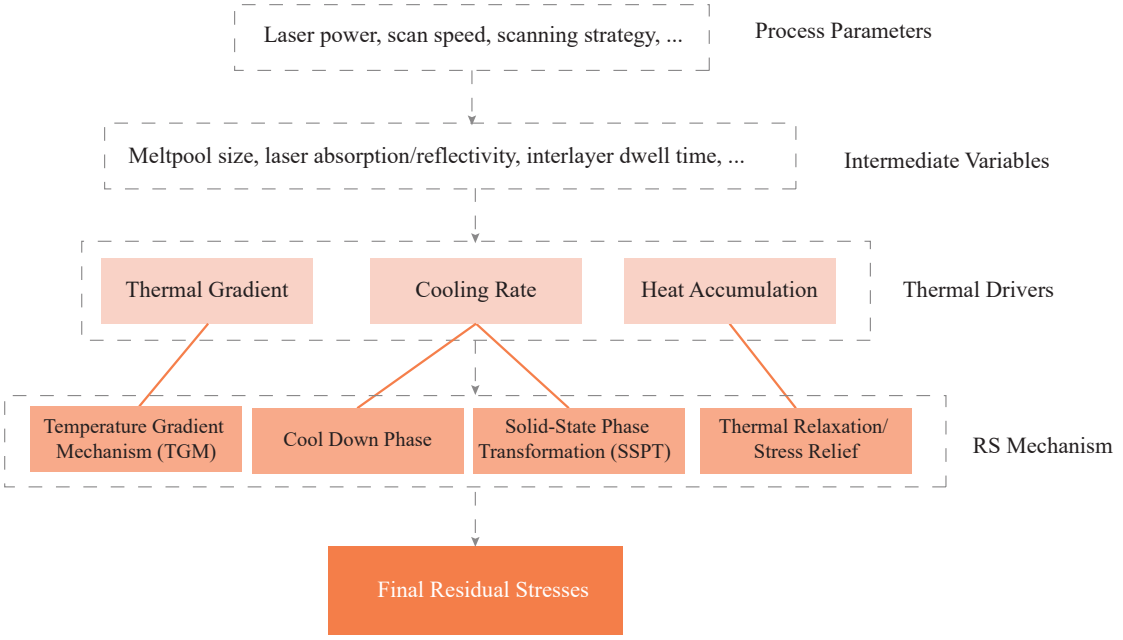


Figure 4: Schematic representation of the relationship between process parameters, process characteristics, thermal drivers, and residual stress (RS) formation mechanisms in DED

2.1. Substrate properties

The substrate or build plate serves as the platform on which the material is deposited. It is typically made from a material similar to the deposited metal, and upon completion of the deposition process, the finished piece is generally separated from the substrate [37]. Due to this close interaction between the end product and the substrate, its properties can have a considerable influence on the part's characteristics.

As the first layers are being deposited during the DED process, the substrate acts as a heat sink, allowing for the rapid conduction of heat, which significantly affects the thermal gradient [23]. Given that the formation of RS is highly

influenced by the thermal gradient during and after deposition, the properties and dimensions of the substrate are important factors to evaluate, as they directly influence the heat sink effect.

Some studies have evaluated the effects of substrate dimensions on melt pool geometry, thermal behaviour and substrate distortion. However, to the best of our knowledge, the direct influence of substrate dimensions on the formation of RS has not yet been evaluated. For instance, Corbin et al. examined the effect of Ti–6Al–4V substrate thickness on distortion and found that thicker substrates exhibited less distortion at the end of the fabrication process compared to thinner ones [38]. In another study, Zhang et al. investigated the effects of various dimensions of CuCr0.8 substrates. They found that the width of the substrate had minimal influence on the depth and width of the single deposited track. In contrast, substrate thickness significantly impacted the process, as both deposition depth and width decreased as substrate thickness increased [39]. Although RS was not directly evaluated in this study, its results confirm that thicker substrates act as more effective heat sinks, creating steeper thermal gradients. Therefore, a steep thermal gradient caused by the heat sink effect of thicker substrates, especially in highly thermally conductive materials such as CuCr0.8, will likely lead to higher RS.

The substrate's mechanical properties can also have an impact on RS in the deposit. In one study, Jeong et al. deposited 316L stainless steel (316L) cubic samples on both heat-treated and non-heat-treated substrates of the same material. As shown in Figure 5, while the trend of RS remained similar for both substrates, the magnitude of RS was generally lower for the heat-treated substrate. This difference was attributed to the lower yield strength of the heat-treated substrate. This lower yield strength facilitated greater plastic deformation, allowing the substrate to accommodate thermal shrinkage during deposition. As a result, less elastic energy was stored, leading to reduced RS [40]. Substrate stiffness can also influence RS. This parameter is further discussed in section 4.6 as the focus of existing research has primarily been on the various substrate design configurations, rather than the intrinsic mechanical property of stiffness itself. Overall, these findings confirm that both the mechanical properties and geometric characteristics of the substrate play a critical role in determining the deformation and final RS in DED-fabricated parts.

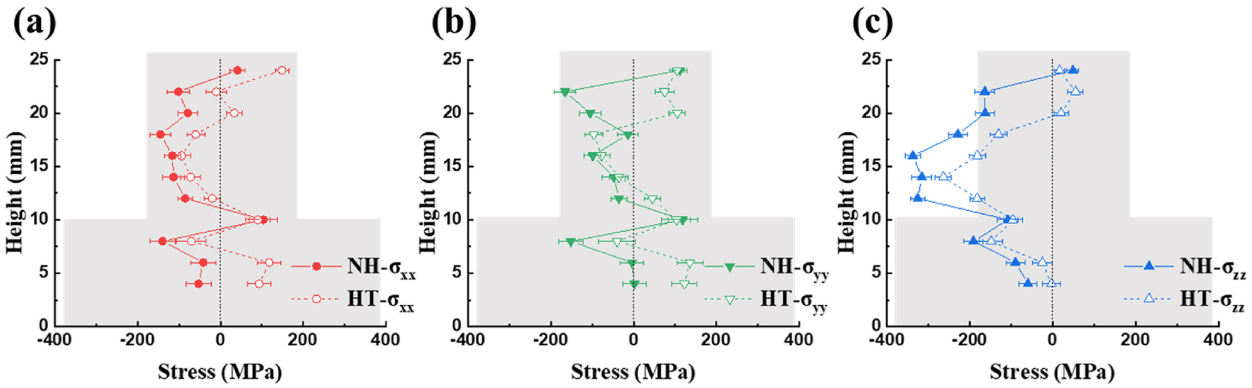


Figure 5: Residual stress distribution in non-heat-treated (NH) and heat-treated (HT) substrates, measured using neutron diffraction: (a) σ_{xx}, (b) σ_{yy}, and (c) σ_{zz}. Reproduced from [40], with permission from Elsevier.

2.2. Heat source power

The power of the heat source is another important parameter in the DED process, significantly influencing the formation of RS. A portion of the incoming energy is absorbed by the feedstock during deposition, some of the energy is reflected and the rest is used to heat the previously deposited layers and create a melt pool on the surface of the deposit (A detailed exploration of the energy distribution associated with the DED process is presented in Section 3.2.). Heat source power has a significant impact on the size of the melt pool and the temperature gradient within the deposited material, which are key factors affecting RS [23].

In one of the earliest studies on the topic, Lai et al. experimented with four different laser powers (1200 W, 1500 W, 1700 W, and 2000 W) to deposit rectangular titanium alloy parts on titanium alloy substrates [41]. RS was measured with the indentation strain-gauge method, in which a strain rosette recorded the strain increment caused by a controlled indentation on the sample surface. The RS were subsequently calculated with Hooke's law. The results showed a direct correlation between laser power and RS, where 1200 W and 2000 W laser power lead to 80 MPa and 360 MPa of RS,

respectively. [41]. In another study, Cheng et al. deposited 30 layers of 316L powder at 300 W, 450 W, 600 W and 800 W laser power and found a linear relation between laser power and the formation of RS [12]. RS was measured with the contour method, and the maximum longitudinal RS increased from 102.2 MPa at 300 W to 339.1 MPa at 800 W. The measured stress values were taken from the longitudinal stress map on the cross-section of the substrate, with the maximum located at the junction between the substrate and the deposited sample. Similar results were observed in other studies [42, 43]. This increasing trend, depicted in Figure 6, arises because a higher laser power produces a larger melt pool, which increases solidification shrinkage, and also creates a steeper thermal gradient in the deposited part. Both of these effects lead to an increase in RS. This elevated energy also influences stress distribution, causing non-uniform RS within the material. Reducing laser power can effectively decrease the thermal gradient and melt pool size, resulting in reduced and more homogeneous RS in the sample [3, 8, 12, 42, 44, 45].

However, some studies offer a different trend. Tong et al., for instance, deposited FeCrCoMnNi onto a 316L substrate using 600 W, 800 W and 1000 W laser power. RS was measured on the as-built specimens by X-ray diffraction (XRD) Prior to the measurements, the surface layer was removed by electropolishing, so the RS was determined at a depth of 1 to 2 mm into the specimens. The tensile RS was highest at 600 W and lower at 800 W, which they attributed to the higher cooling rate at 600 W. At 1000 W the RS increased again, which they attributed to the larger melt pool and the resulting greater volume shrinkage of the solidified layer [46]. It is important to note the in this study The scatter between measurement points was large, so the results should be interpreted with caution. Tian et al. utilised medium and high laser powers to deposit CrMnFeCoNi high-entropy alloy parts on AISI 1045 steel substrates. RS was measured by XRD in the build direction – scanning direction plane at the sample centre. Each measurement was repeated five times, and the results were converted into 2D RS maps and mean RS profiles along the build height. From 1100 W to 1400 W, the peak tensile and compressive RS increased by 40 MPa and 55 MPa, respectively, which was attributed to the higher melt pool temperature and larger melt pool volume causing greater shrinkage strain. Above 1400 W, RS decreased. The peak tensile and compressive RS were 260 MPa (top) and -250 MPa (bottom) at 1400 W, compared with 160 MPa and -153 MPa at 2300 W. They attributed this decrease to greater heat accumulation in the build at high laser power, which partially relieves the RS [47].

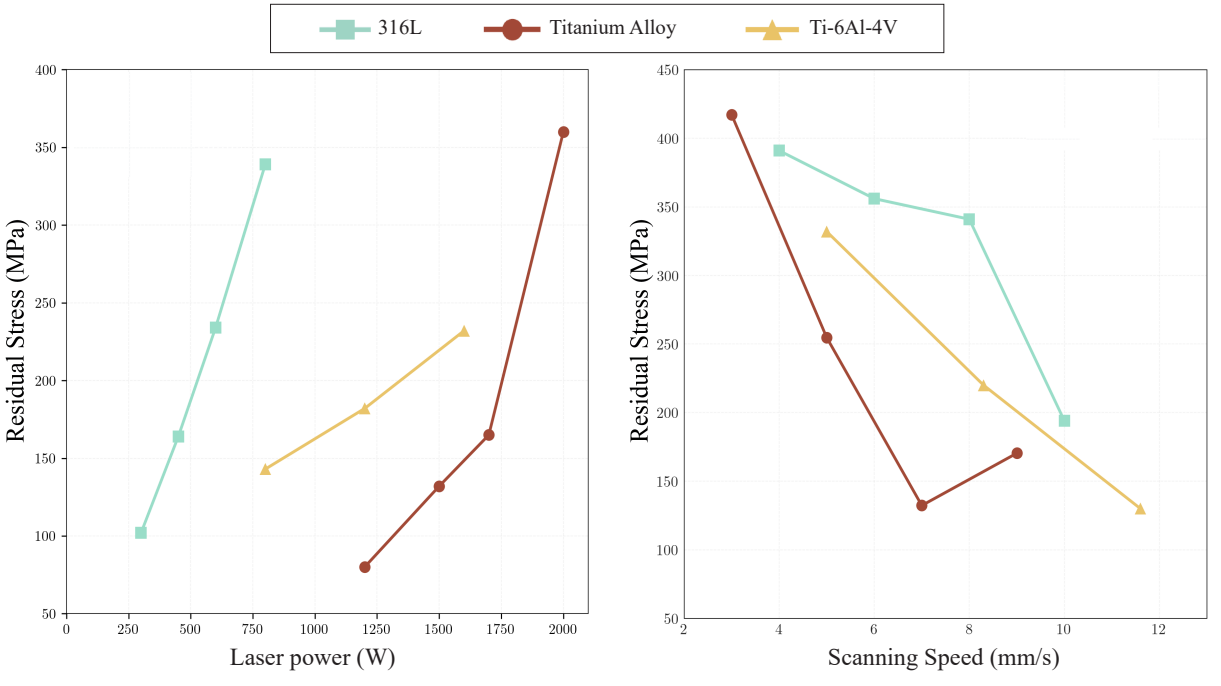


Figure 6: Influence of laser power and scanning speed on RS in 316L [12], Titanium alloy [41] and Ti-6Al-4V [42].

In addition to using a constant laser power, some studies have also explored the use of varying laser power. Xu et al. used both constant (220 W, 320 W, 410 W) and varying laser power to deposit 60 layers of Inconel 718 (IN718) on a hot-rolled IN718 thin-wall substrate to simulate a repair [45]. RS were measured on the as-deposited samples using XRD. Measurements were taken at the mid-length position of the longitudinal plane in the middle region of the deposit, in the longitudinal and normal directions. In samples deposited with constant laser power, the longitudinal tensile RS decreased with increasing laser power (from 80 MPa at 220 W to 16 MPa compressive at 410 W). The opposite was noticed for the normal stress as the stresses were compressive at 220 W, but tensile when using 320 W and 410 W laser power. However, using a gradually decreasing laser power resulted in compressive RS in both directions. This gradient approach reduced the size of the melt pool, reducing the shrinkage effect. It also led to an increased cooling rate and more uniform heat distribution that promoted heat dissipation in the longitudinal direction, which is why it led to large compressive stresses [45]. In a more limited approach, Wu et al. deposited ten layers of Ti-6Al-4V powder on a forged Ti-6Al-4V substrate. A constant laser power of 1500 W was compared with a variable laser power strategy, in which the power was reduced from 1500 W to 1300 W over the initial segment of each layer after the second layer. RS were measured by XRD at Seven measurement points. Five along the length of the deposit and further points through the height at mid-length. The experimental RS were reported only as the average equivalent (von Mises) stress over the measurement points, which were 776.8 MPa for constant power and 621.2 MPa for variable power [48].

Overall, the literature does not support a single, universal relationship between laser power and RS. Studies using small beam diameters and thin layers generally report that RS increases with laser power [12, 41]. Cheng et al. explained this with the TGM, reasoning that higher power increases the temperature gradient and thermal strain, which they attributed to greater heat accumulation. Using an infrared camera, they found that the maximum local temperature gradient in the solid region behind the melt pool rose from about 320 to 806 °C/mm as power increased from 300 W to 800 W, accompanied by larger thermal strain and higher RS [12]. In contrast, Tong et al. and Tian et al., who used larger beam diameters and thicker layers, observed lower RS over part of the power range. Tong et al. attributed the lower RS at 800 W to a lower cooling rate, while Tian et al. attributed the decrease above 1400 W to heat accumulation, which keeps the build hot for longer and allows partial stress relaxation [46, 47]. Heat accumulation is therefore linked to opposite outcomes. Cheng et al. associated it with greater thermal expansion and strain, whereas Tian et al. associated it with stress relief. Which of these effect dominates likely depends on how long the part stays at elevated temperature relative to the time needed for relaxation, which in turn depends on dwell time, part geometry, and substrate. Therefore, Laser power alone is a poor predictor of RS.

2.3. Scanning speed

Scanning speed refers to the velocity at which the laser or energy source moves across the surface of the material during the deposition process. This parameter significantly influences the RS formed during DED, since the fusion depth and melt pool diameter increase the longer the laser dwells in a specific location [49].

Various papers have investigated the effects of scanning speed. For the DED process specifically, most report that an increase in scanning speed results in a reduction of RS [12, 41, 42]. Cheng et al. evaluated the effect of scanning speed on RS in 30 layer thin-walled 316L deposits at fixed laser power. Scanning speed was varied between 4, 6, 8 and 10 mm/s [12]. RS were measured using the contour method focusing on the longitudinal component, due to the transverse stresses being much lower. The maximum longitudinal RS was reported in the substrate. Increasing the scanning speed reduced the maximum longitudinal RS, from roughly 390 MPa at 4 mm/s to roughly 195 MPa at 10 mm/s. In situ infrared (IR) thermography showed that the temperature gradient in the solid region decreased slightly with increasing speed, which the authors linked to faster heat removal by conduction, reducing heat accumulation and thermal strain [12]. Zhan et al. investigated the effect of scanning speed on RS in single-wall Ti-6Al-4V specimens [42]. Scanning speed was varied from 3.3 to 6.6, 10 and 13.3 mm/s, while laser power and powder feed rate were kept constant. RS were measured with laser ultrasonics. The longitudinal stress was measured at five equally spaced points along a line on that surface. The average longitudinal RS decreased with increasing scanning speed, from 366.1 MPa at 3.3 mm/s to 274.3, 167.5 and 98.8 MPa at 6.6, 10 and 13.3 mm/s, respectively. The authors attribute this to the lower heat input at higher speeds, which reduces thermal gradients and stress accumulation [42].

In general, increasing the scan speed at constant laser power lowers the energy input per unit length, which reduces heat accumulation in the part. The part therefore stays cooler, and the temperature difference between the deposit and the surrounding material is smaller, which lowers RS. Close to the melt pool, however, higher speeds lead to faster cooling and steeper local temperature gradients, which on their own would raise RS. The net reduction reported in the literature suggests that the part-scale effect is more dominant than the local effect. Similar results are shown in

Figure 6. These findings appear consistent across the materials studied, as similar trends were observed for Ti-6Al-4V [42], titanium alloy [41], and 316L [12].

Although increasing the scan speed can be beneficial for RS mitigation, it can also lead to higher surface roughness and lack of fusion porosities. Additionally, when introducing higher scanning speeds, laser power often needs to be increased to compensate for the higher speed. This may be limited due to laser power availability. Furthermore, as discussed in the previous section, increasing the laser power can lead to the opposite outcome of elevating RS. This shows that a delicate balance is required between these two parameters. A useful parameter that incorporates both of these variables is energy density, which is be discussed in detail in section 3.1.

2.4. Spot size

Spot size in DED refers to the diameter or width of the laser beam at the position where it interacts with the material. This parameter is typically determined by the machine's optical setup, including the laser beam delivery system and the focusing optics. Therefore, it is often not easily adjustable during the process. However, spot size is still a crucial factor in DED, as it determines the energy absorbed by the deposited material and significantly influences the thermal gradient.

Due to the inherent difficulty in modifying the spot size, its effects on thermal gradients have been underexplored. However, in a relevant study, Nie et al. used laser remelting of DED tracks with two spot sizes (1.4 mm and 2 mm) as a strategy to mitigate RS. They found that at fixed laser power, the smaller spot was more effective at reducing RS [50]. Note that this reflects the stress-relief capability of a remelting pass on an existing deposit, not the RS generated during deposition itself.

For deposition, a smaller spot at fixed power would be expected to produce steeper thermal gradients, which according to the TGM favours higher RS. However, spot size also affects peak temperature, cooling rate and the size of the heat-affected zone, and to the best of our knowledge this has not been tested directly.

2.5. Feed rate

The feed rate in the DED process is defined as the mass flow rate of the feedstock delivered to the melt pool per unit of time [51]. When the feed rate is low, minimal energy is required to melt the powder, which allows the rest of the energy to be used to heat and melt the previous layers (or substrate), resulting in a deeper penetration depth and higher thermal gradient. In contrast, when feed rate is high, more energy is consumed to melt the incoming powder, leading to a shallower melt pool and reduced thermal gradient [52, 53]. Therefore, feed rate is another important parameter that affects the bead formation, porosity, microstructure, fusion between deposited layers, and RS of the final deposit [51].

A study on Ti-6Al-4V by Zhan et al., with results shown in Figure 7, demonstrated that, at a constant laser power (1.0 kW) and scanning speed, increasing the powder feed rate (PFR) from 9 to 13 g/min reduces the longitudinal RS [42]. For details on how RS measurements are performed, refer to Section 2.3. Assuming a laser energy transfer efficiency of about 0.4 (see Section 3.2), roughly 400 W of the 1 kW laser power is absorbed. Melting Ti-6Al-4V powder requires roughly 1.4 MJ/kg (about 1.1 MJ/kg to heat it from room temperature (25 °C) to the liquidus (about 1655 °C), using a mean specific heat of about 0.7 kJ/(kg·K), plus about 0.3 MJ/kg of latent heat of fusion). At this value, melting 9 to 13 g/min of powder requires about 210 to 300 W, which is about 50% of the absorbed power at 9 g/min and about 75% at 13 g/min, assuming full powder catchment. As more laser energy is used to melt the additional powder, less heat reaches the deposit, which leads to a less steep thermal gradient [52, 53]. These values are estimates, because the catchment efficiency was not reported, and in practice only part of the powder reaches the melt pool.

Aleksandr et al. reported similar findings when depositing 1.2709 maraging steel powder. The powder feed rate was evaluated as part of the powder density (Q_p) parameter, described as

$$Q_p = \frac{PFR}{v.d} \tag{1}$$

in which PFR, v, and d represent powder feed rate, scanning speed and laser spot diameter, respectively. RS were measured at the central point of the top surface by XRD, with the cubes still attached to the substrate. Stresses were measured along the scanning direction and the overlap direction. Almost all RS were compressive, and stresses along the scanning direction were generally higher than along the overlap direction. Regarding PFR, they found that by increasing the powder density from 9 g/dm^2 to 16 g/dm^2 (either by increasing the PFR or decreasing the scanning

speed) the magnitude of the compressive RS measured near the surface decreased from around 500 MPa to 100 MPa [54]. The authors interpreted this as a reduction in overall stress magnitude, since the compressive stresses are balanced by tensile ones elsewhere in the part.

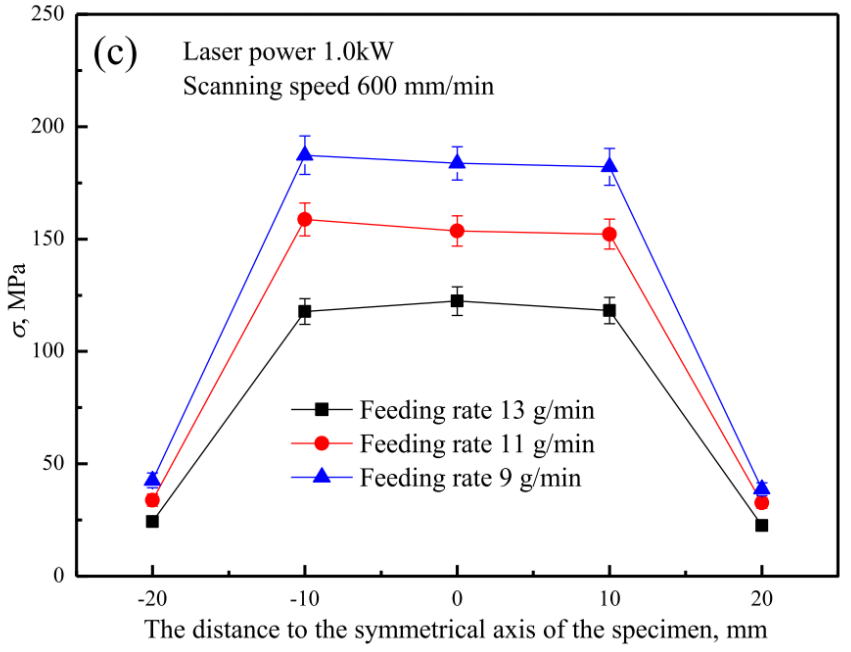


Figure 7: Influence of powder feed rate on RS in a Ti-6Al-4V DED sample. Reproduced from [42], with permission from Elsevier.

2.6. Hatch spacing

Each layer in a three-dimensional structure fabricated by the DED process consists of individually deposited lines. The distance between the centres of two adjacent lines is termed hatch spacing. This value must be set to ensure overlap between adjacent deposition tracks, which is why it is also often expressed as overlap percentage. To achieve high density, the overlap is usually set between 40% to 60%. However, the optimal hatch spacing, which avoids excessive overlap while maintaining density, is often determined empirically through multiple track deposition experiments [23, 49]. Reducing the hatch spacing results in increased remelting of neighbouring tracks, and increases both heat input and thermal gradient within each layer [49, 55]. As a result, smaller hatch spacing, or greater overlap between adjacent tracks, leads to higher thermal stresses [54].

Very few studies have demonstrated the effects of hatch spacing on RS in the DED process. In a study by Aleksandr et al. mentioned earlier in section 2.5 regarding PFR, the authors also investigated the effect of various overlaps. They reported that a lower overlap of 30% resulted in reduced compressive RS compared to the 40-60% overlap range [54]. Liu et al. compared the RS at overlap and non-overlap regions. They deposited IN718 with 25% overlap and measured the RS along a single line across two adjacent passes within one layer, in a cross section perpendicular to the scan direction. They used the Vickers micro-indentation method, following the Carlsson–Larsson approach and observed that RS were higher in magnitude in overlap regions compared to the interior regions of single passes [56]. Similarly, as illustrated in Figure 8, Jinoop et al. built Hastelloy-X rectangular blocks with 50% track overlap and measured RS with XRD on the as deposited surface along and perpendicular to the laser scan direction [57]. They found that RS in the overlap regions was higher and tensile, while in non-overlap regions they showed to be lower and more compressive. The maximum value was 252 ± 24 MPa, found perpendicular to the scan direction. They attributed this to the remelting and re-solidification of the overlap region during the deposition of the adjacent track. In the overlap region, the material is remelted and then shrinks while bonded to the neighbouring solid track, which holds it back and builds up tensile stress. In the non-overlap region, the heat of the adjacent track partly relieves the stress [57].

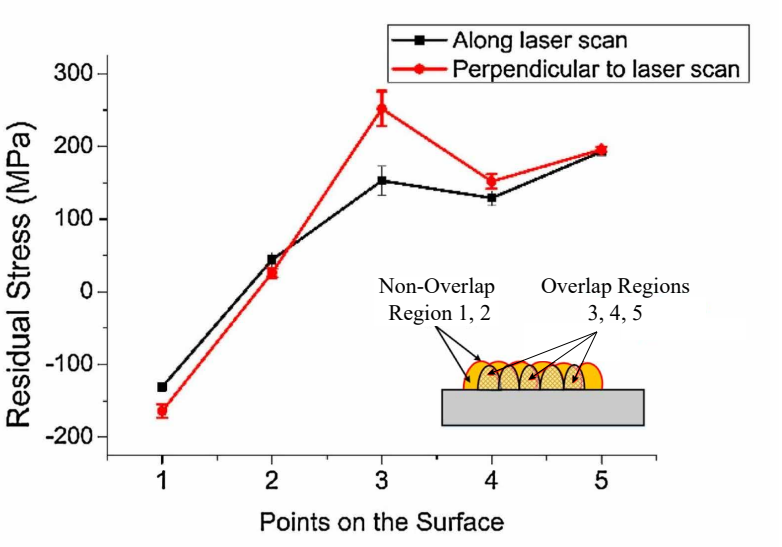


Figure 8: Residual stress on the as-deposited surface in overlap and non-overlap regions. Adapted from [57], with permission from Elsevier.

Although there is limited research on the effects of hatch spacing, these studies suggest that a larger hatch spacing lowers the heat input per unit area and reduces reheating between adjacent tracks, which limits heat accumulation. However, the increase in hatch spacing should not compromise the density of the deposited material.

2.7. Layer thickness

Layer thickness or layer height is defined as the vertical distance between successive layers of deposition. Selecting an optimal thickness is critical as it can have significant effects on defect formation, surface quality and RS magnitude and distribution. However, it is often challenging to maintain a constant layer thickness throughout the deposition process.

At the start of the deposition, the cold substrate rapidly absorbs a significant amount of heat, which leads to a smaller melt pool and therefore a thinner deposition layer. As the deposition continues, heat accumulates, leading to a thickening of layers. Once a balance between the heat input and heat dissipation approaches a more steady state, the layer thickness becomes more uniform [43]. The commanded layer thickness is implemented via the Z-increment or the programmed vertical displacement of the laser head between layers. This Z-increment also governs melt pool penetration depth and interlayer overlap, which has a significant impact on microstructural evolution, thermal gradients, and RS [58].

Despite its importance, relatively few experimental studies have isolated the influence of layer thickness, likely because layer thickness is not independently controllable, as it is constrained by laser focal parameters (e.g., spot size, power density) and powder flow dynamics. Therefore, research has prioritised more controllable variables, such as laser power, scan speed, or deposition pattern, while layer thickness is often held constant to standardise experimental conditions.

However, one study by Yan et al. aimed to determine which of the three parameters (laser power, scanning speed, and layer thickness) is most influential in the formation of RS in austenitic stainless Steel single track thin walls. They deposited 316L powder at laser powers of 400 W, 600 W, and 800 W; scanning speeds of 8 mm/s, 12 mm/s, and 16 mm/s; and layer thicknesses of 200 µm, 400 µm, and 600 µm. RS was measured using the contour method, and results showed that layer thickness had the greatest influence on transverse and through-thickness RS, while laser power had the strongest effect on longitudinal RS. The optimal combination for reducing RS was determined to be lower layer thickness, moderate laser power and a higher scanning speed [59].

2.8. Stand-off distance

The vertical distance between the heat source or nozzle and the deposition is defined as the stand-off distance. This parameter affects important factors of the process such as heat input, bead geometry, cooling rate and deposition

quality. This distance typically ranges from 5 mm to 25 mm in the DED process [50, 60]. To the best of our knowledge, there have not been any studies that investigate the effects of various stand-off distances on RS. However, it has been shown that decreasing the stand-off distance increases the deposition density by minimising porosities and lack of fusion defects during the initial steps of deposition [61].

2.9. Scanning strategy

The scanning strategy in the DED process is defined as the path of the laser or heat source within a single layer and how it compares to its path in the previous layer [3]. Given that the scan strategy directly affects the temperature field, it has a significant effect on the accumulation of RS within produced parts [49].

As described above, the scanning strategy can be divided into two aspects: the path of the heat source within a single layer and the rotation between successive layers. In one of the earliest studies on scanning strategy, Yu et al. focused on the heat source path within a single layer, investigating four different deposition patterns (Unidirectional, offset from outside to inside, offset from inside to outside, and fractal patterns) using 316L powder. They found that the fractal pattern (Figure 9(e)) produced the least substrate deformation, followed by the offset from outside to inside pattern (Figure 9(d)). The unidirectional pattern (Figure 9(a)) showed the most deformation [62]. In a more recent study, Kohler et al. utilised bidirectional, outward spiral and S-shaped patterns (Figure 9(b, c, and f)) to deposit an aluminium alloy using WAAM technology. Each sample consisted of four layers and the pattern rotated by 90° after every layer. Surface RS were measured in the as-deposited condition by XRD. Measurements were taken along a diagonal line across the top surface of the deposit. Results indicated that the bidirectional pattern produced the highest amount of RS, while S-shaped and spiral patterns had lower RS. They attribute this to the fact that both of these patterns produce a more uniform temperature distribution [63]. Mirazimzadeh et al. investigated the deposition of a hexagonal shape using 316L wire by continuous and segmented tool paths (Figure 9(g and h)). RS were measured by XRD with stresses reported as depth profiles. Measurements were taken at three locations at the hexagon joints, where the thermal history is most affected by the toolpath. Their results showed that the segmented toolpath led to shorter thermal cycles and reduced RS in certain areas, likely due to less heat accumulation compared to the uninterrupted continuous deposition [64].

Opting for a different approach, Zhang et al. combined Zig-Zag and contour patterns in a single-layer WAAM deposit, using ER4043 aluminium alloy wire. They first deposited the middle Zig-Zag pattern and then encircled it with 0, 2, 4, and 6 outward spirals (Figure 9(i)). The longitudinal RS was measured by XRD at a depth of 2 mm below the top surface of the deposit, after electrolytic polishing. Five points were measured on the first, third, fifth, seventh, and ninth passes, running from the inner contour next to the hole to the outer edge. The results showed that adding contour passes reduced the tensile RS to the point that with four and six contour passes, the RS at the innermost location became compressive. They attribute this change in RS to the fact that the contour passes smooths out the thermal gradients and cooling rates, and makes a relatively more stable temperature field and gentle cooling rate [65]. From a mechanical point of view, because the contour passes are deposited hot and then contract during cool down, they could also be contracting the inner region and pushing it into compression.

Zhan et al. investigated the effect of five path strategies: two samples with bidirectional scanning strategies (in longitudinal and transverse directions), one with a unidirectional pattern, one with an inward spiral, and one using an island strategy. They also experimented with 90° rotation between layers using the bidirectional scanning strategy. Their results demonstrated that the island scanning strategy and the 90° rotation between layers were effective strategies for the reduction of RS. As for the two samples with bidirectional scanning, the conclusion was that scanning along the shorter side leads to less RS [66].

Zhang et al. also investigated the effects of rotation strategies between successive layers. In Sample A, a unidirectional pattern was used, maintaining the same direction for each layer. Sample B employed a bidirectional pattern, reversing the direction after every layer. Sample C also followed a bidirectional approach but introduced a 90° rotation (Figure 9(k)) between layers. Finally, Sample D was fabricated using an inward spiral path for all layers. They observed that the scanning pattern directly impacts the thermal history and that different thermal histories influence RS. However, they concluded that no direct correspondence could be established between the distribution of RS and the scanning patterns. They did note, however, that the spiral deposition exhibited higher RS [67]. Additionally, Saboori et al. investigated the RS formation on the surfaces of a 316 cube using two distinct deposition strategies. In the first method, each successive layer was deposited with a 90° rotation relative to the preceding layer, while in the second method, a 67° rotation (Figure 9(l)) was implemented. Their results indicated no significant difference in the RS formed on the top surface of both cases. However, on the lateral surfaces, higher stress values were recorded for the

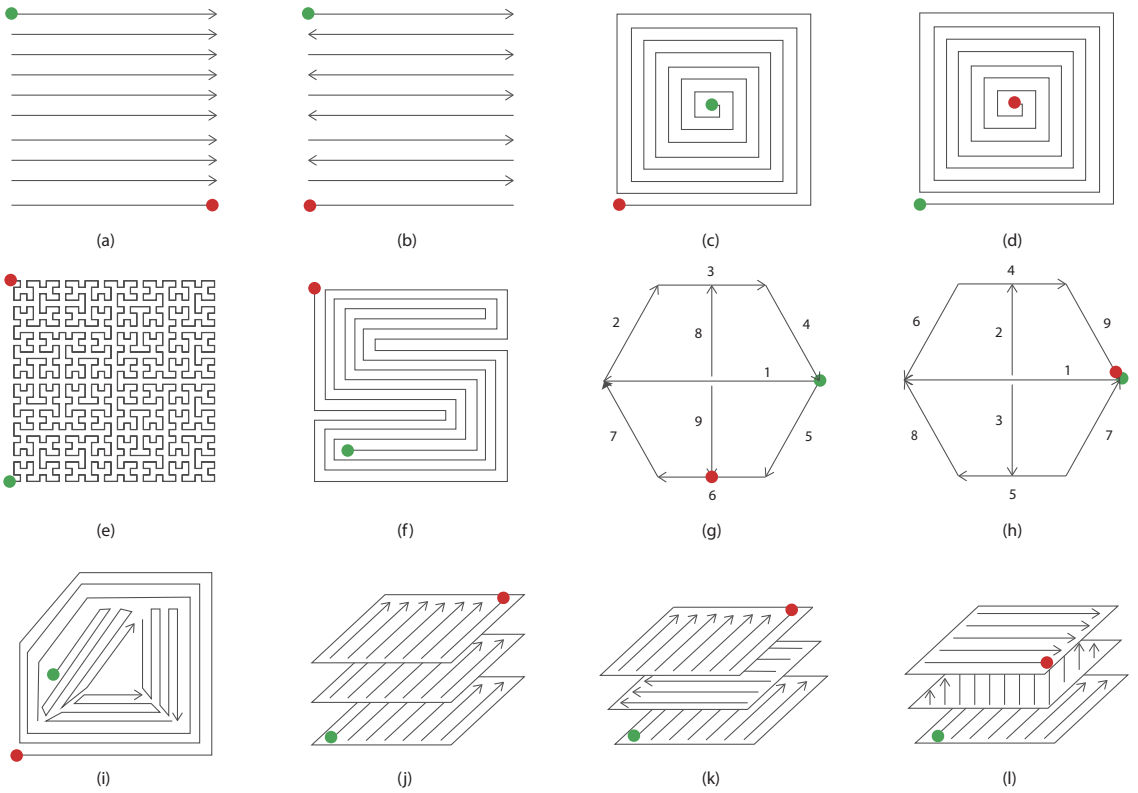


Figure 9: Various scanning patterns in DED: unidirectional (a), bidirectional (b), outward spiral (c), inward spiral (d), fractal (e), S-shaped (f), continuos hexagonal (g), segmented hexagonal (h), zig-zag with contour (i), no interlayer rotation (j), 90° interlayer rotation (k), 67° interlayer rotation (l). Green indicates the start and red the end of deposition. Numbers in the figure indicate the sequence of deposited tracks.

90° deposition strategy [68]. Aversa et al. also investigated the effects of different scanning directions and found that the RS using the 90° rotation strategy was lower than that of the 60° deposition strategy [69]. In a more recent study, Piscopo et al. performed similar experiments, comparing three deposition paths of outward spiral, 90° and 67°. Their findings, shown in Figure 10, are in corroboration with the previous studies showing that the 90° deposition strategy resulted in the least RS build-up. The spiral strategy showed the highest amounts of RS [70].

Lastly, Woo et al. experimented with three deposition methods: bidirectional, 90° rotation and island pattern [71]. They built five-layer functionally graded material specimens by DED on an S45C steel substrate, grading from 316L to a ferritic carbon steel (P21) in 25 vol.% steps. RS were measured by neutron diffraction along the specimen centre line through the thickness, with a stress uncertainty mostly below ±60 MPa. They found that the range of stress was significantly decreased from 950 MPa in the back-and-forth method to 680 MPa in the 90° rotation and to 430 MPa in the island deposition strategy. The trends were consistent with contour method and deep hole drilling results. The authors argue that strategies like having shorter deposition length (island strategy) and rotating the deposition direction in each layer reduce the heat input. They also disperse heat across multiple directions and promote a more uniform thermal gradient, rather than concentrating it along the building direction. This eventually leads to a reduction in the accumulation of RS [71].

In summary, these studies demonstrate that both the scanning path and the rotation between layers can have a significant impact on the development of RS in the deposited material. While it is difficult to reach a definite conclusion on which strategies are best for the mitigation of RS, some common trends are observed. The island and segmented scanning strategies have been shown to be most effective by dividing the deposit into smaller sections, thus minimising

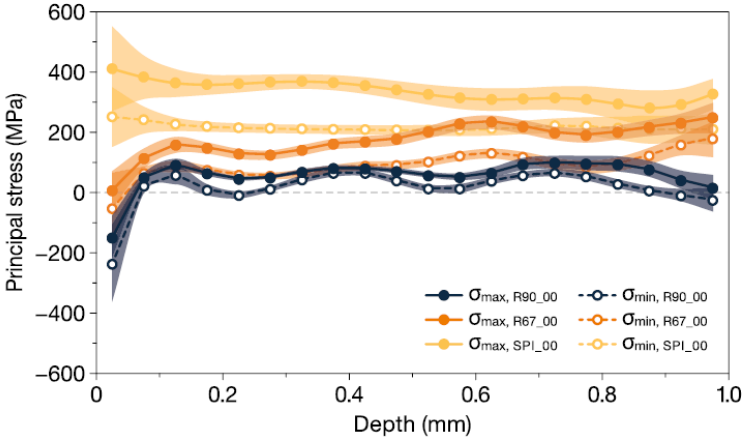


Figure 10: Minimum and maximum distribution of RS measured on the top surface of samples with 0°, 67° and 90° rotation between layers. Reproduced from [70], with permission from Springer.

heat accumulation [66, 71]. The 90° rotation between layers has also been shown to be an effective strategy as it prevents stress build-up along a single direction [68–71]. In contrast, unidirectional scanning has led to the highest amounts of RS [62, 66, 72].

2.10. Interlayer dwell time

Upon finishing the deposition of each layer in the DED process, the laser moves to the initial position for the deposition of the next layer. At this stage, the laser can either immediately start the deposition of the next layer or a pause can be introduced in the process [73]. This pause between the deposition of successive layers is referred to as the interlayer dwell time [74].

Adjusting the dwell time is an important factor in controlling the heat input of the DED process. On one hand, introducing a pause between layers can allow excess heat to dissipate, thereby reducing heat accumulation and the overall thermal gradient [73–75]. On the other hand, longer dwell times can lead to the significant cooling of previously deposited layers, which then creates a high interlayer thermal gradient when the next layer is deposited [70, 76]. This parameter can be significantly important when manufacturing large components, where the time gap between successive layers can be substantial [77].

Several works have investigated the effects of dwell time. From these studies, it is clear that the impact of this process parameter is more material-dependent than the previously discussed parameters. The most notable study was conducted by Denlinger et al., who investigated the effect of dwell time on Ti-6Al-4V and Inconel 625 thin walls, demonstrating contradictory results [16]. Dwell times of 0, 20 and 40 s were applied between layers. RS was measured on the substrate after the build using the incremental hole-drilling method. A single measurement was taken per sample, and the longitudinal stress component was reported. As shown in Figure 11, in the Ti-6Al-4V samples, introducing dwell times of up to 40 s led to an increase in RS, while in the Inconel 625, a reduction in RS was recorded with increasing dwell time. They recognise that the introduction of dwell time is commonly used to reduce RS, but argue that the material being used is an important factor to consider. In the case of Ti-6Al-4V, recrystallisation occurs at temperatures around 600°C, which relaxes plastic strain and self-anneals the part when layers are deposited in rapid succession. If a pause is introduced, the component will spend less time above the recrystallisation temperature, thereby hindering the removal of built-up stresses. Lee et al. achieved similar results when depositing Ti-6Al-4V and found that shorter interlayer cooling time led to less RS [16, 78]. Conversely, a study by Zhan et al. reported a slight decrease in RS with the introduction of dwell times of 20 to 60 s. However, their quenched martensitic microstructure shows that the bulk never remained hot enough to recrystallise; Therefore, dwell time did not interrupt recrystallisation. Instead, longer pauses simply cooled the solid between melts, reducing thermal accumulation, leading to a slight decrease in RS [42].

As for Inconel 625, Mohsin Khan et al. applied a 2-minute dwell time and observed an increase in tensile RS, contradicting Denlinger et al.'s findings. They attributed this increase in RS to excessive cooling of each deposited layer, which amplified the thermal gradient when the subsequent layer was added [79]. Although the lack of detailed thermal

data limits direct comparison, it is plausible that the 2-minute pause was excessively long compared to Denlinger's 20–40 s range, leading to over-cooling and negating the benefits of reduced heat accumulation [16, 79]. Further insight into nickel superalloys' behaviour is provided by Li et al., who investigated the effects of dwell times of 15 s, 30 s, and 45 s on the RS of an IN718 alloy [80]. They observed a reduction in RS at 30 s and 45 s dwell time, consistent with the findings of Denlinger et al. on Inconel 625 [80]. Mehmeti et al. investigated the effects of dwell time on another nickel-based superalloy (CM247LC); However, rather than applying dwell time between each layer, they applied a 45 s dwell time between each 4 mm of deposition, which was also when they rotated the scan direction by 180°. The study found that these intermittent dwells effectively minimised thermal gradients, lowering RS well below the material's yield strength. The aim of this approach was to balance the reduction of RS with process efficiency, as interlayer dwell time significantly slows down the DED process [81]. These studies suggest that moderate dwell times may provide sufficient cooling to relieve stress in nickel-based superalloys, without introducing large thermal gradients.

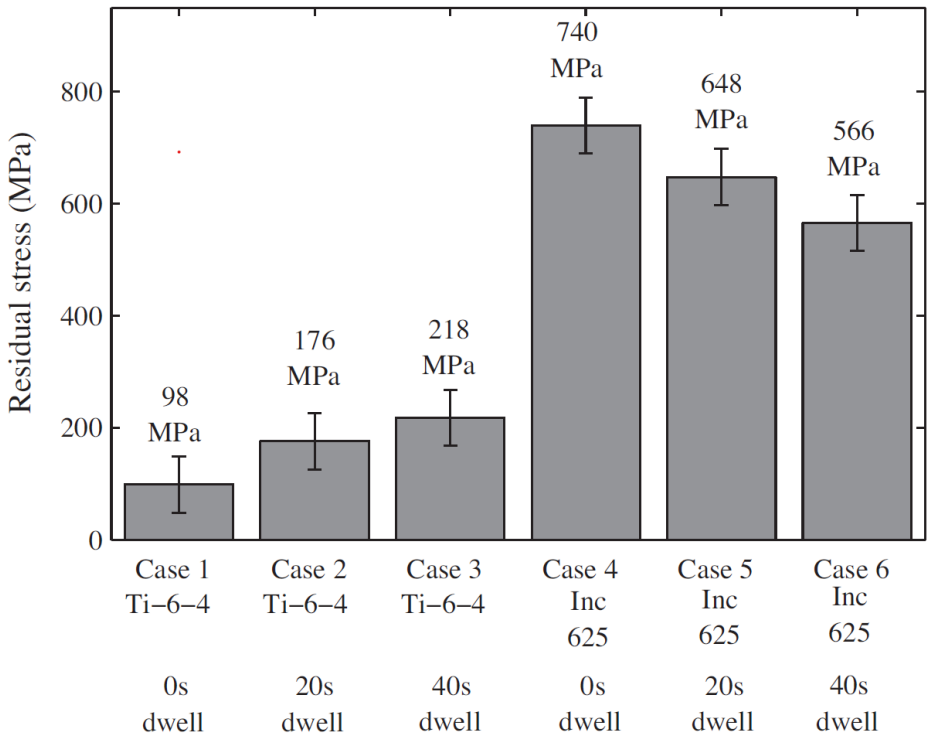


Figure 11: Residual stress measurements for Ti-6Al-4V and Inconel 625 with different dwell times. Reproduced from [16], with permission from Elsevier.

Piscopo et al. investigated the effects of dwell time (10 s and 20 s) on 316L deposits. Their findings revealed that introducing dwell time increased RS. While dwell time reduced overall heat accumulation, it amplified thermal gradients between successive layers, leading to higher RS. Additionally, longer dwell times (20 s) reduced heat retention, causing incomplete fusion and increased porosity [70]. Kumar et al. investigated the effect of interlayer dwell times in ferritic steel. They found that longer dwell times of 400 s increased tensile RS compared to shorter dwell times of 100 s, attributing this to greater thermal gradients and constrained contraction during cooling. However, the study did not include a condition with no dwell time, so its impact on RS remains underexplored.

In conclusion, introducing a pause between layers can reduce heat accumulation and potentially reduce RS, but it can also lead to an increased thermal gradient during the deposition of the next layer. It can also lead to the formation of defects such as lack of fusion pores [70]. Another important point is that the effectiveness of this approach is highly dependent on the material being processed and the chosen dwell time. Beyond quality considerations, the introduction of dwell time extends the total manufacturing duration, which may not be economically viable [74].

2.11. Laser mode

In the DED process, two distinct laser modes can be utilised: continuous wave (CW) and pulsed wave (PW), sometimes also referred to as modulated laser mode. As their name suggests, in the CW mode, the laser remains on throughout the entire deposition process. In PW mode, however, the laser power is periodically modulated. It can cycle between high and low power levels, or between on and off states. While the majority of DED studies have been conducted using CW laser mode, notable findings have been recently made through the use of PW laser in DED.

In PW mode, when the laser turns on, the material heats up and expands similarly to the CW mode, which creates compressive stresses. However, the subsequent laser off period leads to a sudden temperature drop and material contraction, which creates tensile stresses. When the laser turns on again, heat is transmitted to the previously solidified area, causing another cycle of expansion and resulting compressive stresses. This cyclic thermal stress in PW mode, compared to the single "compression-tension" thermal stress characteristic of CW mode, helps reduce tensile RS [12]. Additionally, this reheating of previously solidified areas can have effects similar to the annealing process, which relieves RS [8].

Zou et al. deposited 30-layer 316L blocks using both CW and PW laser modes. RS was measured using the contour method. Using PW laser (10 Hz, 75% duty cycle), they observed less concentrated, lower RS. Specifically, they noted that using PW laser mode resulted in a 75% reduction in the tensile RS in the middle region of the deposit, as can be seen in the 2D mapping of RS in Figure 13. They also reported a 42% reduction of RS between the deposit and the substrate. In addition to the cyclic compression-tension effect, the authors attributed this reduction in RS to a smaller temperature gradient (about 25% lower than in CW mode) in PW mode, leading to reduced thermal strain. Moreover, PW mode minimised heat accumulation, and maximum temperature, resulting in more homogeneous stress distribution [8, 82].

Cheng et al. expanded this analysis by testing with low and high laser power in CW and PW (10 Hz and 50% duty cycle) modes in 316L thin walls [83]. RS was measured mainly with the contour method. For the two high-energy cases, XRD was used as a cross-check at six depths along the substrate centreline, on transverse cut surfaces. The two techniques showed similar trends, with the values of the contour method slightly lower than the XRD ones. Interestingly, they observed that under low laser power (300 W for CW and 600 W for PW), the longitudinal RS at the junction was lower in the CW sample. However, when laser power was increased (600 W for CW and 1200 W for PW), the PW laser samples showed lower RS. The authors attributed this trend to the extent of remelting during deposition. At low laser power, the PW molten pool was small and the remelted zone covered only about 9.7% of its area, so stress relief was minimal. At high laser power, the PW molten pool was larger and the remelted zone covered about 19.8% of its area, facilitating repeated melting and solidification cycles that promoted stress relaxation. This behaviour is illustrated in Figure 12, where the remelting zone in the high-power PW case is wider and deeper compared to the other cases [83]. They also reported that the density and manufacturing efficiency of the PW deposit were comparable to the CW samples [12].

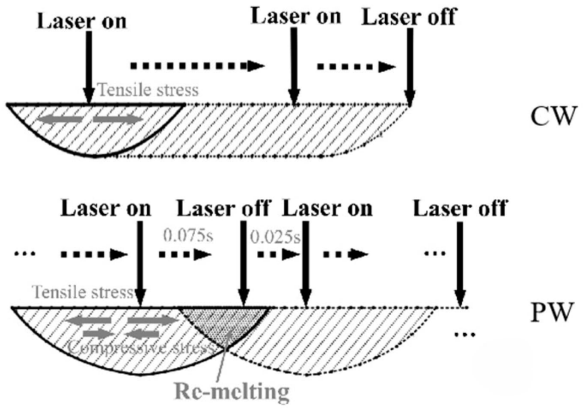


Figure 12: Schematic diagrams of thermal stress state during deposition using CW and PW Laser modes. Adapted from [12], with permission from MDPI.

These studies highlight the effectiveness of PW laser mode in reducing RS in DED by promoting cyclic thermal stress, enhancing localised remelting, and minimising thermal gradients. Optimal frequency and duty cycle further enhance stress mitigation while maintaining deposition quality.

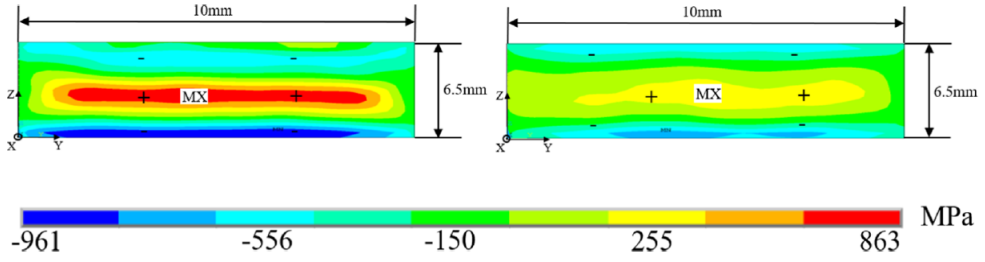


Figure 13: 2-D mapping of the longitudinal RS (σ_x) in deposited blocks obtained using the contour method. (a) CW 600 W, (b) PW 800 W. Reproduced from [8], with permission from Elsevier.

2.12. Summary

It is clear from the number of studies and their sometimes contradicting results that the DED process is a very complicated manufacturing technique. The formation of RS in this process depends on a multitude of factors that are not yet completely understood due to the relative recency of this process. However, if the goal is to mitigate these RS as much as possible, some constant trends can be seen in the literature. The most significant results were obtained by adjusting the laser power. Multiple studies have shown that a decrease in laser power has led to a decrease of RS, some of them by as much as 77%. This can be effectively done by reducing the laser power as much as possible before the appearance of defects such as pores and lack of fusion. A varying laser power approach can also be used, in which heat input starts at a higher laser power and gradually reduces as the process continues. Another effective method is adjusting the scanning strategy. Changing the scanning pattern to a more segmented one, and with rotations between layers, also leads to less RS in the final part. For a summary of the effect of all DED parameters on RS, the reader is referred to Table 2.

Table 2. Effect of DED parameters on RS.

Parameter	Adjustment for lower RS	Range of Values / Technique	Mechanism	Material
Laser power	Lower laser power (except in superalloys)	300 - 3000 W	Lower laser power produces a less steep thermal gradient and smaller melt pools, both contributing to reduced RS.	Titanium alloy [41] Ti-6Al-4V [42, 43] 316L [12] Maraging steel [54] FeCrCoMnNi [46] CrMnFeCoNi [47]
Scanning speed	Higher scanning speed	4 - 20 mm/s	At the layer level, a higher scan speed lowers the energy input per unit length and reduces heat accumulation.	Titanium alloy [41] Ti-6Al-4V [42] 316L [12]
Spot size	Bigger spot size	0.6 - 4 mm	In theory, bigger spot sizes lead to less heat concentration, which decreases the thermal gradient, leading to a reduction in RS	316L [50]
Powder feed rate (PFR)	Higher PFR	0.4 - 30 gr/min	High PFR means that more energy is used to melt the powder, so a lower thermal gradient occurs in the part	Maraging steel [54] Ti-6Al-4V [42]
Hatch spacing / Overlap	Higher hatch spacing	Hatch spacing: 0,25 - 1,5 mm Overlap: 40-60%	Increased hatch spacing reduces both heat input and thermal gradient	Maraging steel [54] IN718 [56, 84]
Heat input	High heat inputs [85, 86] Low heat inputs [27, 87]	200-650 J/mm	Higher temperatures lead to more stress relief but also cause larger melt pools and higher peak temperatures	Filler steel [85, 86] IN718, SS316, and 800H [27] Carbon steel [87]

Table 2. Effect of DED parameters on RS (continued)

Parameter	Adjustment for lower RS	Range of Values / Technique	Mechanism	Material
Energy Density	Lower ED [54, 88, 89] Higher ED [89, 90]	75-300 J/mm 20-167 J/mm^2 100-300 J/mm^3	It is a balance between stress relief at higher temperatures and greater thermal gradients causing more stress.	Maraging steel [54] Fe-Cr alloy [88] Fe-50Cu [89] Fe [89] Ti-6Al-4V [90]
Scanning strategy	Rotation between layers [66–71] Fragmented / island scanning patterns [62–67, 70, 71]	Interlayer: 90°, 60°, 67°, 45° rotation Intralayer: Unidirectional, bidirectional, fractal pattern, inward spiral, outward spiral, S shaped, island, continuous, segmented	Rotation between layers helps reduce heat gradient in the same direction. Segmented strategies, reduce heat accumulation, reducing RS.	316L [62, 64, 68–70] H13 steel [71] Al-4046 [63] Aluminium alloy [65] Ti-6Al-4V [66, 72] IN718 [67]
Interlayer dwell time	Material-specific dwell time optimization	10 - 1800 s	Dwell time reduces heat accumulation, but also increases thermal gradient during the deposition of the next layer. A balance between these two mechanisms is needed to reduce RS, and is material specific.	IN625 [16, 79] IN718 [80] CM247LC [81] 316L [70] Ti-6Al-4V [16, 42, 78]
Laser mode	PW mode	Frequency: 5-10 Hz Duty cycle: 50-75%	Cyclic thermal stress in PW mode helps reduce RS.	316L [8, 12, 82, 83]

3. Energy input and thermal response

As described in the previous section, most DED parameters influence one another as well as the RS in the final part. Combined with the complex mechanisms behind the formation of these stresses, this results in an intricate relationship that is difficult to interpret one parameter at a time. Since these variables are strongly interconnected, it is useful to have a parameter that incorporates the most influential ones, providing a clearer picture of how they affect RS development. For this reason, this section examines several attempts at defining metrics that combine many of these parameters with additional ones, such as the intrinsic characteristics of the process, including the material used and the laser absorptance. The objective of these metrics is to clarify how the parameters work together, and to provide a means of comparing different cases and studies.

3.1. Heat input and energy density

Heat input is defined as the amount of transferred energy per unit length during deposition [91, 92]. It is usually defined as

$$HI = \frac{P}{v} \tag{2}$$

Where P is the net power in Watts, and v is the travel speed of the energy source [92].

On the other hand, Energy density, which is generally understood as the amount of energy per unit area or volume, has been defined in different ways across various sources [3, 49, 54, 55, 93, 94]. Despite these variations, a consistent aspect across these definitions is that energy density is directly proportional to laser power and inversely proportional to scanning speed. The difference lies in the parameters chosen to define the area or the volume of the material. These can be hatch spacing, laser spot diameter, layer thickness or a combination thereof. In this work, we refer to energy density as:

$$E = \frac{P}{v \cdot d \cdot t} \tag{3}$$

where P, v, d, and t refer to laser power, scanning speed, laser spot diameter, and layer thickness, respectively. This definition is chosen given that incorporating both layer thickness and laser spot diameter provides a more comprehensive representation of volumetric energy density than using only one of the above parameters. Hatch spacing was not considered, as laser spot diameter is more commonly reported in the literature, making comparison of results across different studies relatively easier.

Both heat input and energy density incorporate several aspects of the DED process, which makes them useful parameters to consider. Although not always the case, heat input is often mentioned in the context of the WAAM process, while energy density is more often used in powder DED studies.

A study by Srivastava et al. observed that increasing heat input increases the RS in the material. They deposited 12-layer, single-track thin walls, using 1.2 mm ER70S-6 mild steel wire on ASTM A36 substrates. Each wall was built with either a fixed heat input or a two-, three- or four-tier layer-wise heat input, so that the heat input dropped in successive layers. RS was predicted with a thermo-mechanical FE model and validated experimentally with an XRD residual stress measurement system. Measurements were taken on the upper surface of the substrate. Compared with the fixed heat input, the varying heat inputs reduced longitudinal RS by 8.54%, 3.59% and 13.07% (two-, three- and four-tier, respectively) and average transverse RS by 1.3%, 13.34% and 25.83%. The Authors attribute this reduction in stress in the multi-tier heat input cases to the reduced accumulated heat in successive layers, which lowers the layer-wise peak temperature and temperature gradients Compared with the single-tier case [87]. In a numerical study, Wu et al. investigated the effect of heat input on the RS of different materials (IN718, SS316, and 800H) [27]. As shown in Figure 14, in all cases, it was also observed that increasing the heat input from roughly 275 J/mm to 375 J/mm led to an increase in longitudinal stresses. This behaviour was attributed to higher heat inputs causing larger melt pools and higher peak temperatures, which can both increase the RS in produced parts [27].

In contrast, other works have shown that heat input and RS are inversely related. Wandtke et al. conducted experiments of depositing a filler steel material using different heat inputs and found that high heat inputs (650 J/mm) led to lower longitudinal RS than lower ones (200 J/mm) (Figure 15). They attribute this to lower cooling time, which

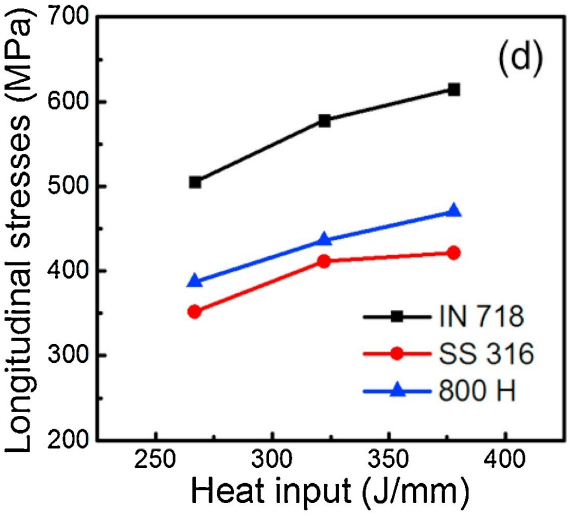


Figure 14: Effects of heat input on longitudinal stresses for three alloys.Adapted from [27], with permission from Elsevier.

causes layers to be partially tempered and not be able to release their RS [85]. Other studies by the same group showed similar results, demonstrating that an increase in heat input leads to a decrease in RS [86].

Some contradictory findings were also observed in the powder-based processes regarding the relation between energy density and RS. For example, Aleksandr et al. who investigated the effects of different parameters during the deposition of 1.2709 maraging steel powder, found that when looking at energy density alone, its increase led to an increase in RS [54]. Similarly, Yue et al. showed that increasing the energy density when depositing Fe-Cr alloy powder also led to an increased RS [88].

However, when Vyatskikh et al. experimented with depositing pure Fe and Fe-50Cu powders using different energy densities, they noticed that for pure Fe samples, higher energy density yielded less RS in both the surface and bulk of the material, but for Fe-50Cu samples, a higher energy density led to more RS in the bulk of the material and had no significant effect on the surface RS [89]. Lastly, a study by Wang et al. also demonstrated that, in Ti-6Al-4V, an increase in energy density decreases RS. Initially, when using high energy density, greater thermal gradients lead to higher elastic stresses, but these stresses eventually exceed the yield strength and cause plastic deformation and therefore stress relief. At low energy densities, however, the stresses remain elastic. Without stress relief in the form of plastic deformation, these stresses accumulate, resulting in higher RS [90].

As these studies show, the topic of energy density is quite complex and relatively underexplored. In this section, we aim to get a better understanding of this relationship by analysing data from the cited literature in section 2 using residual stress versus energy density plots. Energy densities were calculated based on Equation 3, using only studies that provided the necessary information. We have looked into the three most studied materials in the literature. Figures 16, 17 and 18 represent the results for 316L, IN718, and Ti-6Al-4V, respectively.

In Figure 16 a direct relation is observed between Energy density and RS, confirming that in most cases an increase in energy density leads to an increase in RS. The same trend is observed for IN718 and Ti-6Al-4V in Figures 17 and 18. However, data availability for these two materials is more limited, and in the case of Ti-6Al-4V, many data points originate from a single study, making it more difficult to draw definitive conclusions.

It is important to note that some of the studies mentioned in section 2 were not included in these graphs because of different manufacturing conditions. For example, the study by Wang et al., which investigated various energy densities, employed a 30 s dwell time between each layer. This parameter may have significantly influenced their results, as they observed a decrease in RS with increasing energy density, contrary to what the trend in the graphs shows [90]. Additionally, some studies were excluded due to the application of post-processing treatments. For instance, the study by Li et al. on 316L reported that during the milling process, a larger blade radius increased both plastic deformation and surface RS [95]. These changes altered the as-built RS, making direct comparison with untreated samples challenging. Other studies were not included simply because essential parameters for calculating energy

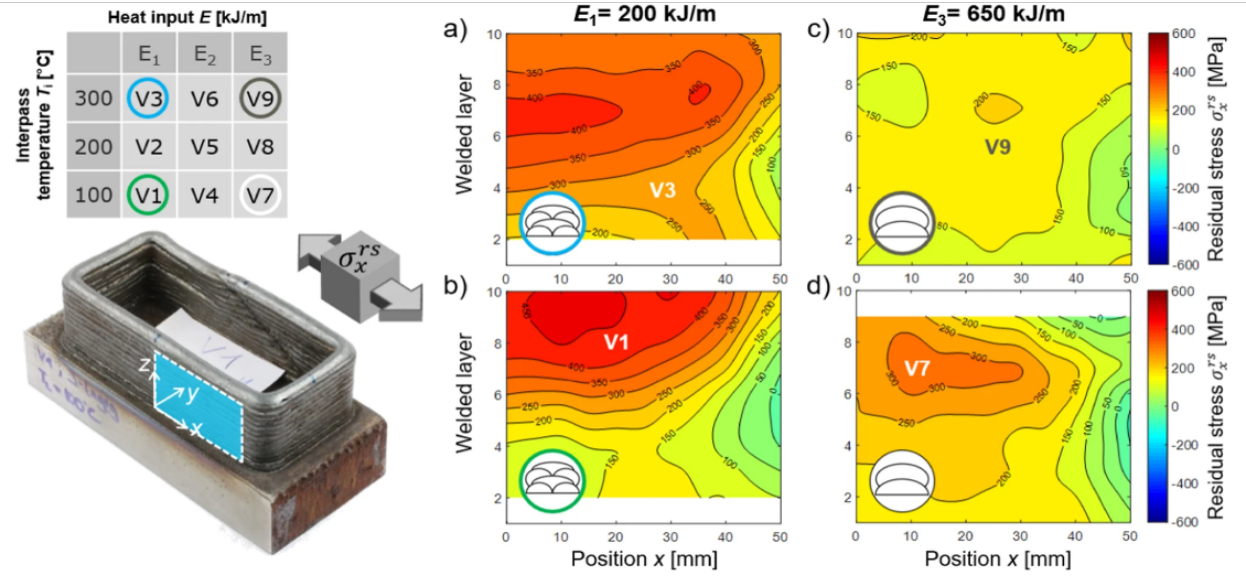


Figure 15: Distribution of the longitudinal residual stress ($\sigma_x^{rs}(x,z)$) on the surface of the WAAM specimen wall (V1, V3, V7, and V9) with different heat input (E), interpass temperature (T_i), and deposition pattern. Reproduced from [85], with permission from Springer.

density, such as laser spot diameter or layer thickness, were not reported. Without this information, it wasn't possible to include them in a consistent comparison. Authors are encouraged to give careful consideration to reporting all relevant processing parameters, as this helps ensure that their valuable results can be used more effectively in future analyses and comparisons across studies.

Another factor to consider is the variety of methods used to measure RS. The depth at which RS is measured can vary significantly between techniques, making it even more difficult to compare results across different studies. There were not enough studies to analyse each method separately, as most were represented by only one or two publications. However, the graph data points have been grouped by measurement method to facilitate comparison.

Although these graphs indicate a trend of increase in RS as the energy density increases, they also indicate that energy density is not the only factor influencing RS. In the case of the study by Piscopo et al. on 316L (blue squares in Figure 16), different values of RS (93 MPa, 240 MPa, and 350 MPa) are observed for the same energy density. These values correspond to 90°, 67°, and 0° of rotation between layers, showcasing that the deposition pattern has a significant role in the formation of RS [70]. Similarly, in the case of Zhan et al.'s study on Ti-6Al-4V, two distinct values for RS have been observed at the same energy density of 147 J/mm^3 in Figure 18 . In this case, higher laser power combined with faster scanning speed led to less RS compared to lower laser powers and slower scanning speed [42]. Also, the study by Zou et al. showed different values of RS for the same energy; the difference in this study was in the choice of pulsed versus continuos laser mode [82].

These findings indicate that while energy density offers a convenient, readily calculable first-order metric for predicting or mitigating RS, it captures only the input side of the thermal problem. A given energy input can produce noticeably different thermal responses, which lead to different thermal gradients, cooling rates, and degrees of heat accumulation. Therefore, the following section examines additional factors that, while less directly tunable than the core process parameters, exert a comparable influence on the thermal history of the part and, through it, on the development of RS.

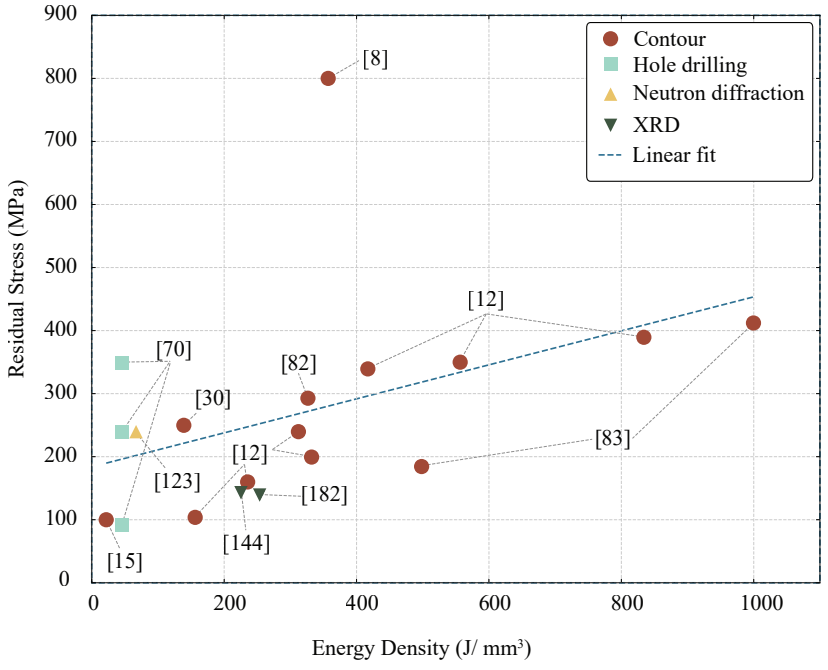


Figure 16: Effect of laser energy density on residual stress in 316L DED fabricated parts.

3.2. Material optical and thermal transport properties

The previous section addressed deposition parameters that can be readily tuned and their influence on RS. However, several parameters relevant to the thermal history of the deposit are considerably less straightforward to control. This is either because they are intrinsic material properties, because they are indirectly influenced by the more easily adjustable process parameters, or because they are constrained by fixed boundary conditions such as the part geometry and the ambient temperature. While their relationship to RS has received comparatively little attention in the DED literature, these parameters have a large impact on the thermal history of the deposited part, which in turn exerts a strong influence on the resulting RS state. This section, therefore, focuses on the parameters that set the energy balance of the process; such as the laser power efficiency, the optical absorptance of the material, and its thermal transport properties. The first two determine how much laser energy is actually utilized during deposition, while the thermal transport properties determine how that energy is subsequently redistributed and dissipated. Several of these parameters are combined in the normalized enthalpy metric, which is discussed later in this section. In line with the ASTM E284 convention of reserving "-ance" for a property of a specific specimen and "-ity" for a property of the kind of material [96]. As an example, the term absorptance is preferred over absorptivity, although the latter is widely used for the same quantity in the DED literature.

Figure 19 illustrates how the total laser energy is distributed during the DED process. This figure was derived from the works of Lia et al. [97] and Liu et al. [98]. Lia et al. describe the process with a simple energy balance, in which the incident laser energy (Q_{in}) is either absorbed or lost [97]:

$$Q_{in} = Q_{abs} + Q_{lost} \tag{4}$$

Each term is then split in two. The absorbed energy is the sum of the energy absorbed directly by the substrate ($Q_{abs,sub}$) and the energy absorbed by the powder stream and carried into the melt pool ($Q_{abs,powder}$). The lost energy is the sum of the energy reflected from the substrate ($Q_{ref,sub}$) and the energy lost to the powder stream through reflection, evaporation, or unfused powder ($Q_{lost,powder}$):

$$Q_{in} = [Q_{abs,sub} + Q_{abs,powder}] + [Q_{ref,sub} + Q_{lost,powder}] \tag{5}$$

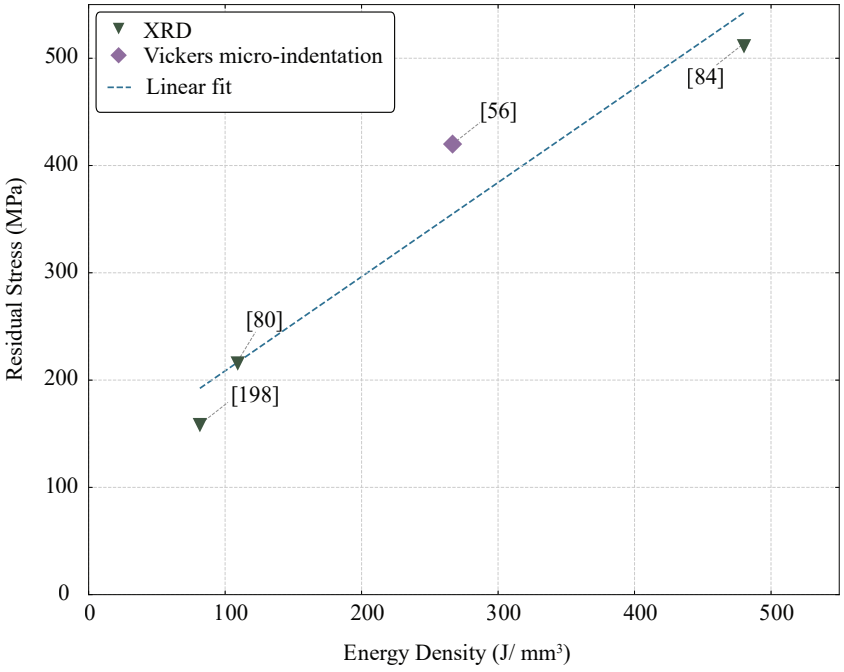


Figure 17: Effect of laser energy density on residual stress in IN718 DED fabricated parts.

Using a different classification, Liu et al. divide this energy into two section: energy that is transmitted to the melt pool and non transmitted energy [98]. A similar power balance for coaxial DED was developed earlier by Pinkerton and Li. Above the melt pool, the laser power is divided into power reflected by the powder, power absorbed by the powder, and power reaching the surface. Powder that misses the pool is treated as lost, while powder that hits the pool is absorbed by it. Of the power absorbed by the pool, most is lost by conduction to the substrate, with evaporation becoming significant at higher temperatures [99]. The powder stream also attenuates the beam before it reaches the melt pool, and Pinkerton modelled this by treating the particles as isothermal lumped capacity elements that absorb part of the beam energy [100].

3.2.1. Energy transfer efficiency

In an early study on the process efficiency of the laser-engineered net-shaping process, which can be considered as a subset of DED, Unocic and DuPont used the laser energy transfer efficiency parameter (η_a) to quantify how much of the total laser energy is transmitted to the workpiece. They defined this parameter as

$$\eta_a = \frac{E_{cal}}{P \cdot t} \tag{6}$$

in which E_{cal} is the total energy absorbed by the workpiece, P is the laser output power and t is the laser "on" time. This parameter will always be less than one because, as demonstrated in figure 19, some energy is lost before reaching the melt pool. Laser energy transfer efficiency was measured in the range of 30–50%, and was shown to be insensitive to laser power, travel speed, and powder feed rate. This allowed the authors to adopt a representative constant value (0.4) for subsequent melting-efficiency calculations [101].

However, the assumption of a constant energy transfer efficiency should be treated with caution for two principal reasons. First, substrate material appears to play a significant role in this parameter. The authors speculate that a more reflective substrate than the H-13 tool steel used in their study, such as copper, would yield a noticeably lower energy transfer efficiency. The second point of caution is in regards to the insensitivity of this parameter to laser power, travel speed and powder flow rate. The apparent power-insensitivity is characteristic of conduction-mode melting. At

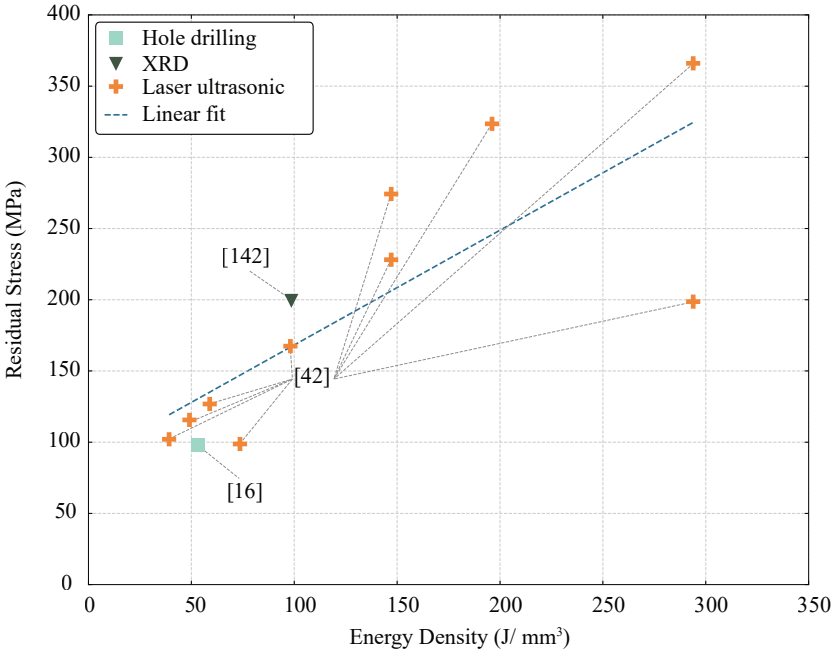


Figure 18: Effect of laser energy density on residual stress in Ti-6Al-4V DED fabricated parts.

sufficiently high power densities a transition to keyhole-mode melting may occur, resulting in increased absorptance [102]. Although, DED typically operates at power densities below the threshold required for keyhole formation, making conduction-mode melting the predominant regime.

Concerning the powder feed rate insensitivity, several studies have investigated this phenomenon, although without explicitly referring to the energy transfer efficiency parameter. Lia et al. reported that unfused powder can represent a substantial source of energy loss, accounting for approximately 11% of the laser energy for Inconel 625 and 14% for Ti-6Al-4V at a laser power of 1 kW. These values were obtained using a custom water-cooled tube calorimeter that directly captured the substrate's absorbed energy from the coolant temperature rise [97]. In another work, Devesse et al. studied the powder attenuation in 316L powder streams using a ray-tracing model that traced the laser beam through the simulated particle cloud to compute the resulting attenuated energy pattern at the substrate [103].To isolate the effect of the powder particles, the substrate was assumed to absorb all incident light, which gives an upper limit for the energy entering the melt pool. For a 400 W beam, the model predicted that 93-95% of the incident laser energy reached the melt pool surface, either as direct light or as heat carried by in-flight particles. The remainder was lost primarily to reflected light escaping the interaction zone and, to a lesser degree, to particles missing the melt pool entirely. The actual energy absorbed into the melt pool would be lower, as the absorbed fraction of the incident light depends on the material, surface geometry, and temperature of the melt pool. With respect to particle size, the smallest particle set exhibited the greatest beam attenuation yet also yielded the highest total absorbed energy. This apparent contradiction was attributed to the superior focusing behaviour of smaller particles. Although a larger fraction of the incident beam was intercepted, proportionally fewer particles missed the melt pool, thereby reducing the associated overspray losses relative to the larger particle sets [103]. It is worth noting that in this study the reported absorbed energy does not account for the reflectance of the melt pool itself; it represents only the fraction of laser and particle-carried energy that survives the powder cloud and reaches the workpiece surface, corresponding to an idealized case where the substrate absorption factor is set to one.

Another important consideration regarding the influence of powder is its shadowing effect on the incident laser beam. A high-fidelity CFD-DEM study by Aggarwal et al., validated through high-speed imaging, investigated laser beam shadowing during DED of titanium powder (45–106 µm) using a 500 W Gaussian beam and powder feed rate of 4 g/min. Argon was used as carrier, shaping and optics gas [104]. They found that in-flight particle-laser interaction

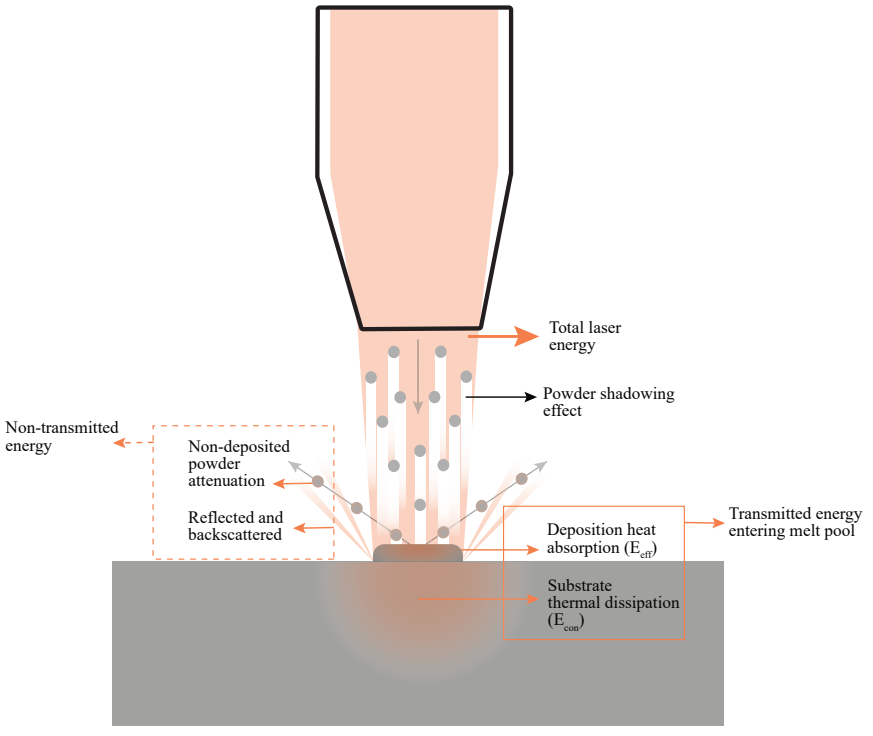


Figure 19: Distribution of laser energy in the DED process, showing the primary energy transfer pathways and loss mechanisms.

significantly deformed the beam from its initial Gaussian profile, with attenuation strongly dependent on the distance from the nozzle outlet and on the shaping gas flow rate. At 10 mm from the nozzle, the predicted attenuation was 25.4% for 3 l/min and 4.3% for 6 l/min shaping gas; at 18 mm it rose to 64.5% and 36.7%, respectively, with instantaneous values approaching 70% owing to the random distribution of powder particles in the stream. It should be noted, however, that these results are not directly comparable to the ray-tracing findings of Devesse et al., as the reported attenuation quantifies the reduction in transmitted laser intensity and does not account for the energy absorbed by the powder particles, which may subsequently be transferred to the melt pool upon particle incorporation. Nevertheless, these findings highlight that the presence of powder influences the fraction of the incident laser energy that directly reaches the melt pool. Despite these limitations, the relevance of energy transfer efficiency extends beyond its role as a stand-alone metric.

Other factors can also have an influence on laser absorptance, which will be briefly mentioned for completeness, though a detailed discussion is outside the scope of this article. The laser wavelength is one of these parameters. In general, as the laser wavelength increases from ultraviolet to infrared, the absorptivity of metals tends to decrease. However, DED systems largely employ lasers in the near-infrared range rather than the ultraviolet or blue range, mainly due to the limited availability, greater cost and technical complexity of scaling such laser sources to the power levels required for metal melting. Within the infrared range, laser choice still influences process efficiency. Nd:YAG lasers, the most widely used laser type in metal DED, operate at near 1.07 µm and are absorbed more efficiently than CO_2 lasers by most metals, which operate at an order of magnitude further into the infrared range at 10.6 µm [37]. Another such parameter is the surface oxide layer. The presence of an oxide layer is typically the reason why the absorptance measured in practice is higher than the theoretical values calculated for an ideal, oxide-free metal surface. Thick oxide layers can entrap the laser beam which can lead to an increase in absorptivity [105]. A study by Abedi and Hoseinpour

Gollo has shown that increasing the Cr_2O_3 oxide layer thickness on AISI 304 stainless steel led to an increase in absorptance [106]. The same study also looked into the effect of surface roughness, another relevant parameter to absorptance, and reached similar conclusion that increasing roughness increases absorptance [106]. Surface roughens affects absorptance through two mechanisms. The first is that increased roughness increases the likelihood of the laser beam being absorbed rather than reflected, as the beam undergoes multiple reflections within the grooves of the rough surface. Secondly, when the roughness is more regular, it can generate surface electromagnetic waves and in the specific case where the roughness pattern's spacing approaches the laser's wavelength, this can cause a resonance effect [105]. An additional factor that affects the absorptance is the vapour plume attenuation. When the laser energy is high enough, material evaporated from the surface, together with the powder flow, can form a vapour plume in the beam path, which may become partially ionized into a plasma. The plume can attenuate the beam through absorption, scattering and refraction [107]. The plasma contribution is wavelength dependent and is generally stronger for CO_2 lasers than for shorter-wavelength lasers such as Nd:YAG [108]. The effect of the plasma is also visible in the choice of shielding gas: in CO_2 laser welding, helium is less prone to plasma formation than argon because of its higher ionisation potential, which can increase penetration, although the benefit depends on welding speed [108]. Lastly, the temperature of the surface receiving the laser radiation is also an important factor affecting absorptance. Absorptance usually increases with temperature; as a result, it is not constant during the DED process but evolves as the material heats up [109, 110]. Unfortunately, very limited data is available in this regard, particularly at the elevated temperatures relevant to DED. Given that in opaque materials, absorptance is the complement of reflectance [107], reflectance is not discussed separately. Any factor that changes the surface reflectance also changes the fraction of laser energy absorbed.

While absorptance governs how much of the laser power enters the part, thermal diffusivity and melt pool convection govern the rate and depth to which that absorbed energy spreads. Thermal diffusivity is defined as the thermal conductivity divided by the product of density and specific heat capacity. Therefore, a material with higher thermal diffusivity will absorb the energy and reach an equilibrium state quicker than a material with lower thermal diffusivity [111]. Apart from the material properties, thermal diffusivity can vary with temperature as well, although the variability is usually less than 10% [105]. However, due to the rapid heating and cooling cycles inherent to DED, even these small variations can significantly affect the temperature distribution in the part.

3.2.2. Normalized Enthalpy

As discussed above, understanding AM processes and being able to compare across different materials and printing conditions is a very complex undertaking. Heat input and energy density offer a convenient way to compare conditions, although they necessarily simplify a process governed by both processing parameters and material properties. For this reason, more recent studies, especially in the LPBF field, have been using normalized enthalpy as an Complementary metric to incorporate both process parameters and material characteristics.

Normalized enthalpy was first introduced in 2011 by Hann et al. for laser welds as

$$H^* = \frac{\Delta H}{h_s} = \frac{\eta C P}{\rho h_s \sqrt{\sigma^3 \alpha v}} \tag{7}$$

Where ΔH is the peak enthalpy of the surface layer, h_s is the enthalpy of melting, η is the absorptivity of the surface, C is a constant, P is laser power, ρ is density, σ is the half-width of the Gaussian laser beam at the workpiece surface, α is thermal diffusivity and v is scanning speed [112]. This parameter was proposed as a complement to energy density by incorporating both material properties and process parameters.

Here, η is the surface absorptivity of the material, as defined in the original formulation, and should not be confused with the process-level energy transfer efficiency discussed in the previous section. However, as discussed in the previous section, treating η as a constant material parameter is a simplification, since the energy actually coupled into the workpiece during DED also depends on process-dependent factors, which a constant value does not capture. The process itself matters as well. Normalized enthalpy is more commonly applied to LPBF, where η can differ considerably from that in DED. In addition, the equation does not account for melt pool flow and heat loss through convection, which can vary considerably with the process and machine setup.

Because of these limitations, normalized enthalpy values can only be compared meaningfully between studies when the inputs behind them are known. In Section 3.1, studies could be compared directly because the values neeeded for the comparison were more readily available. The same applies here. Reporting the material, the value of η used, and

other relevant details would allow normalized enthalpy to be recalculated and compared consistently across studies, and would help move towards a standardized use of the parameter.

Normalized Enthalpy was first introduced in AM in a LPBF study by king et al. in which this parameter was used to characterize the transition between conduction and keyhole-mode melting for 316L [113]. Since then, normalized enthalpy has been increasingly adopted as a metric for comparing the effects of different process parameters, including its use for determining optimal parameters in novel LPBF materials [114, 115], and as an input feature in machine-learning-based melt pool prediction models [116].

Its first introduction in DED was in a study by Kistler et al. that investigated the effects of processing parameters on single tracks deposited IN718 powder. They found that normalized enthalpy correlated linearly with fusion zone area when laser power and processing speed were varied. However, this correlation did not hold when the working distance was varied (7.9, 9.3, 10.7 and 12.1 mm). Fusion zone area instead followed a parabolic trend. Changing the working distance moves the substrate through the powder focus, which changes the area covered by the powder stream and thus the powder capture efficiency of the melt pool. The largest fusion zone occurred with a focused powder stream, while working distances above and below the focus captured less powder and gave smaller fusion zones. Because beam diameter is already included in the normalized enthalpy calculation, the authors attributed this behaviour to powder flow distribution, which the metric does not account for, although beam–powder interactions may also contribute [117]. This observation appears to align with the preceding discussion on laser energy transfer efficiency, suggesting a limitation of normalized enthalpy-based approaches in their inability to account for powder flow behaviour and particle dynamics during the DED process.

The use of normalized enthalpy in DED is still at an early stage. Adopting it as a complementary metric alongside heat input and energy density would enable a more holistic interpretation of how energy is delivered, distributed, and absorbed in DED.

4. In-situ RS reduction

Aside from changing process parameters, RS can be controlled by utilising in-situ strategies. Most of the strategies mentioned in this section are still in the early stage of research regarding their integration in the DED process; however, they are worth examining to understand their potential impact on RS. Additionally, the direct effectiveness of some of these strategies on RS may be limited, but they provide valuable insights for RS mitigation, as many of them focus on controlling thermal gradients, which have been proven to be an important factor in the formation of RS in AM.

4.1. Feedback control systems

Due to the complexity and speed of the DED process, it is challenging to manually control all aspects. Therefore, various closed-loop control methods have been employed to improve the properties of the parts produced by this process. The most commonly used are Proportional-Integral-Derivative (PID) control, adaptive control, and feed-forward control, or a combination thereof. The PID controller regulates process parameters by adjusting system settings based on predefined control rules. In adaptive control, however, these rules are more flexible and adjust dynamically in response to real-time process variations. Lastly, feed-forward control is model-based or experience-based. Instead of reacting to measured deviations, it uses a process simulation or data from previous builds to predict the process behaviour in advance, and adjusts the process parameters before deposition starts. Each of these control systems can operate with either real-time control, which continuously adjusts during the process, or layer-by-layer control, which modifies parameters after each layer's deposition. These two strategies have significantly different time constants. Real-time control responds to fast dynamics such as melt pool fluctuations within a single track, whereas layer-by-layer control reacts on the timescale of a full layer [23, 118–122].

Each of these control systems can operate with either real-time control, which continuously adjusts during the process, or layer-by-layer control, which modifies parameters after each layer's deposition. These two strategies have significantly different time constants: real-time control can respond to fast dynamics such as melt pool fluctuations within a single track, whereas layer-by-layer control reacts on the timescale of a full layer and is better suited to slower effects such as heat accumulation across layers.

In a recent study, Zhang et al. investigated the effects of offline energy control and online height control on the RS of 50-layer 316L thin walls, measured by neutron diffraction [123]. In the offline energy control, laser power or scanning speed was adjusted layer by layer according to a schedule calculated before deposition, aiming for a constant median layer temperature of 600 °C. The online control measured the layer height error after each layer and adjusted the PFR

for the next layer. Without control, the walls showed tensile normal residual stresses with a mean of 56 ± 23 MPa along the build direction. Layer height control shifted the normal stresses to compression at a mean of -124 ± 86 MPa, but with a high maximum absolute RS of 313 MPa among all three stresses. Adding Laser power based energy control to the height control, for a target median layer temperature of 600 °C, reduced the maximum absolute RS by 26% (313 to 232 MPa). Laser power based control alone gave a mean stress of -35 ± 24 MPa and a maximum of 89 MPa, while scanning speed based control gave a mean of 12 ± 31 MPa and a maximum of 142 MPa [123].

To the best of our knowledge, there has not been any other study that explores the direct effect of using feedback control on RS formation. However, the parameters monitored and controlled in the literature have a direct influence on RS. Temperature, for instance, is the most commonly monitored variable in the DED process, while laser power is the most frequently adjusted parameter; both of which, as previously discussed, play a crucial role in RS formation [23, 37, 120, 124–126].

Song et al. used a two-input single-output controller to manufacture a turbine blade, demonstrating that controlling temperature and layer height by adjusting the laser power led to better geometrical accuracy [121]. Similarly, Webster et al. revealed that controlling the melt pool temperature significantly reduced the grain size in the manufactured thin-walled structures [127]. However, while temperature control during the DED process can help mitigate the high thermal gradients inherent to the process, it alone does not guarantee reduced RS [37, 119, 124, 126, 126]. Thus, regulating other parameters, such as cooling rate and thermal gradient, can be a more effective approach for controlling RS formation. Thus, regulating other parameters, such as cooling rate and thermal gradient, can be a more effective approach for controlling RS formation

Su et al. demonstrated that by controlling the melt pool width through laser power adjustments, they were able to reduce thermal build-up in the melt pool [128]. Another study, conducted by Shin et al., aimed to control the melt pool height by monitoring the difference in temperature between the middle of the melt pool and its sides. They found a direct correlation between the temperature difference and the melt pool height. This temperature difference was kept constant by adjusting the laser power accordingly. The results were a reduction of 3D geometric error from 10.49% to approximately 4% for different deposition geometries [129]. Controlling layer height was also explored in laser-wire DED. Heralic et al. used a 3D scanner to measure the height of the deposition after each layer and adjusted the vertical offset of the robot to control the height of the next layer and maintain a stable build height. They also modified the wire feed rate to compensate for deviations in layer height, using an iterative learning control approach to improve the surface consistency [130].

Devesse et al. took a different approach [131]. Instead of relying on simple models fitted to experimental data, they built their controller on a physical model of how heat spreads through the material. The controller adjusts the laser power based on several temperature measurements at the surface, with the goal of keeping the melt pool width at a target value. In simulations, the melt pool reached its target width in about 10 ms with only a small overshoot (3%), and it stayed on target afterwards. The controller also followed changes in the target width quickly. These results come from simulations only, and experimental validation was still to be done [131]. Gibson et al. also controlled the melt pool size, which led to improved geometrical accuracy. This was achieved by real-time laser power adjustments during laser-wire DED. They also experimented with layer-by-layer control by adjusting scanning speed and deposition rate to control the average laser power per layer. These methods reduced energy density by ~23% and enhanced deposition efficiency while maintaining dimensional precision [94].

In another study, Farshidianfar et al. were able to keep a constant cooling rate throughout the build of a thin-wall part by adjusting the laser travel speed in real-time. This resulted in a consistent hardness profile across the produced samples [132]. In this study, the cooling rate was monitored with the help of a computational tool. In contrast, Akbari and Kovacevic established an empirical relationship between the cooling rate and melt pool area, which could be used to control the cooling rate in a more practical manner [133–135].

Lastly, Nassar et al. employed a different approach by controlling the deposition pattern of 3D Ti-6Al-4V sample. They monitored the substrate temperature before the deposition of each track. If the local temperature at a hatch location was below a specified threshold, the deposition proceeded as usual. However, if the temperature was too high, that specific track was temporarily skipped and revisited later. This intra-layer closed-loop control strategy resulted in a more uniform distribution of micro hardness throughout the deposited component, along with vertically aligned columnar grains [136].

Though RS outcomes were not explicitly measured in these works, they offer a valuable foundation for further investigation into how closed-loop control could be used to alleviate RS. Given that RS is highly dependent on factors such as thermal gradients and cooling rates, the control strategies discussed provide useful methods for controlling

these critical parameters. Thus, the integration of feedback control into DED could represent a promising avenue for more effective RS mitigation.

4.2. Build-plate preheating

When deposition begins on a room-temperature build plate, the heat from the initial layers rapidly dissipates into the substrate causing a heat sink effect. This results in a steep thermal gradient in the first layers, causing rapid solidification, which can influence dimensional accuracy and contribute to increased RS [75]. Heating the build-plate prior to deposition decreases the maximum temperature gradient during deposition and also limits the stress magnitude to the yield stress of the material at elevated temperatures. Since most materials exhibit lower yield stress at elevated temperatures, greater stress relaxation occurs through plastic deformation if the substrate is preheated. The result will be lower distortion and maximum RS in the produced part [3, 28, 38, 137].

Build plate preheating is one of the most common methods used to reduce RS in additive manufacturing [5, 6, 12, 70]. Corbin et al. evaluated the effects of both substrate thickness and temperature on distortion by depositing Ti–6Al–4V powder on thick and thin substrates of the same material [38]. They demonstrated that having a preheated substrate significantly reduces the thermal gradient near the melt pool during the deposition of the initial layer, which consequently reduces the amount of distortion. As demonstrated in Figure 20, in thin substrates, preheating reduced the first layer distortion by 27.4%. However, when preheating thick substrates, no measurable effects were found on the first layer distortion. Instead, the distortion rate during deposition increased by up to 390%, and the final distortion after cool down was larger than for the non-preheated substrates. The authors attributed these effects to both the higher stiffness of thick substrates and the larger through-thickness thermal gradient when preheated. They also considered the softening of Ti–6Al–4V at elevated temperatures. As the temperature rises, the stiffness of the material decreases, which lessens the constraint against bending. In addition, stress relaxation occurs when the material reaches a critical temperature (stress relaxation isotherm), approximately 690 °C for Ti–6Al–4V, above which the material softens and creeps, so internal stresses begin to dissipate. In this study, the substrate was preheated from the top surface, and the heat diffused downward. In thin substrates, the heat could penetrate through the full thickness (the bottom surface reached about 600 °C), allowing the stress relaxation isotherm to reach the bottom surface. This relieved internal stresses more uniformly and helped reduce overall distortion. However, in thick substrates, the heat could not reach the bottom surface as effectively (the bottom surface reached only about 350 °C). As a result, only the upper region underwent stress relaxation, while the cooler bottom remained stiff, leading to greater distortion accumulation during and after deposition [38].

In other studies, Baek et al. investigated the effects of substrate preheating (100-500 °C) on M4 steel parts and found that higher preheating temperatures resulted in lower cooling rates. They identified this as the primary cause for the reduction in thermal stress of the final part [138]. Similarly, Mohsin Khan et al.'s experiments on substrate preheating while depositing IN625 powder demonstrated favourable outcomes, with a significant reduction in RS achieved through the introduction of build plate preheating [79]. Bieg et al. conducted experiments with 316L and Ferro 55 cubes and observed that samples preheated to 500°C in both materials exhibited reduced compressive RS [139]

Additionally, substrate preheating at above 200 °C has been demonstrated to be effective in reducing crack formation in M4 steel parts and having more isotropic properties [138]. Zhang et al. also showed improving surface quality at preheating temperature of above 400 °C for Ni60A [140]. However, it can also lead to some adverse effects. The same studies above showed a reduction in mechanical properties such as strength and toughness [138] and a segregation of materials [140]. Preheating at higher temperatures has also caused coarsening of the microstructure as in [28] for a titanium alloy at 800 °C of preheating.

4.3. Localised heating and melting

Heating large build plates for the entire length of the deposition process can be inefficient, which is why localised preheating has been proposed as a substitute technique [141]. When implementing localised heating, the temperature of the solid material around the melt pool is raised (below the solidus), which promotes stress relief and reduces thermal stresses during deposition. However, the larger temperature difference between the locally heated region and the surrounding material also increases the thermal gradient, which may lead to larger thermal stresses during the final cool-down. A balance between these two mechanisms is therefore needed when applying localised heating during deposition [142].

Fan et al. added a stationary rectangular induction coil, parallel to the substrate at a distance of 9 mm. The substrate was lowered by 0.5 mm after each layer deposition, which kept the coil at a constant position relative to the deposition

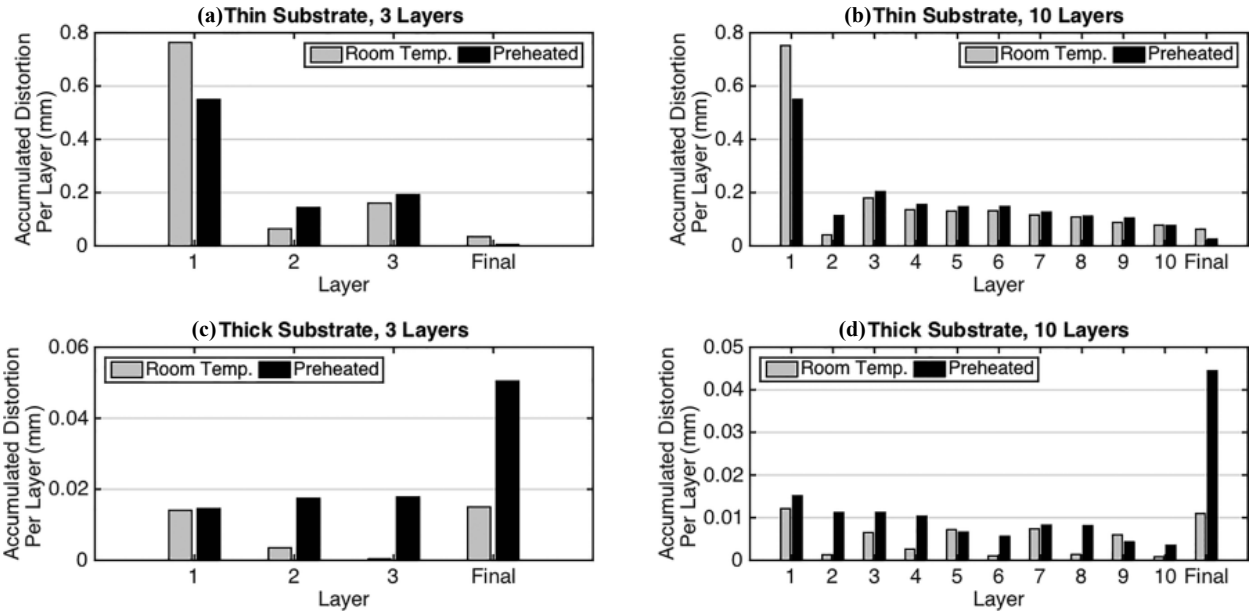


Figure 20: Incremental distortion accumulated during each layer for thin substrate with three layers of deposition (a), thin substrate with ten layers of deposition (b), thick substrate with three layers of deposition (c), and thick substrate with ten layers of deposition (d). Reproduced from [38], with permission from ASME.

zone and provided localised preheating for every layer [142]. The results in both longitudinal and transverse directions were adverse. In the longitudinal direction, there was an increase in tensile RS, and in the transverse direction, a decrease in compressive RS [142]. Using a different approach, Gao et al. implemented an in-situ reheating strategy by rescanning each deposited layer with lower laser power. They believed that doing so would result in a slower cooling rate and reduced thermal gradient; however, they did not investigate the effects on the thermal gradient or RS directly [143]. In these studies, the heating temperature and laser power were chosen in a way that would only increase the temperature of the deposit.

However, some studies have investigated the effects of remelting the previous layers. Reducing RS is not the primary objective of this technique; rather, remelting is used as a treatment to obtain parts with finer microstructure, fewer pores, higher density, and improved surface quality. Given that during remelting the part does not need to be transferred to another machine or machine station, and the same laser used for deposition is employed for remelting, this type of post-processing is viewed as very efficient [50, 144]. During remelting, the laser interacts with the previously solidified material rather than with powder. Thanumoorthy et al. argue that the solid deposited metal reflects more of the laser energy than powder, resulting in a smaller melt pool, and that its higher thermal conductivity leads to lower thermal gradients, and therefore lower thermal RS, than in the as-built case [18, 44, 144].

Nie et al. investigated the use of different energy densities to remelt each 316L deposited layer after depositing with 600 W laser power. They found that in most cases, laser remelting led to a reduction in RS. The authors attributed this to the increased temperatures of the previously deposited layers caused by remelting, which reduced the temperature gradient during the deposition of new layers, ultimately lessening the RS. As the energy density of the remelting passes decreased from case 1 (600 W) to case 4 (400 W), the reheating effects on the previous layers diminished. In case 4, there was no significant reduction in the thermal gradient; however, the material's exposure to two cyclic heating and cooling processes resulted in an increase in RS compared to the as-built sample (360 MPa vs. 322 MPa). The authors also suggest that pores in the more porous as-built sample, which lack fixed connections to the surrounding material, help release RS, whereas the denser LR4 sample could not relax in this way [50].

Remelting only after the deposition of a completed part has also been studied, with contrasting results. Thanumoorthy et al. remelted the top surface of IN718 blocks (deposited at 400 W laser power) and observed a significant reduction in surface RS, from 666.7 MPa in the as-built state to between 107.7 and 217.1 MPa. Lower laser power coupled with higher scan speed resulted in greater RS reduction, with the best results obtained at 150 W laser power and a scan speed of 19 mm/s [44]. In contrast, Cho et al. deposited 316L samples at 800 W laser power and remelted the

top surface at various laser powers ranging from 600 to 1200 W. They found that remelted samples showed an increase in RS compared to as-built ones at measurement directions of 0° (145.6 to 201.7 MPa), 45° (124 to 132.3 MPa), and 90° (18.8 to 130.8 MPa) [144]. The as-built surface RS differed considerably between these studies, and the material (316L vs. IN718) and the remelting strategy also differ, which should be taken into account when comparing the outcomes.

As the studies above indicate, remelting alone cannot be classified as a process that is either beneficial or detrimental to the behaviour of RS in DED parts. The mechanisms behind it are more important to consider. If remelting passes, especially in the case of interlayer reheating, reduce the thermal gradient between deposited layers, the effect may be beneficial. However, if they only introduce an additional heating and cooling cycle without lowering the thermal gradient, the effect can be detrimental to the RS. Therefore, the initial stress state of the part, the material, and the build conditions need to be considered when selecting remelting parameters. Additionally, remelting has also been shown to reduce porosities, increase density and produce a finer microstructure, but it does come at the expense of increased processing time and extra energy input [18, 50, 145, 146].

4.4. Controlled cooling

Although the deposition phase shapes the initial thermal conditions, the cooling process is also significant in determining the thermal gradient and the evolution of RS within the material. Ideally, all deposited layers should have the same cooling rate in order to have uniform mechanical properties [132]. However, at constant laser power and absorption coefficient, heat dissipation slows as the number of layers increases in the DED process, resulting in higher peak temperatures and steeper thermal gradients. Because heat dissipation capacity typically drops compared to the capacity available at the substrate, various studies have explored active cooling strategies to exert more direct control over cooling rates. While RS reduction was not the primary focus of these works, their impact on cooling behaviour remains significant, given the strong correlation between cooling rate and RS formation.

Wu et al. utilised compressed CO_2 for interpass cooling in the WAAM process. They demonstrated that active cooling reduces both the peak temperature and the temperature variations. They demonstrated that active cooling reduces the peak temperature and the heat build-up. This lowered the post-build distortion of the substrate, with reported maximum reductions of 81% in longitudinal and 69% in transverse distortion. Additionally, a significant decrease in total build time was observed compared to no use of active cooling, because the rapid cooling after each layer shortened the interlayer dwell time that natural cooling requires [147]. In another study, Li et al. found that by implementing thermoelectric cooling in the WAAM process, there was a 56.8% reduction in bead width error, which led to more geometrically accurate parts [148]. Other active cooling strategies explored include the use of water-cooling tanks [149, 150], cooling the substrate with running water, and compressed air [151].

As observed, many of these strategies rely on gases or fans, which are primarily beneficial for wire-based DED processes rather than powder-based ones. Another more accessible approach for controlling the cooling rate is process parameter adjustment. Farshidianfar et al. used closed-loop control to maintain a stable cooling rate by gradually increasing the travel speed of each deposited layer [132]. Pixner et al. experimented with different scanning patterns and found that spacing out the deposition of individual beads, which allows for brief cooling between passes, led to improved geometric accuracy [152]. Additionally, interlayer dwell time adjustments, as discussed in Section 2.10, remain a widely used strategy for managing heat accumulation. These studies demonstrate that the cooling rate can be effectively controlled and that doing so improves geometric accuracy. However, further research is needed to fully understand the impact of cooling rate control on RS formation.

4.5. Ultrasonic vibration

In ultrasonic-assisted DED (UA-DED), an ultrasonic transducer is incorporated into a conventional DED system for the purpose of delivering vibration energy to the melt pool [153]. The ultrasonic device can transmit acoustic energy directly to the substrate, or it can be integrated into a moving ultrasonic vibration setup, where it moves in synchronisation with the heat source. In this case the ultrasonic probe can be in direct contact with the melt pool, or with the solidified deposit behind the melt pool [154]. When connected to the build plate, the setup is easy to implement; however, the intensity of the ultrasonic waves decreases as the build height increases. On the other hand, in the moving setup, there is a risk of contamination due to direct contact between the ultrasonic head and the deposited material [154]. Therefore, careful consideration must be given when selecting the appropriate configuration. Moving probes that do not contact the material (air-coupled) have also been implemented. This type of setup lowers the risk of contamination, but at the cost of a weaker ultrasonic effect, since air coupling transmits energy less effectively than direct contact [155].

The addition of ultrasonic waves has been shown to significantly impact melt pool flow, solidification behaviour, and defect development [153, 156, 157]. As the acoustic waves create alternating high and low pressure phases in the melt pool, bubbles form, expand, compress, and eventually collapse at high speeds [156]. The collapse of these bubbles causes the refinement of the coarse primary dendrites, creating a more refined microstructure [73, 154, 156]. The acoustic flow also affects the solidification process by enhancing the internal flow of the melt, which homogenises both the temperature field and the solute distribution. This results in reduced thermal gradients and a more uniform microstructure [156]. An additional effect occurs after solidification, with recrystallisation. The ultrasonic impact increases the range of dislocation movement, promoting their merging and annihilation, which can contribute to a reduction in RS [156, 158].

Li et al. applied non-contact ultrasonic vibration (20 kHz, 40 µm) to deposit Fe-Cr-B powder on 42CrMoA steel [155]. The transmitter was mounted on a robotic arm, moved with the laser head, and was placed 50, 80 or 110 mm from the melt pool. Residual stress was measured by portable X-ray diffraction on the substrate surface, but only to validate a thermo-mechanical finite element model. The simulation predicted lower peak tensile stress with ultrasound (down 45.6% at 80 mm), a smoother stress gradient near the interface, a more uniform temperature field and a slower cooling rate. The authors link the lower stress to these thermal changes. The lowest simulated peak stress occurred at 50 mm, but 80 mm gave the best overall result because it avoided the pores seen at 50 mm and the microcrack seen at 110 mm [155]. In another study by Diao et al., ER321 austenitic stainless steel was deposited using WAAM and ultrasonic impact. The introduction of ultrasonic waves caused a reduction in dislocation density. Because dislocations are sources of local lattice distortion, this suggests a reduction in localised stress fields and hence in RS [156]. The authors do not specify which RS type is affected, but since the evidence is microstructural, the reduction is more plausibly type II and type III than type I.

While not using ultrasonic vibrations, Imširović et al. had some valuable findings related to vibrations and RS. Using an electromagnetic vibration system, they introduced in-situ subsonic waves while producing thin-wall samples and found that adding vibrations resulted in a more uniform RS distribution. The deviation of stresses in different directions was significantly reduced, with anisotropic RS distribution decreasing by 60% [159]. These studies suggest that ultrasonic vibrations, and potentially other types of vibrations, can have a positive effect on reducing RS while also improving microstructure and mechanical performance [24, 153, 157]. However, further investigation is needed to fully understand the underlying mechanisms.

4.6. Build-plate stiffness

Another factor that is not often discussed in regard to RS formation in AM is the yield ability of the substrate. When material is allowed to expand and contract freely due to thermal cycles, no RS should be generated in the piece. In AM, however, the substrate acts as a constraint that can significantly affect RS formation. Studies have examined substrate modification to manage such mechanical constraints as a means of mitigating RS and cracking. For instance, Lu et al. investigated the effect of adding grooves to the substrate in parts produced with LPBF. Figure 21 illustrates how these grooves enable substrate expansion during heating and facilitate stress recovery during cooling by reducing resistance to deformation. This results in lower tensile RS at the end of the process, which can also assist in minimising cracks [160]. They report that this substrate structure reduces RS by 50%. In a later study, they performed similar experiments with the DED process and explained that the aim is to reduce the local stiffness of the top half of the substrate mechanically. This process allows metal strains to form more fully and hence reduces RS. This, however, comes at the expense of a slight loss in geometric precision [161]. In another study, Jing et al. attempted to reduce the stiffness of the substrate by incorporating long holes or support legs in the substrate. They found that these adjustments allowed for greater strain relaxation, which led to a reduction in RS [162].

These studies demonstrate that a change in substrate stiffness will minimise the creation of RS in the material. This is particularly useful for depositing large parts, as they usually require thicker, less ductile substrates, which can lead to stress concentration around the substrate [163]. Adding grooves, holes, or support legs will increase the flexibility of the substrate, therefore contributing to the reduction of RS.

4.7. Rolling

Rolling-assisted AM is another technique being explored as a means to reduce RS in AM material. It works by compressing the surface in contact with rollers, causing plastic deformation and grain refinement as well as introducing compressive stresses [164]. These compressive stresses counteract the tensile stresses that develop during the deposition process. The final RS profile results from the interaction between these two forces [165]. Rolling is

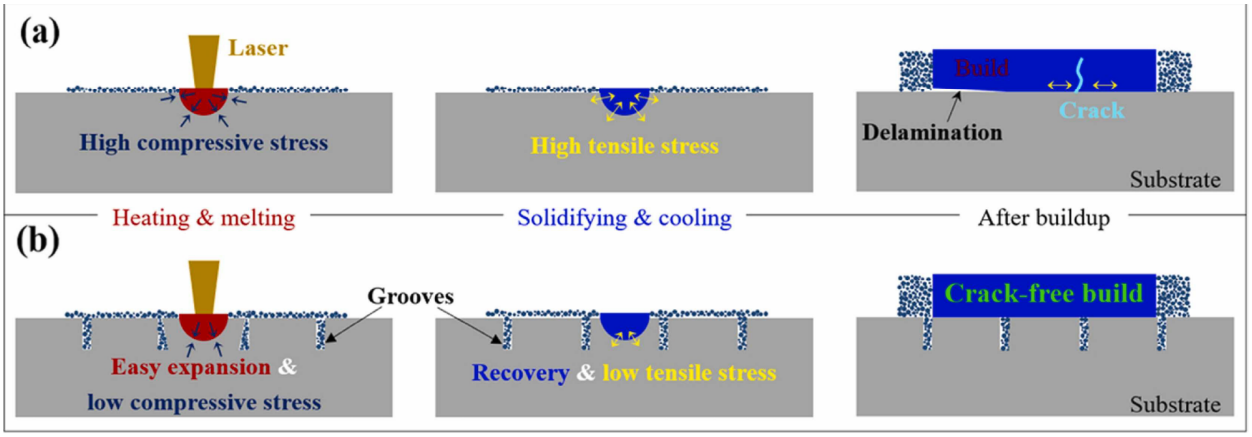


Figure 21: Formation of RS and cracks without (a) and with substrate grooves (b). Adapted from [161], with permission from Taylor & Francis.

predominantly used in the WAAM process and can be integrated in several ways. One approach is in-situ rolling, where a roller follows the energy source during deposition, applying deformation while the material remains hot, sometimes also referred to as hot rolling. Alternatively, inter-pass rolling is conducted at the end of each deposited layer. Lastly, post-process rolling is performed after the entire part has been deposited [154]. There have also been different approaches regarding the direction of rolling and the design of the roller profiles [166].

The first study to implement in-situ rolling was done by Zhang et al. In this study, as the energy source advanced, a micro-roller followed it continuously, deforming the surface while still hot. This resulted in a flatter deposition surface rather than a domed one, which offered several benefits, such as more uniform layer thickness, reduced material waste due to less material flowing to the sides, and improved ease of depositing subsequent layers. The ability to control deposition layer thickness is particularly advantageous for enhancing dimensional accuracy and addressing the common issue of disparity between the theoretical and actual deposition heights. They also conclude that in-situ rolled parts tend to exhibit a more compact microstructure with finer grains and increased tensile strength [167]. Regarding the effects on RS and distortion, Colegrove et al. carried out a study investigating various rolling-assisted configurations, including in-situ rolling of a low-carbon steel. They utilised a profiled roller featuring a grooved surface designed to match the domed shape of the deposited bead. It applied deformation to the freshly deposited material at a distance of 130 mm behind the welding torch. The specimens were rigidly clamped during the deposition and rolling processes to constrain deformation. After completing the final layer, the clamps were released, allowing RS to redistribute and induce measurable out-of-plane distortion. Interestingly, their findings indicated that in-situ rolling had no effect on the distortion of the samples. However, as seen in Figure 22, this technique led to a decrease of RS in the longitudinal and transverse direction while simultaneously increasing stress in the normal direction [168]. The same study investigated inter-pass rolling using both a profiled roller, as described above, and a slotted roller incorporating a deep (10 mm) longitudinal slot that physically constrained lateral material flow. The experiments demonstrated that the slotted roller provided a more effective reduction in RS and distortion when compared to rollers with no lateral restraints. However, in both cases, a significant reduction in peak RS was observed in the longitudinal direction [168]. The same authors investigated the interpass rolling for deposited titanium wire, yielding similar results. Interpass rolling with a profiled roller significantly reduced the peak tensile stress at the interface between the baseplate and the deposit, while also inducing substantial compressive stress near the top of the deposit [169, 170].

Conversely, when Honnige et al. investigated the effects of interpass rolling on Ti-6Al-4V they found that although rolling had a positive impact on the material texture, it had no significant effect on the RS [171]. However, when applying interpass rolling to IN718 deposits, they observed a notable reduction in RS and part distortion [172]. They also experimented on aluminium deposits and found that using high loads while interpass rolling generated significant compressive stresses, while lower loads had little impact. Additionally, they investigated post-deposition side-rolling and found it very effective for controlling RS and distortion [165].

The variability in interpass rolling outcomes can be attributed to the fact that while rollers do effectively mitigate RS near the surface, the subsequent deposition layer will recreate some of these stresses [168]. Therefore, the final RS

profile will be dependent on the balance between the relieved RS and the newly generated ones in the subsequent layer, which can be dependent on many factors such as material properties, applied load and process parameters [165, 168]. It is worth noting that rolling has also been incorporated in powder DED; however, to the best of our knowledge, there has not been a discussion on its effects on RS in the produced parts [173, 174].

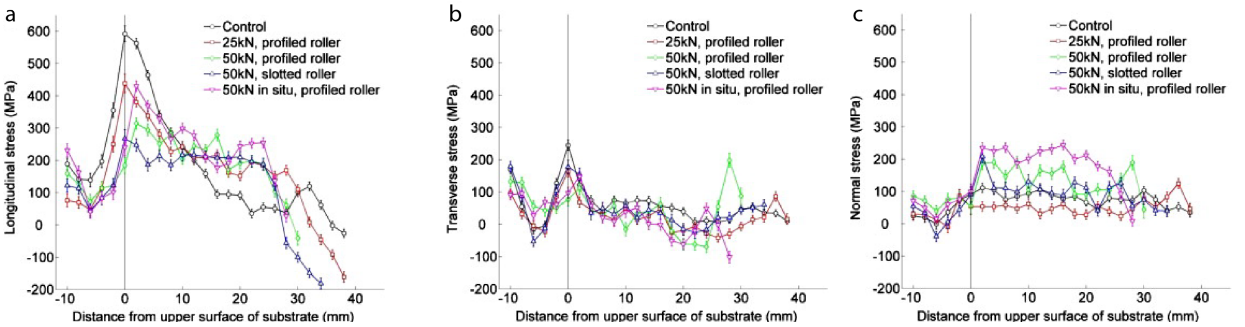


Figure 22: a) Longitudinal, (b) transverse and (c) normal RS vs. distance from the top of the baseplate. Diffraction peak-fitting error is indicated to one standard deviation. Adapted from [168], with permission from Elsevier.

Finally, although these methods can be effective in reducing RS, they do come with some difficulties. For instance, in in-situ rolling, the distance between the heat source and roller should be accurately calculated for rolling to occur at the desired temperature. This can be especially challenging in higher layers, as heat accumulation causes a different cooling rate than the initial layers. The rolling force should also be carefully considered to control the depth of the recrystallised zone and preserve a flat layer surface [166, 167].

4.8. Summary

These in-situ RS reduction techniques all offer varying degrees of success and have varying levels of complexity. Preheating the build plate or substrate is one simple and effective way of reducing stresses; however, it can be both expensive and time-consuming to apply, especially in larger components. In this context, localised preheating shows to be a promising substitute, but further studies are needed to evaluate its effect on different materials. Feedback control is another valuable method, as it gives the ability to manage a wide range of DED parameters. Although it has not been extensively explored for RS reduction, it shows significant potential in this regard. Cooling rate control, through either active cooling or process parameter adjustment, can also improve geometric accuracy, although its direct effect on RS formation still requires further research. A summary of all in-situ RS reduction techniques is presented in Table 4.

Table 3. In-situ mitigation methods of RS.

Parameter	Adjustment for lower RS	Range of Values / Technique	Mechanism	Material
Feedback Control	Minimised thermal input		Controlling energy fluence and layer height by adjusting PFR, laser power and scanning speed.	316L [123]
Build-plate preheating	Elevated build plate temperature	100 - 500°C	Reduction of thermal gradient between build plate and deposit.	M4 steel [138] IN625 [79] 316L and Ferro 5 steel [139]
Localised preheating	Stress relief and redistribution except in [142, 144]	Heating with induction coil or rescanning with laser	Higher temperatures reduce thermal gradients and encourage stress relief.	Ti-6Al-4V [142] 316L [50, 144] IN718 [44]
Controlled cooling	Reducing peak temperatures and enhancing heat dissipation (potentially)	CO_2 gas cooling [147] Thermoelectric cooling [148] Water-cooling tanks [149, 150] Compressed air [151] Closed loop control of travel speed [132] different scanning patterns [152]	Reduction of heat build-up and temperature variations.	Ti-6Al-4V [147] 2325 Al alloy [148] Structural steel [149] Mild steel [150] IN718 [151] 316L [132]
Ultrasonic vibration	Introduction of ultrasonic vibration	Vibration frequency: 20-25 kHz Ultrasonic power: 40-1000 W	Creates a more homogenous thermal gradient by affecting melt pool dynamics and solidification behaviour	ER321 austenitic SS [156]
Build plate stiffness	Lower stiffness	Adding grooves [160, 161] [LPBF] Holes or support legs [162]	Reducing stiffness enables expansion during heating and aids stress relief during cooling by reducing deformation resistance.	Ti-6Al-4V [160–162]
Deformation (Rolling)	Application of rolling, with results varying by material and rolling direction	Different roller geometries and pressures	Compressive stresses induced by the rollers counteract the surface tensile stresses.	Low-carbon steel [168] Ti-6Al-4V [170] Ti-6Al-4V [165] Titanium wire [169] IN718 [172] Aluminium [165]

5. Post-process RS reduction

Despite the efforts to minimise RS during the deposition process in DED, some amount of RS is certain to be present in the developed parts. Therefore, it is beneficial to also explore post-processing techniques to further reduce RS and improve part performance.

5.1. Heat treatment

Heat treatment is commonly used in conventionally manufactured materials to improve mechanical properties and modify microstructure. It consists of controlled heating and cooling of the material, which can be done using various approaches depending on the material and desired outcomes. One of these treatments is solution treatment, which usually involves high temperatures to cause compounds to enter solid solutions, followed by rapid cooling to maintain solution properties [84]. Although not directly used to alleviate RS, some studies have demonstrated the positive impact of this process on reducing RS. Another popular treatment is stress relieving, which is specifically designed to mitigate RS [24].

Due to rapid solidification and steep thermal gradients, as-built DED parts usually exhibit columnar grains and a high dislocation density [23, 49, 175, 176]. Applying post-process heat treatments, such as stress relieving, can have an impact on this microstructure and reduce dislocation density. Stress relieving involves heating the material to a temperature below its critical temperature, holding it until the temperature is uniform throughout, and then cooling it slowly to room temperature [177]. However, this exposure time at elevated temperatures should be kept short if recrystallisation and grain growth are not desired [5]. Given the material-dependent nature and the variety of heat treatment methods, a detailed review falls beyond the scope of this article [89]. In this section, we provide a concise overview of recent research on the application of heat treatments in DED-fabricated components that have led to a reduction in RS. For clarity, the results are categorised based on the materials used in the studies.

For IN718, Jinoop et al. conducted two solution treatments on laser additive manufactured samples at 950°C and 1050°C for 1 h, followed by water quenching, which induced compressive stresses in the material. They reported a 17.5% and 50% reduction in RS for the respective treatments [84]. In another study on DED IN718 bars, Careri et al. compared three post-processing routes: machining only, heat treatment followed by machining, and machining followed by double ageing. Machining followed by double ageing gave the lowest RS together with high hardness [178]. Double ageing consisted of heating the samples at 718°C for 8 h, cooling to and holding at 621°C for another 8 h before finally air-cooling to room temperature. While the machined-only surfaces showed high tensile RS (up to about 1.4 GPa), the surface RS after double ageing was close to zero or slightly compressive. The hardness increase was attributed to the formation of strengthening phases [178]. Honnige et al. used a combination of the above methods by combining solution treatment at 970–980°C, followed by ageing treatment as mentioned above. As shown in Figure 23, they reported a significant reduction in RS, especially in the longitudinal direction [172].

Similarly, for Inconel 625, Mohsin Khan et al. employed a two-step heat treatment process involving an initial solution treatment at 1150°C for 2 h, followed by water quenching, and further ageing at 700°C for 24 h, followed by final water quenching. This thermal treatment resulted in a significant decrease in RS compared to as-deposited samples. This decrease was linked to microstructural changes involving recrystallisation of the original columnar dendritic microstructure into equiaxed grains and dissolution of the brittle Laves phases [79]. Paranthaman et al. also report similar results, stating that stress relief at 870-980°C helped alleviate RS [176]. Jinoop et al. investigated Hastelloy-X samples with results presented in Figure 24. They subjected the prepared DED samples to heat-treatment at 1177°C for 2 h, followed by water quenching. They measured RS using XRD and found that this heat treatment reversed the tensile RS into compressive RS and attributed this effect to the induction of compressive stresses during the water quenching phase [179].

As for 316L, Li et al. investigated the effects of different heat treatment temperatures on the microstructure, tensile properties, and RS. However, for RS analysis, they only compare the heat treatment at 400°C with the as-built samples, because higher temperatures lead to surface oxidation, which affects RS but also reduces the area of actual load bearing. They found that heat treatment at 400°C for 2 h followed by air cooling reduced the RS by 53.7% without significantly compromising yield strength or ultimate tensile strength and with a slight increase in ductility [95]. In another study, Aversa et al. implemented a heat treatment at 600°C and noticed a partial RS reduction while maintaining mechanical properties. The heat treatment at 800°C, however, led to an almost complete mitigation of RS but with 20% reduction in yield strength. The authors concluded that heat treatment at 800°C would be more beneficial for complex parts where RS could significantly impact the geometry, whereas for applications requiring high strength, the 600°C heat

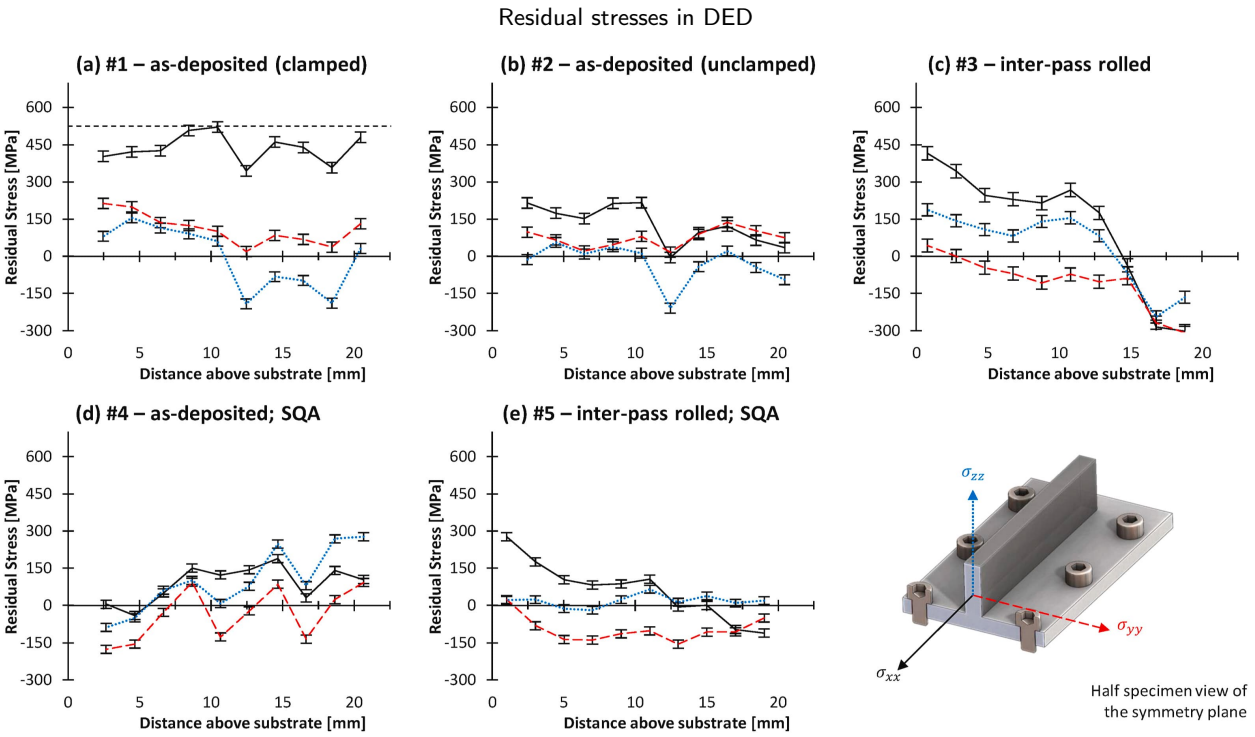


Figure 23: Calculated RS in the three principal directions in the deposit of (a) the as-deposited control specimen before and (b) after unclamping; (c) the inter-pass rolled specimen; (d) and (e) the solution treated, quenched and aged version of (b) and (c). The horizontal dashed line in (a) indicates the longitudinal yield strength. Reproduced from [172], with permission from Elsevier.

treatment would be a more suitable choice [69]. Vinoth et al. used a different approach. In one case, they conducted a stress relief treatment by heating the samples to 600°C for 2 h, followed by furnace cooling. In the second approach, they performed a solution treatment by heating the samples to 1000°C for 2 h, followed by water quenching. The stress-relieved samples exhibited coarser equiaxed grains, texture relaxation, and reduced anisotropy. In contrast, the solution-treated samples showed more pronounced microstructural evolution, including significant grain refinement due to rapid quenching, resulting in highly equiaxed grains with diminished texture anisotropy. The solution-treated samples also demonstrated superior ductility and more uniform hardness distribution, suggesting effective mitigation of stress concentration and more homogeneous stress relaxation. While RS levels were inferred indirectly through these microstructural and mechanical property changes rather than quantified experimentally, the results indicate that the solution treatment provided optimal stress relief while enhancing overall material performance.

Other studies have examined the impact of heat treatment on Scalmalloy and FeCrCoMnNi alloys, with the result that effective heat treatment can help mitigate RS. For Scalmalloy, low-temperature heat treatments were effective in lowering RS without degrading mechanical properties; however, at high temperatures, the authors noticed an increase in RS [180]. For FeCrCoMnNi, heat treatment at 700°C and 1100°C relaxed the tensile RS and improved ductility, while the Ultimate tensile strength stayed about the same and the yield stress dropped slightly due to grain coarsening [46].

Overall, post-process heat treatments clearly play an important role in reducing RS in DED components. Depending on the material and the specific treatment, techniques like stress relieving, solution treatment, and ageing can convert tensile stresses into compressive ones, reduce dislocation density, and, in some cases improve mechanical properties. While the choice of temperature and duration needs to be carefully balanced to avoid unwanted grain growth or strength loss, the studies discussed here show that well-designed heat treatments can effectively manage RS and enhance part performance.

5.2. Peening methods

As one of the most popular surface treatment processes in manufacturing, shot peening finds applications in numerous industries [25, 181]. Typically, it is used as a post-process treatment; however, given the unique nature

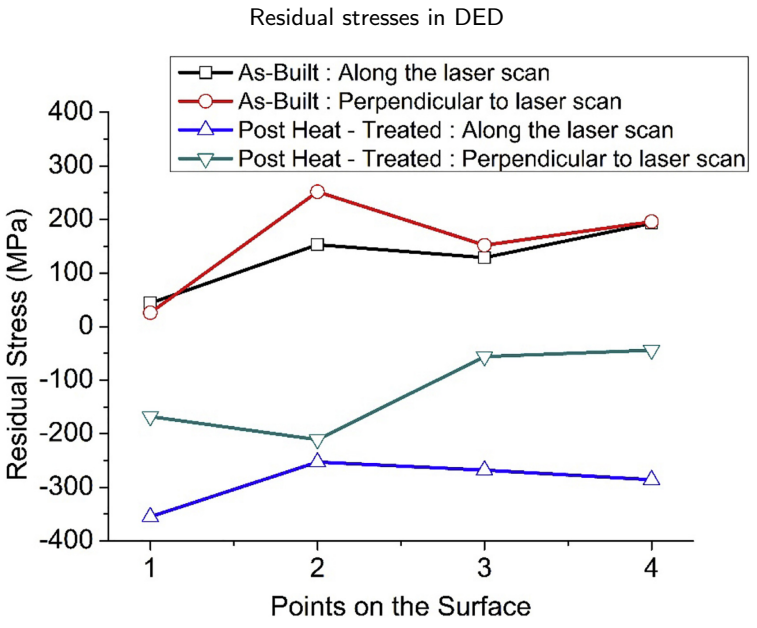


Figure 24: Residual stress on as-built and heat-treated Hastelloy-X samples measured using XRD. Reproduced from [179], with permission from Elsevier.

of AM, in addition to exploring it as a post-process treatment, recent studies have also explored the use of this method between deposited layers. This approach aims to determine whether the favourable effects of shot peening can extend beyond surface enhancement to improve bulk material properties [18]. The primary goal of shot peening is to apply a protective layer of compressive stress on the surface of fabricated parts to avoid or delay crack initiation and propagation [74, 181]. This compressive stress layer can be applied in several ways, the most common ways being mechanical shot peening, laser shock peening, and ultrasonic peening [3].

5.2.1. Mechanical shot peening

In mechanical shot peening, often simply referred to as shot peening (SP), sand or metallic spheres are blasted onto the surface of the material using compressed air [25, 182]. This high-velocity impact induces local plastic deformation at the impact surface, which causes strain hardening and compressive RS in the near-surface region of the material. [18, 25]. Zhang et al. investigated a hybrid process using a Fe-Cr-Ni-B-Si alloy, where SP was performed on the surface of the deposited material after each layer of DED. Their results showed that in the hybrid sample, the surface stresses were compressive, while in the DED sample, the surface stresses were found to be tensile [183]. Mithal et al. utilised a similar approach using 316L but came to a different conclusion. In their study, they determined that the compressive RS induced by peening were completely relieved due to the deposition of subsequent layers [15]. In addition to the difference in material, several other key distinctions likely contributed to these contradicting outcomes. Zhang et al. performed SP after each layer and while the surface had not yet cooled down, whereas Mithal et al. applied SP only after every 10 layers and once the part had cooled to room temperature [15, 183]. Moreover, the nominal layer height in the study by Mithal et al. was approximately 1 mm, compared to 0.2 mm in Zhang et al.'s study, further reducing the effectiveness of SP due to a limited penetration depth of around 0.1–0.8 mm.

In general, SP is considered to be the most affordable and efficient peening technique since other techniques, such as ultrasonic peening and laser shock peening, often require a redesign of the AM system and also involve the cost of additional expensive equipment, such as powerful lasers [25]. However, SP does tend to be less effective than other treatments because of lower penetration depth and comparatively lower magnitude of induced compressive RS [25].

5.2.2. Laser shock peening

The most widely adopted peening method in AM is laser shock peening (LSP). Like conventional SP, LSP introduces compressive RS, but it replaces physical media with high-power pulsed laser-generated shock waves [6]. A brief, high-intensity laser pulse creates plasma within the confined space, resulting in pressure waves that induce localised plastic deformation [184]. An ablative layer is typically applied to minimise thermal effects, ensuring that

the surface experiences only the mechanical shock wave generated by the plasma [18, 154]. A transparent confining medium, such as water, is also often used to enhance the pressure exerted on the surface [184].

As mentioned above LSP can be applied as a post-process treatment or between deposited layers. Most DED studies focus on the addition of LSP after deposition has been completed. Sun et al., for example, deposited a 2319 aluminium wall by WAAM. LSP was done on both sides of the printed wall with a pulse energy of 15 J, duration of 15 ns, and 4 mm circular spot size at 50% overlap. The RS was measured on the top and middle of the wall. Both areas showed a transformation of tensile to compressive RS [185]. Another study by the same team investigated the effects of LSP on Ti-6Al-4V thin walls produced by DED. The LSP samples showed a compressive stress of around 200 MPa compared to the 100 MPa tensile stress of untreated samples. The affected depth was measured to be around 0.7 mm, and a refinement of microstructure in the surface layer was noticed [186]. Many other studies have been conducted on this and other titanium alloys produced by various DED processes with similar results. As expected, all studies reported compressive RS in the surface and sub-surface layers of LSP-treated samples. The maximum compressive RS was around 200-700 MPa, depending on the material and LSP parameters. This high range of compressive stress can be attributed to different DED processes, different XRD measurement techniques and most importantly, different LSP parameters [187–191]. For example, An et al. experimented with TC17 and reported a compressive RS of 240 MPA with a laser energy of 5 J and 20 ns pulse duration, while Chi et al. experimented with Ti17 and recorded 740 MPa of compressive RS when using a 20 J laser energy at 15 ns pulse duration [190, 191].

In a study on 316L, Mithal et al. demonstrated the importance of an ablative coating. They showed that under the same pulse energy of 10 J, spot size of 3 mm, and pulse width of 18 ns, the sample with no coating failed to demonstrate compressive RS while the sample with an ablative coating showed a value 480 MPa compressive RS. Even changing the spot size to 2 mm, which causes a 10 times increase in power density, could not cause compressive RS to form on the surface of the sample. They attributed this to the fact that the absence of an ablative layer creates a thin layer of tensile RS due to thermal effects [192]. Similar results were obtained when using other materials such as steel [181] and aluminium [193] welding wires.

Compared to post-process LSP, few studies have examined the effects of layer-by-layer LSP applied during the build. The first study to address this gap was conducted by Sealy et al.. They used 420 stainless steel powder to deposit 85-layer cylinders using the laser engineered net shaping process, which is a subset of DED. LSP was applied every 5 layers (with peening performed outside the printing machine, using ablative and confining layers) using a 1064 nm Nd:YAG laser with a pulse energy of 700 mJ, a pulse duration of 8 ns, and a spot diameter of 1 mm. The authors reported that interlayer LSP introduced compressive RS up to 400 MPa in the build direction, along with a secondary compressive RS region 1 mm below the surface, demonstrating that thermal effects from subsequent layers did not fully cancel prior LSP benefits. However, they highlighted thermal cancellation as a key challenge, where heat from deposition partially relaxed compressive RS, especially at higher laser powers due to deeper thermal penetration [194].

In another study, Lu et al. deposited a total of three 1 mm-thick Ti-6Al-4V layers via DED, applying LSP (7.6 J, 3 mm spot size, 10 ns pulse duration,a dn 5 Hz frequency) after the first and second layers but not the final layer. Their results showed compressive RS extending 0.8 mm deep, with higher compressive RS levels achieved through multiple LSP coverage layers. Notably, the final deposited layer didn't erase prior LSP effects, as re-melting only penetrated at a depth of 0.3 mm, preserving the deeper compressive stress zone [36].

Using a different approach, Zhou et al. compared final surface LSP (SLSP) and layer-by-layer LSP (LLSP) treatments integrated into a hybrid DED system without the use of an ablative or confining layer. In their setup, a pulsed LSP laser with pulse width of 20 ns and 25 mJ pulse energy (0.4 mm laser spot diameter) followed the deposition laser at a fixed offset of 5 mm. Figure 25 illustrates the RS profile for all conditions up to a depth of 2.5 mm. Both SLSP and LLSP introduced compressive RS near the surface, extending to approximately 0.5 mm and 0.75 mm, respectively. Below this depth, while stresses became tensile, the LLSP sample maintained significantly reduced tensile stresses compared to untreated and SLSP samples throughout the measured 2.5 mm depth [195]. These findings are notable because even with the absence of ablative and confining layers, which could not have been applied due to their reduction of process efficiency, a measurable depth effect was achieved [166, 195].

5.2.3. Ultrasonic peening

Ultrasonic peening (UP), also known as ultrasonic impact treatment, uses an electromechanical transducer to apply high-frequency ultrasonic energy and induce plastic deformation and compressive RS to the material's surface [18, 196]. In a study by Yang et al., Ti-6Al-4V powder was deposited via WAAM in two geometries: a single-layer deposit and a seven-layer stack. Each deposited layer underwent two UP passes, and control samples were left untreated.

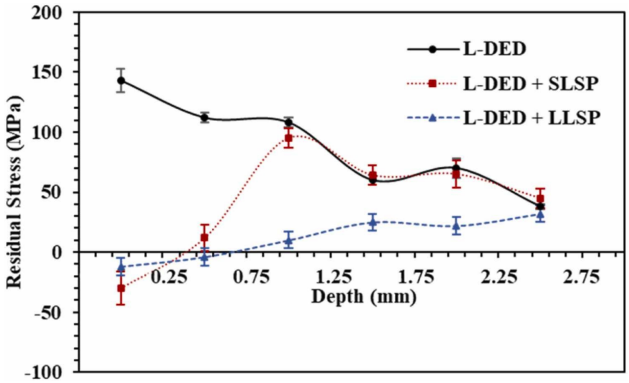


Figure 25: Residual stress distribution of DED, surface Laser shot peened and layer-by-layer laser shot peened samples. Adapted from [195], with permission from Elsevier.

While the untreated seven-layer sample exhibited significantly higher RS than its single-layer counterpart, UP treatment brought the RS in both geometries to nearly identical levels. This finding strongly suggests that UP effectively mitigates RS accumulation across successive layers [197]. In another work, Wang and Shi investigated the effects of UP on a nickel-based superalloy produced by LMD. They found that UP significantly reduced horizontal RS and transformed vertical RS from tensile to compressive [198]. In a more recent study by Zhang et al., GH4169 superalloy powder was deposited, and UP was applied to the deposited layers during the process. Both transverse and longitudinal RS were transformed to compressive stresses ranging from 200 MPa to 900 MPa [199]. Even the application of UP after every four layers, rather than every layer, was shown to lead to a considerable reduction in RS in both directions [200].

Although the extent of complexity, cost, and results heavily depend on the material and varying conditions [181], the significant number of studies on peening strategies for reducing RS reflects its widespread acceptance as an effective method for reducing or transforming RS, even in the emerging field of AM. Their relatively low cost and simple application, especially for mechanical and ultrasonic peening, have led to their popular adoption. However, there always needs to be a balance between minimizing the RS without impacting the microstructure that improves the other mechanical properties.

6. Conclusion

RS in produced parts are not a problem to be entirely solved or eliminated, they are a natural consequence of manufacturing processes. The optimal approach is to understand the mechanisms behind them and, based on that, try to control these stresses. This is especially true in AM, where many of these mechanisms operate simultaneously and have a significant impact on one another. The next step is the implementation of this knowledge in a step by step approach. Prior to starting the fabrication process, the process parameters must be chosen carefully. For laser power, lower values appear to be the obvious choice, especially when smaller beam diameters and thinner layers are involved. However, the literature does not support a single, universal relationship. With larger beam diameters and thicker layers, lower RS has been observed over part of the power range, attributed either to a lower cooling rate or to heat accumulation that allows partial stress relaxation. As for scanning speed, higher values are generally associated with preferable outcomes. The choice of scanning strategy has one of the most influential impacts on RS, with segmented paths and rotation between layers being more favourable. Island and segmented strategies divide the deposit into smaller sections and limit heat accumulation, while rotation between layers prevents stress build-up along a single direction. Introducing a pause between layers can also reduce heat accumulation and potentially RS, but it can increase the thermal gradient during the next layer, promote lack of fusion pores, and extend the build time, which may not be economically viable. Its effectiveness also depends strongly on the material and the dwell time. Finally, pulsed-wave laser mode has been shown to reduce RS by promoting cyclic thermal stress, enhancing localised remelting, and minimising thermal gradients.

Although it is relatively simpler to investigate the effects of process parameters individually, this approach does not give a global view and can often show seemingly contradictory results. Process parameters can also be highly material dependent, as is the case for parameters such as interlayer dwell time. Therefore, To have a more comprehensive view, parameters such as energy density and normalized enthalpy are useful to examine. Energy density is easily calculated

and offers a quick initial means of comparing the effects of different parameter changes simultaneously. The general trend indicates that an increase in energy density is accompanied by an increase in RS. However, energy density does not account for intrinsic material-dependent characteristics, which is why the normalized enthalpy metric has been proposed to include them. Although the introduction of this metric in DED is quite recent and its relevance to RS is yet to be established. More broadly, the interactions between parameters and their dependence on the material are not always sufficiently taken into account in the literature. Future studies should therefore pay closer attention to the intrinsic material properties and the laser-material interactions.

Even with well-chosen process parameters, there is a limit to how much RS can be controlled through process parameters alone. This is where hybrid technologies have significant potential. Combining DED with processes such as interlayer machining, interlayer rolling or peening, laser remelting, in-situ heating, or the addition of ultrasonic vibrations can impact the produced RS directly rather than only limiting their formation. Because these processes are applied during fabrication, they can modify the thermal history, relax stresses, or introduce compressive stresses layer by layer, instead of correcting the part after it is built. Their effect is not always beneficial, however, and depends on the mechanism involved. Remelting reduces RS only if it lowers the thermal gradient between layers. If it merely adds a heating and cooling cycle, it can raise them. It can also reduce porosity and refine the microstructure, but at the cost of longer processing time and extra energy input. Substrate preheating has shown to reduce cracking, but high preheating temperatures have been linked to lower strength and toughness, material segregation, and microstructure coarsening. Ultrasonic vibrations appear to reduce RS while improving microstructure and mechanical performance, although the underlying mechanisms still need to be clarified. Lowering the stiffness of the substrate, for example with grooves, holes, or support legs, can also reduce RS. This is particularly useful for large parts, which usually require thicker, less ductile substrates that cause stress concentration. These in-situ methods are also accompanied by practical difficulties. In in-situ rolling, for instance, the distance between the heat source and the roller must be calculated accurately so that rolling occurs at the desired temperature. This is harder in upper layers, where heat accumulation changes the cooling rate, and the rolling force must be controlled to preserve a flat layer surface.

Feedback control can make these processes more reliable. By using in-situ measurements of temperature, melt pool size, or layer height to adjust the process parameters or trigger the hybrid steps during the build, the process can respond to deviations as they occur instead of relying on fixed settings chosen beforehand. RS were not explicitly measured in the closed-loop control studies reviewed, but these studies offer a useful foundation, since they control the thermal gradients and cooling rates on which RS depend. Closed-loop control that gradually increased the travel speed of each layer kept the cooling rate stable, and spacing out the deposition of individual beads improved geometrical accuracy. Controlling the cooling rate therefore appears to improve geometrical accuracy, but its effect on RS still needs further research.

As a final step, post-process treatments are effective at reducing the RS induced during the AM process. The choice of treatment depends on whether the whole part needs to be treated, as with heat treatment, or only its surface, as with shot peening. Depending on the material, heat treatments such as stress relieving, solution treatment, and ageing can reduce RS and, in some cases, improve mechanical properties, as long as temperature and duration are balanced to avoid grain growth and loss of strength. Among the peening techniques, mechanical shot peening is generally the most affordable and efficient, since ultrasonic peening and laser shock peening often require a redesign of the AM system and expensive equipment. however, Laser shock peening can be integrated into a hybrid DED process. In this setup, the ablative and confining layers normally used in laser shock peening are not utilised; nevertheless, both final-surface treatment and layer-by-layer treatment introduce compressive RS near the surface. Below this zone the stresses become tensile, but layer-by-layer treatment keeps them lower than final-surface treatment or no treatment overall. The large number of studies on peening reflects its acceptance as an effective method for reducing or transforming RS, although the results depend on the material and conditions. While being very effective at RS reduction, post-process methods generally add cost to the overall production chain, whether through the additional time required to produce a part or the cost of the treatment itself. Where possible, RS should therefore be mitigated during the process, with post-process treatments reserved for cases where this is not sufficient.

The extensive body of experimental work on DED reviewed here, shows that RS remain a serious and persistent issue. The large variations in results, and in the interpretation of the mechanisms involved when changing each parameter, also suggest that experimental studies alone may not be enough to fully understand the complex interactions taking place during the process. Some of these parameters are also difficult to measure experimentally, such as the temperature field and cooling rates inside the part, the melt pool flow, the heat lost through convection, and the energy actually absorbed by the workpiece. Simulations, of course with experimental validation, are therefore very important.

They make it possible to change one parameter at a time while keeping the others fixed, which is hard to do in practice, and they give access to quantities that cannot be measured directly. They would also help with the normalized enthalpy calculations, for example by providing realistic values of η and by accounting for the melt pool flow and convection that the equation neglects.

In summary, this article set out to provide an overview of the existing literature, highlight the gaps, and outline best practices. Along the way, it compiled data from many studies, calculated energy density and grouped it by material. It also examined absorptance efficiency and normalized enthalpy, which are rarely discussed in RS reviews. In conclusion, this review has shown that, although the RS problem is complex, a stepwise approach makes it manageable.

References

[1] Mikell P Groover. *Fundamentals of modern manufacturing: materials, processes, and systems*. John Wiley & Sons, 2010.

[2] N.S. Rossini, M. Dassisti, K.Y. Benyounis, and A.G. Olabi. Methods of measuring residual stresses in components. *Materials & Design*, 35:572–588, March 2012.

[3] Shu-guang Chen, Han-jun Gao, Yi-du Zhang, Qiong Wu, Zi-han Gao, and Xin Zhou. Review on residual stresses in metal additive manufacturing: formation mechanisms, parameter dependencies, prediction and control approaches. *Journal of Materials Research and Technology*, 17:2950–2974, March 2022.

[4] P.J. Withers and H.K.D.H. Bhadeshia. Residual stress. Part 2 – Nature and origins. *Materials Science and Technology*, 17(4):366–375, April 2001.

[5] C. Li, Z.Y. Liu, X.Y. Fang, and Y.B. Guo. Residual Stress in Metal Additive Manufacturing. *Procedia CIRP*, 71:348–353, 2018.

[6] Nabin Bastola, Muhammad P. Jahan, Nithin Rangasamy, and Chandra Sekhar Rakurty. A Review of the Residual Stress Generation in Metal Additive Manufacturing: Analysis of Cause, Measurement, Effects, and Prevention. *Micromachines*, 14(7):1480, July 2023.

[7] R. Acevedo, P. Sedlak, R. Kolman, and M. Fredel. Residual stress analysis of additive manufacturing of metallic parts using ultrasonic waves: State of the art review. *Journal of Materials Research and Technology*, 9(4):9457–9477, July 2020.

[8] Xi Zou, Zhou Yan, Ke Zou, Shuai Gang Zhang, Wenyang Liu, and Lijun Song. Residual stress control of 316L stainless steel using pulsed-wave laser additive manufacturing. *Optics & Laser Technology*, 150:107910, June 2022.

[9] Kevin Carpenter and Ali Tabei. On Residual Stress Development, Prevention, and Compensation in Metal Additive Manufacturing. *Materials*, 13(2):255, January 2020.

[10] Amanda S. Wu, Donald W. Brown, Mukul Kumar, Gilbert F. Gallegos, and Wayne E. King. An Experimental Investigation into Additive Manufacturing-Induced Residual Stresses in 316L Stainless Steel. *Metallurgical and Materials Transactions A*, 45(13):6260–6270, September 2014.

[11] P.J. Withers, M. Turski, L. Edwards, P.J. Bouchard, and D.J. Buttle. Recent advances in residual stress measurement. *International Journal of Pressure Vessels and Piping*, 85(3):118–127, March 2008.

[12] Manping Cheng, Xi Zou, Yang Pan, Yan Zhou, Wenyang Liu, and Lijun Song. Residual Stress Control Using Process Optimization in Directed Energy Deposition. *Materials*, 16(19):6610, October 2023.

[13] Yousub Lee, Thomas Feldhausen, Chris M. Fancher, Peeyush Nandwana, Sudarsanam S. Babu, Srdjan Simunovic, and Lonnie J. Love. Prediction of residual strain/stress validated with neutron diffraction method for wire-feed hybrid additive/subtractive manufacturing. *Additive Manufacturing*, 79:103920, January 2024.

[14] Niyanth Sridharan, Jeffrey Bunn, Michael Kottman, Chris M. Fancher, Andrew Payzant, Mark Noakes, Andrzej Nycz, Lonnie Love, Badri Narayanan, and S.S. Babu. Consumable development to tailor residual stress in parts fabricated using directed energy deposition processes. *Additive Manufacturing*, 39:101837, March 2021.

[15] Abeer Mithal, Niroj Maharjan, Nicholas Yew Jin Tan, Youxiang Chew, and Sridhar Idapalapati. Understanding residual stress evolution in directed energy deposition with interlayer deformation. *Journal of Manufacturing Science and Engineering*, 146(11):1–25, August 2024.

[16] Erik R. Denlinger, Jarred C. Heigel, Pan Michaleris, and T.A. Palmer. Effect of inter-layer dwell time on distortion and residual stress in additive manufacturing of titanium and nickel alloys. *Journal of Materials Processing Technology*, 215:123–131, January 2015.

[17] Wei Chen, Lianyong Xu, Yongdian Han, Lei Zhao, and Hongyang Jing. Control of residual stress in metal additive manufacturing by low-temperature solid-state phase transformation: An experimental and numerical study. *Additive Manufacturing*, 42:102016, June 2021.

[18] Michael P. Sealy, Gurucharan Madireddy, Robert E. Williams, Prahalada Rao, and Maziar Toursangsaraki. Hybrid Processes in Additive Manufacturing. *Journal of Manufacturing Science and Engineering*, 140(6), March 2018.

[19] Xiaoqiang Zhang, Ze Chai, Huabin Chen, Jijin Xu, Luming Xu, Hao Lu, and Xiaoqi Chen. A novel method to prevent cracking in directed energy deposition of Inconel 738 by in-situ doping Inconel 718. *Materials & Design*, 197:109214, January 2021.

[20] Eike Tim Koopmann, Tim Jäger, Christoph Kaminsky, and Henning Zeidler. Development of heating strategies to reduce crack formation in the manufacturing process of tool components using directed energy deposition. *Progress in Additive Manufacturing*, 10(3):1745–1753, March 2025.

[21] P.J. Withers and H.K.D.H. Bhadeshia. Residual stress. Part 1 – Measurement techniques. *Materials Science and Technology*, 17(4):355–365, April 2001.

[22] Wen Chen, Thomas Voisin, Yin Zhang, Jean-Baptiste Forien, Christopher M. Spadaccini, David L. McDowell, Ting Zhu, and Y. Morris Wang. Microscale residual stresses in additively manufactured stainless steel. *Nature Communications*, 10(1), September 2019.

[23] T. DebRoy, H.L. Wei, J.S. Zuback, T. Mukherjee, J.W. Elmer, J.O. Milewski, A.M. Beese, A. Wilson-Heid, A. De, and W. Zhang. Additive manufacturing of metallic components – Process, structure and properties. *Progress in Materials Science*, 92:112–224, March 2018.

[24] David Svetlizky, Baolong Zheng, Alexandra Vyatskikh, Mitun Das, Susmita Bose, Amit Bandyopadhyay, Julie M. Schoenung, Enrique J. Lavernia, and Noam Eliaz. Laser-based directed energy deposition (DED-LB) of advanced materials. *Materials Science and Engineering:*

A, 840:142967, April 2022.

[25] Yang Liu, Jing Shi, and Yachao Wang. Evolution, Control, and Mitigation of Residual Stresses in Additively Manufactured Metallic Materials: A Review. *Advanced Engineering Materials*, 25(22), October 2023.

[26] Peter Mercelis and Jean Pierre Kruth. Residual stresses in selective laser sintering and selective laser melting. *Rapid Prototyping Journal*, 12(5):254–265, October 2006.

[27] Q. Wu, T. Mukherjee, A. De, and T. DebRoy. Residual stresses in wire-arc additive manufacturing – Hierarchy of influential variables. *Additive Manufacturing*, 35:101355, October 2020.

[28] Xufei Lu, Miguel Cervera, Michele Chiumenti, and Xin Lin. Residual Stresses Control in Additive Manufacturing. *Journal of Manufacturing and Materials Processing*, 5(4):138, December 2021.

[29] T. Mukherjee, V. Manvatkar, A. De, and T. DebRoy. Mitigation of thermal distortion during additive manufacturing. *Scripta Materialia*, 127:79–83, January 2017.

[30] Da Guo, Kun Yan, Mark D. Callaghan, Dominik Daisenberger, Mark Chatterton, Jiadong Chen, Andrew Wisbey, and Wajira Mirihanage. Solidification microstructure and residual stress correlations in direct energy deposited type 316L stainless steel. *Materials & Design*, 207:109782, September 2021.

[31] A Sahraeidolatkhaneh, A Ariaseta, G Aydin, M Nilsen, and F Sikström. Influence of Substrate Preheating on Processing Dynamics and Microstructure of Alloy 718 Produced by Directed Energy Deposition Using a Laser Beam and Wire. *Metals*, 15(11), October 2025.

[32] Bikash Kumar and Balila Nagamani Jaya. Thermal Stability and Residual Stresses in Additively Manufactured Single and Multi-material Systems. *Metallurgical and Materials Transactions A*, 54(5):1808–1824, May 2023.

[33] Ali Kazemi Movahed, Reza Ghanavati, Abdollah Saboori, and Luca Iuliano. A Review of Strategies for In Situ Mitigating of Residual Stress in Laser-Based Metal Additive Manufacturing: Insights, Innovations, and Challenges. *Acta Metallurgica Sinica (English Letters)*, July 2025.

[34] Pengfei Tan, Fei Shen, Biao Li, and Kun Zhou. A thermo-metallurgical-mechanical model for selective laser melting of Ti-6Al-4V. *Materials & Design*, 168:107642, April 2019.

[35] Peng Rong, Qingsong Bai, Ming Yin, Wei Li, Yanxuan Song, and Fenglei Zheng. Thermal mechanical modeling and residual stress prediction for laser direct energy deposition of 30CrNi2MoVA steel considering solid-state phase transformation. *Journal of Materials Research and Technology*, 30:7727–7740, May 2024.

[36] Haifei Lu, Liujun Wu, Huiliang Wei, Jie Cai, Kaiyu Luo, Xiang Xu, and Jinzhong Lu. Microstructural evolution and tensile property enhancement of remanufactured Ti-6Al-4V using hybrid manufacturing of laser directed energy deposition with laser shock peening. *Additive Manufacturing*, 55:102877, July 2022.

[37] Scott M. Thompson, Linkan Bian, Nima Shamsaei, and Aref Yadollahi. An overview of Direct Laser Deposition for additive manufacturing; Part I: Transport phenomena, modeling and diagnostics. *Additive Manufacturing*, 8:36–62, October 2015.

[38] David J. Corbin, Abdalla R. Nassar, Edward W. Reutzel, Allison M. Beese, and Pan Michaleris. Effect of Substrate Thickness and Preheating on the Distortion of Laser Deposited Ti–6Al–4V. *Journal of Manufacturing Science and Engineering*, 140(6), March 2018.

[39] Baopeng Zhang, Zhanxiang Gao, Haifeng Xiao, Xu Yang, Yunpeng Li, and Haihong Zhu. Size effects and optimization during laser directed energy deposition on high thermal conductivity copper alloys. *Journal of Materials Research and Technology*, 33:4389–4399, November 2024.

[40] Sang Guk Jeong, Soung Yeoul Ahn, Eun Seong Kim, Gangaraju Manogna Karthik, Youl Baik, Daehee Seong, You Sub Kim, Wanchuck Woo, and Hyoung Seop Kim. Effect of substrate yield strength and grain size on the residual stress of direct energy deposition additive manufacturing measured by neutron diffraction. *Materials Science and Engineering: A*, 851:143632, August 2022.

[41] You Bin Lai, Wei Jun Liu, Ji Bin Zhao, Yu Hui Zhao, Fu Yu Wang, and Wen Chao Han. Experimental Study on Residual Stress in Titanium Alloy Laser Additive Manufacturing. *Applied Mechanics and Materials*, 431:20–26, October 2013.

[42] Yu Zhan, Chen Liu, Junjian Zhang, Guanzhong Mo, and Changsheng Liu. Measurement of residual stress in laser additive manufacturing TC4 titanium alloy with the laser ultrasonic technique. *Materials Science and Engineering: A*, 762:138093, August 2019.

[43] Xufei Lu, Xin Lin, Michele Chiumenti, Miguel Cervera, Yunlong Hu, Xianglin Ji, Liang Ma, Haiou Yang, and Weidong Huang. Residual stress and distortion of rectangular and S-shaped Ti-6Al-4V parts by Directed Energy Deposition: Modelling and experimental calibration. *Additive Manufacturing*, 26:166–179, March 2019.

[44] Raja S Thanumoorthy, Satyajeet Vijay Jadhav, R Oyyaravelu, Srikanth Bontha, and Balan A S S. Effect of surface remelting on the characteristics of IN718 components fabricated using laser powder directed energy deposition. *Engineering Research Express*, 6(3):035548, August 2024.

[45] Luming Xu, Ze Chai, Huabin Chen, Xiaoqiang Zhang, Jibing Xie, and Xiaoqi Chen. Tailoring Laves phase and mechanical properties of directed energy deposited Inconel 718 thin-wall via a gradient laser power method. *Materials Science and Engineering: A*, 824:141822, September 2021.

[46] Zhaopeng Tong, Xudong Ren, Jiafei Jiao, Wangfan Zhou, Yunpeng Ren, Yunxia Ye, Enoch Asuako Larson, and Jiayang Gu. Laser additive manufacturing of FeCrCoMnNi high-entropy alloy: Effect of heat treatment on microstructure, residual stress and mechanical property. *Journal of Alloys and Compounds*, 785:1144–1159, May 2019.

[47] Yuan Tian, Yunzhuo Lu, and R. Lakshmi Narayan. Optimization of tensile properties and anisotropy in a cryogenically treated laser additively manufactured high entropy alloy. *International Journal of Plasticity*, 178:104015, July 2024.

[48] Di Wu, Jiyuan Tian, Maocheng Liao, Man Zhao, and Gang Liu. Study on the effect of variable laser power on residual stress distribution in laser directed energy deposition of Ti-6Al-4V. *CIRP Journal of Manufacturing Science and Technology*, 55:322–332, December 2024.

[49] Ian Gibson, David Rosen, and Brent Stucker. *Additive Manufacturing Technologies: 3D Printing, Rapid Prototyping, and Direct Digital Manufacturing*. Springer New York, 2015.

[50] Hailin Nie, Hang Liu, Chao Wang, Yuru Wu, Shimin Zhu, and Jun Luo. A new laser remelting strategy for direct energy deposition of 316L stainless steel. *Proceedings of the Institution of Mechanical Engineers, Part B: Journal of Engineering Manufacture*, January 2024.

[51] Dong-Gyu Ahn. Directed Energy Deposition (DED) Process: State of the Art. *International Journal of Precision Engineering and Manufacturing-Green Technology*, 8(2):703–742, February 2021.

[52] Adrita Dass and Atieh Moridi. State of the Art in Directed Energy Deposition: From Additive Manufacturing to Materials Design. *Coatings*, 9(7):418, June 2019.

[53] Avinash Gonnabattula, Raja S. Thanumoorthy, Srikanth Bontha, ASS Balan, V. Anil Kumar, and Anand K. Kanjarla. Process parameter optimization for laser directed energy deposition (LDED) of Ti-6Al-4V using single-track experiments with small laser spot size. *Optics & Laser Technology*, 175:110861, August 2024.

[54] Kulish Aleksandr, Salvatore Ferdinando, Rech Joel, Courbon Joel, Munoz Jordan, and Joffre Thomas. Effect of direct energy deposition parameters on morphology, residual stresses, density, and microstructure of 1.2709 maraging steel. *The International Journal of Advanced Manufacturing Technology*, 117(3–4):1287–1301, August 2021.

[55] Abhishek Shrivastava, S. Anand Kumar, and Samrat Rao. Postprocessing challenges in metal AM: Strategies for achieving homogeneous microstructure in Ni-based superalloys. In *Advances in Metal Additive Manufacturing*, pages 179–202. Elsevier, 2023.

[56] Fencheng Liu, Xin Lin, Gaolin Yang, Menghua Song, Jing Chen, and Weidong Huang. Microstructure and residual stress of laser rapid formed Inconel 718 nickel-base superalloy. *Optics & Laser Technology*, 43(1):208–213, February 2011.

[57] A.N. Jinoop, C.P. Paul, and K.S. Bindra. Laser assisted direct energy deposition of Hastelloy-X. *Optics & Laser Technology*, 109:14–19, January 2019.

[58] H. Zheng, J.F. Peng, X. Sun, H.M. Xie, Y.H. Ding, and W. He. Distribution of microstructure, elastic modulus and residual stress near the interface in laser repaired GH4169 superalloy. *Journal of Alloys and Compounds*, 966:171625, December 2023.

[59] Zhou Yan, Xi Zou, Simeng Li, Guoyun Luo, and Lijun Song. A Study on the Thermo-Mechanical History, Residual Stress, and Dynamic Recrystallization Mechanisms in Additively Manufactured Austenitic Stainless Steels. *Metals*, 12(7):1109, June 2022.

[60] Mehran Ghasempour-Mouziraji, Joana Lagarinhos, Daniel Afonso, and Ricardo Alves de Sousa. A review study on metal powder materials and processing parameters in Laser Metal Deposition. *Optics & Laser Technology*, 170:110226, March 2024.

[61] G. A. W. Sweet, I. W. Donaldson, C. T. Schade, and D. P. Bishop. Laser-Based Directed Energy Deposition (L-DED) Processing of Water Atomized 42CrMo4 Powder. *Lasers in Manufacturing and Materials Processing*, 10(1):32–63, November 2022.

[62] Jun Yu, Xin Lin, Liang Ma, Junjie Wang, Xingling Fu, Jing Chen, and Weidong Huang. Influence of laser deposition patterns on part distortion, interior quality and mechanical properties by laser solid forming (LSF). *Materials Science and Engineering: A*, 528(3):1094–1104, January 2011.

[63] Markus Köhler, Li Sun, Jonas Hensel, Sakari Pallaspuro, Jukka Kömi, Klaus Dilger, and Zhiliang Zhang. Comparative study of deposition patterns for DED-Arc additive manufacturing of Al-4046. *Materials & Design*, 210:110122, November 2021.

[64] Seyedeh Elnaz Mirazimzadeh, Bita Mohajernia, Syamak Pazireh, Jill Urbanic, and Ofelia Jianu. Investigation of residual stresses of multi-layer multi-track components built by directed energy deposition: experimental, numerical, and time-series machine-learning studies. *The International Journal of Advanced Manufacturing Technology*, 130(1–2):329–351, November 2023.

[65] Chi Zhang, Chen Shen, Xueming Hua, Fang Li, Yuelong Zhang, and Yanyan Zhu. Influence of wire-arc additive manufacturing path planning strategy on the residual stress status in one single buildup layer. *The International Journal of Advanced Manufacturing Technology*, 111(3–4):797–806, October 2020.

[66] Y. Zhan, H. Xu, W. Du, and C. Liu. Study on the Effect of Scanning Strategy on Residual Stress in Laser Additive Manufacturing with the Laser Ultrasound Technique. *Experimental Mechanics*, 62(4):563–572, November 2021.

[67] Yang Zhang, Hongyang Jing, Lianyong Xu, Yongdian Han, and Lei Zhao. Effects of different scanning patterns on nickel alloy-directed energy deposition based on thermal analysis. *Virtual and Physical Prototyping*, 16(sup1):S98–S115, March 2021.

[68] Abdollah Saboori, Gabriele Piscopo, Manuel Lai, Alessandro Salmi, and Sara Biamino. An investigation on the effect of deposition pattern on the microstructure, mechanical properties and residual stress of 316L produced by Directed Energy Deposition. *Materials Science and Engineering: A*, 780:139179, April 2020.

[69] Alberta Aversa, Gabriele Piscopo, Alessandro Salmi, and Mariangela Lombardi. Effect of Heat Treatments on Residual Stress and Properties of AISI 316L Steel Processed by Directed Energy Deposition. *Journal of Materials Engineering and Performance*, 29(9):6002–6013, September 2020.

[70] Gabriele Piscopo and Luca Iuliano. Evaluating the Effect of Deposition Strategy on Mechanical Characteristics of 316L Parts Produced by Laser Powder Directed Energy Deposition Process. *Lasers in Manufacturing and Materials Processing*, 11(2):419–436, April 2024.

[71] Wanchuck Woo, Dong-Kyu Kim, Ed.J. Kingston, Vladmir Luzin, Floriana Salvemini, and Michael R. Hill. Effect of interlayers and scanning strategies on through-thickness residual stress distributions in additive manufactured ferritic-austenitic steel structure. *Materials Science and Engineering: A*, 744:618–629, January 2019.

[72] Sudheer Kumar Polamuri, Avinash Mishra, Srihari Chitral, Venkata Kiran Degala, and Ajay Kumar. Thermal–mechanical analysis of Ti-6Al-4V components in wire-arc directed energy deposition using a novel in situ trapezoidal-parallelogram overlapping (TPO) model. *Progress in Additive Manufacturing*, February 2025.

[73] Jingjing Shi, Ning Qian, Shihao Sun, Honghua Su, Wenfeng Ding, and Yucan Fu. Enhancement of material microstructure and properties in Arc wire-based direct energy deposition: A short review. *Journal of Advanced Manufacturing Science and Technology*, 4(4), 2024.

[74] Jin-Long Su, Fu-Lin Jiang, Jie Teng, Le-Qun Chen, Guillermo Requena, Ming Yan, Lai-Chang Zhang, Y. Morris Wang, Ilya V. Okulov, Hong-Mei Zhu, Guo-Wei Bo, You-Xiang Chew, and Chao-Lin Tan. Laser additive manufacturing of titanium alloys: process, materials and post-processing. *Rare Metals*, July 2024.

[75] Yun Zhao, Yazhou Jia, Shujun Chen, Junbiao Shi, and Fang Li. Process planning strategy for wire-arc additive manufacturing: Thermal behavior considerations. *Additive Manufacturing*, 32:100935, March 2020.

[76] Amritesh Kumar, Swarup Bag, and V.C. Srivastava. Role of inter-layer dwell time on residual stress generation of a thin wall structure by directed energy deposition of ferritic steel. *Materials Chemistry and Physics*, 340:130807, August 2025.

[77] Zhuqing Wang, Erik Denlinger, Panagiotis Michaleris, Alexandru D. Stoica, Dong Ma, and Allison M. Beese. Residual stress mapping in Inconel 625 fabricated through additive manufacturing: Method for neutron diffraction measurements to validate thermomechanical model predictions. *Materials & Design*, 113:169–177, January 2017.

[78] Yousub Lee, Yashwanth Bandari, Peeyush Nandwana, Brian. T. Gibson, Brad Richardson, and Srdjan Simunovic. Effect of Interlayer Cooling Time, Constraint and Tool Path Strategy on Deformation of Large Components Made by Laser Metal Deposition with Wire. *Applied Sciences*, 9(23):5115, November 2019.

[79] K. Mohsin Khan, Thella Babu Rao, B. N. Manjunath, K. Abhinav, A. R. Vinod, and Raffi Mohammed. Studies on the Effect of Substrate Preheating, Interlayer Dwell, and Heat Treatment on Microstructure, Residual Stress, and Mechanical Properties of IN625 Superalloy Built by Direct Metal Deposition. *Journal of Engineering Materials and Technology*, 145(4), May 2023.

[80] Pengfei Li, Jing Liu, Jianzhong Zhou, Aixin Feng, Yadong Gong, Jinzhong Lu, and Xiankai Meng. In-situ and off-line deformations of cylindrical walls manufactured by directed energy deposition with different dwell times. *Measurement*, 198:111402, July 2022.

[81] Aldi Mehmeti, Prveen Bidare, Stano Imbrogno, David Wimpenny, Khamis Essa, and Stefan Dimov. Surface integrity of hybrid CM247LC/Inconel 718 components produced by laser-directed energy deposition. *The International Journal of Advanced Manufacturing Technology*, 121(7–8):4961–4980, July 2022.

[82] Xi Zou, Tengfei Chang, Zhou Yan, Zi Song Zhao, Yang Pan, Wenyang Liu, and Lijun Song. Control of thermal strain and residual stress in pulsed-wave direct laser deposition. *Optics & Laser Technology*, 163:109386, August 2023.

[83] Manping Cheng, Xi Zou, Tengfei Chang, Qi Cao, Houlai Ju, Guoyun Luo, Zhengwen Zou, and Zhenxing Wu. Residual Stresses of 316L Stainless Steel Laser Direct Metal During Pulsed-Wave and Continuous-Wave Laser Additive Manufacturing: A Comparative Study. *Coatings*, 14(12):1598, December 2024.

[84] A.N. Jinoop, C.P. Paul, S.K. Mishra, and K.S. Bindra. Laser Additive Manufacturing using directed energy deposition of Inconel-718 wall structures with tailored characteristics. *Vacuum*, 166:270–278, August 2019.

[85] K. Wandtke, D. Schroepfer, R. Scharf-Wildenhain, A. Haelsig, T. Kannengiesser, A. Kromm, and J. Hensel. Influence of the WAAM process and design aspects on residual stresses in high-strength structural steels. *Welding in the World*, 67(4):987–996, March 2023.

[86] R. Scharf-Wildenhain, A. Haelsig, J. Hensel, K. Wandtke, D. Schroepfer, and T. Kannengiesser. Heat control and design-related effects on the properties and welding stresses in WAAM components of high-strength structural steels. *Welding in the World*, 67(4):955–965, December 2022.

[87] Shekhar Srivastava, Rajiv Kumar Garg, Anish Sachdeva, and Vishal S. Sharma. A multi-tier layer-wise thermal management study for long-scale wire-arc additive manufacturing. *Journal of Materials Processing Technology*, 306:117651, August 2022.

[88] Haitao Yue, Ning Lv, Chenguang Guo, Lijuan Zhao, Yihan Jiang, Weibing Dai, Qiang Li, and Jianzhuo Zhang. Effects of energy density on the mechanical properties, residual stress, and fatigue damage of Fe-Cr alloy fabricated by laser-directed energy deposition. *The International Journal of Advanced Manufacturing Technology*, 127(7–8):3965–3977, June 2023.

[89] Aleksandra L. Vyatskikh, Xin Wang, James Haley, Baolong Zheng, Lorenzo Valdevit, Enrique J. Lavernia, and Julie M. Schoenung. Residual stress mitigation in directed energy deposition. *Materials Science and Engineering: A*, 871:144845, April 2023.

[90] Ruixin Wang, Chaoyue Chen, Tingwei Cao, Ruixin Zhao, Yuyang Hou, Songzhe Xu, Tao Hu, Xia Li, Wenjun Zhao, Gang Ji, Ninshu Ma, Jiang Wang, and Zhongming Ren. Thermal distortion evolution and residual stress characteristics of Ti-6Al-4V alloy by laser-directed energy deposition: In-situ monitoring, contour method, and XRD. *Thin-Walled Structures*, 211:113131, June 2025.

[91] Nor Ana Rosli, Mohd Rizal Alkahari, Mohd Fadzli bin Abdollah, Shajahan Maidin, Faiz Redza Ramli, and Safarudin Gazali Herawan. Review on effect of heat input for wire arc additive manufacturing process. *Journal of Materials Research and Technology*, 11:2127–2145, March 2021.

[92] Federico M. Sciammarella and Benyamin Salehi Najafabadi. Processing Parameter DOE for 316L Using Directed Energy Deposition. *Journal of Manufacturing and Materials Processing*, 2(3):61, September 2018.

[93] John D Williams and Carl R Deckard. Advances in modeling the effects of selected parameters on the SLS process. *Rapid Prototyping Journal*, 4(2):90–100, 1998.

[94] B.T. Gibson, Y.K. Bandari, B.S. Richardson, W.C. Henry, E.J. Vetland, T.W. Sundermann, and L.J. Love. Melt pool size control through multiple closed-loop modalities in laser-wire directed energy deposition of Ti-6Al-4V. *Additive Manufacturing*, 32:100993, March 2020.

[95] Pengfei Li, Yadong Gong, Chunyou Liang, Yuying Yang, and Ming Cai. Effect of post-heat treatment on residual stress and tensile strength of hybrid additive and subtractive manufacturing. *The International Journal of Advanced Manufacturing Technology*, 103(5–8):2579–2592, April 2019.

[96] ASTM International. Standard Terminology of Appearance. Technical report, ASTM International, West Conshohocken, PA, August 1999. E284-99a.

[97] Frederick Lia, Joshua Park, Jay Tressler, and Richard Martukanitz. Partitioning of laser energy during directed energy deposition. *Additive Manufacturing*, 18:31–39, December 2017.

[98] Wen Liu, Bin Zeng, Weiren Xiong, and Songrong Luo. Unraveling the Mechanism of Energy Utilization Efficiency Regulating Melt Pool Dimensions and Tensile Properties of 316L Stainless Steel in Laser Directed Energy Deposition. *Journal of Manufacturing and Materials Processing*, 10(2):61, February 2026.

[99] A J Pinkerton and L Li. An analytical model of energy distribution in laser direct metal deposition. *Proceedings of the Institution of Mechanical Engineers, Part B: Journal of Engineering Manufacture*, 218(4):363–374, April 2004.

[100] Andrew J Pinkerton. An analytical model of beam attenuation and powder heating during coaxial laser direct metal deposition. *Journal of Physics D: Applied Physics*, 40(23):7323–7334, December 2007.

[101] R. R. Unocic and J. N. DuPont. Process efficiency measurements in the laser engineered net shaping process. *Metallurgical and Materials Transactions B*, 35(1):143–152, February 2004.

[102] Johannes Trapp, Alexander M. Rubenchik, Gabe Guss, and Manyalibo J. Matthews. In situ absorptivity measurements of metallic powders during laser powder-bed fusion additive manufacturing. *Applied Materials Today*, 9:341–349, December 2017.

[103] Wim Devesse, Dieter De Baere, and Patrick Guillaume. Modeling of laser beam and powder flow interaction in laser cladding using ray-tracing. *Journal of Laser Applications*, 27(S2):S29208, February 2015.
[104] Akash Aggarwal, Vigneashwara Pandiyan, Christian Leinenbach, and Marc Leparoux. Investigating laser beam shadowing and powder particle dynamics in directed energy deposition through high-fidelity modelling and high-speed imaging. *Additive Manufacturing*, 91:104344, July 2024.
[105] A.M. Prokhorov. *Laser Heating of Metals*. CRC Press, 2018.
[106] Hamid Reza Abedi and Mohammad Hoseinpour Gollo. An experimental study of the effects of surface roughness and coating of Cr2O3 layer on the laser-forming process. *Optics & Laser Technology*, 109:336–347, January 2019.
[107] Martin Von Allmen and Andreas Blatter. *Laser-Beam Interactions with Materials: Physical Principles and Applications*, volume 2 of *Springer Series in Materials Science*. Springer Berlin Heidelberg, Berlin, Heidelberg, 1995.
[108] William M. Steen and Jyotirmoy Mazumder. *Laser Material Processing*. Springer, London, 2010.
[109] J. Xie, A. Kar, J. A. Rothenflue, and W. P. Latham. Temperature-dependent absorptivity and cutting capability of CO2, Nd:YAG and chemical oxygen–iodine lasers. *Journal of Laser Applications*, 9(2):77–85, April 1997.
[110] R. Indhu, V. Vivek, L. Sarathkumar, A. Bharatish, and S. Soundarapandian. Overview of Laser Absorptivity Measurement Techniques for Material Processing. *Lasers in Manufacturing and Materials Processing*, 5(4):458–481, December 2018.
[111] T. L. Bergman and Frank P. Incropera, editors. *Fundamentals of heat and mass transfer*. Wiley, Hoboken, NJ, 7th ed edition, 2011.
[112] D B Hann, J Iammi, and J Folkes. A simple methodology for predicting laser-weld properties from material and laser parameters. *Journal of Physics D: Applied Physics*, 44(44):445401, October 2011.
[113] Wayne E. King, Holly D. Barth, Victor M. Castillo, Gilbert F. Gallegos, John W. Gibbs, Douglas E. Hahn, Chandrika Kamath, and Alexander M. Rubenchik. Observation of keyhole-mode laser melting in laser powder-bed fusion additive manufacturing. *Journal of Materials Processing Technology*, 214(12):2915–2925, December 2014.
[114] Hossein Ghasemi-Tabasi, Jamasp Jhabvala, Eric Boillat, Toni Ivas, Rita Drissi-Daoudi, and Roland E. Logé. An effective rule for translating optimal selective laser melting processing parameters from one material to another. *Additive Manufacturing*, 36:101496, December 2020.
[115] Simon Bergmueller, Lukas Gerhold, Lorenz Fuchs, Lukas Kaserer, and Gerhard Leichtfried. Systematic approach to process parameter optimization for laser powder bed fusion of low-alloy steel based on melting modes. *The International Journal of Advanced Manufacturing Technology*, 126(9):4385–4398, June 2023.
[116] Viktor Coen, Louca Goossens, and Brecht Van Hooreweder. Methodology and experimental validation of analytical melt pool models for laser powder bed fusion. *Journal of Materials Processing Technology*, 304:117547, June 2022.
[117] Nathan A. Kistler, Abdalla R. Nassar, Edward W. Reutzel, and David J. Corbin. Effect of directed energy deposition processing parameters on laser deposited Inconel® 718: Microstructure, fusion zone morphology, and hardness. *Journal of Laser Applications*, 29(2), 2017.
[118] Yachao Wang and Jing Shi. Recrystallization behavior and tensile properties of laser metal deposited Inconel 718 upon in-situ ultrasonic impact peening and heat treatment. *Materials Science and Engineering: A*, 786:139434, June 2020.
[119] Nima Shamsaei, Aref Yadollahi, Linkan Bian, and Scott M. Thompson. An overview of Direct Laser Deposition for additive manufacturing; Part II: Mechanical behavior, process parameter optimization and control. *Additive Manufacturing*, 8:12–35, October 2015.
[120] Stefano Baraldo, Ambra Vandone, Anna Valente, and Emanuele Carpanzano. Closed-Loop Control by Laser Power Modulation in Direct Energy Deposition Additive Manufacturing. In *Proceedings of 5th International Conference on the Industry 4.0 Model for Advanced Manufacturing*, pages 129–143. Springer International Publishing, 2020.
[121] Lijun Song, Vijayavel Bagavath-Singh, Bhaskar Dutta, and Jyoti Mazumder. Control of melt pool temperature and deposition height during direct metal deposition process. *The International Journal of Advanced Manufacturing Technology*, 58(1–4):247–256, May 2011.
[122] Nashit Ali, Luca Tomesani, Alessandro Ascari, and Alessandro Fortunato. Fabrication of Thin Walls with and without Close Loop Control as a Function of Scan Strategy Via Direct Energy Deposition. *Lasers in Manufacturing and Materials Processing*, 9(1):81–101, February 2022.
[123] Weijun Zhang, Muqing Yang, Wenqi Mao, Shogo Takesue, and Masakazu Soshi. The effect of productive and quality deposition strategies on residual stress for Directed Energy Deposition (DED) process. *Manufacturing Letters*, 41:868–878, October 2024.
[124] Ziyad Smoqi, Benjamin D. Bevans, Aniruddha Gaikwad, James Craig, Alan Abul-Haj, Brent Roeder, Bill Macy, Jeffrey E. Shield, and Prahalada Rao. Closed-loop control of meltpool temperature in directed energy deposition. *Materials & Design*, 215:110508, March 2022.
[125] Guijun Bi, Andres Gasser, Konrad Wissenbach, Alexander Drenker, and Reinhart Poprawe. Characterization of the process control for the direct laser metallic powder deposition. *Surface and Coatings Technology*, 201(6):2676–2683, December 2006.
[126] Lie Tang and Robert G. Landers. Melt Pool Temperature Control for Laser Metal Deposition Processes—Part I: Online Temperature Control. *Journal of Manufacturing Science and Engineering*, 132(1), January 2010.
[127] Samantha Webster, Jihoon Jeong, Jon-Erik Mogonye, James Zuback, Shuheng Liao, Julian Rocher, Kornel Ehmann, and Jian Cao. Effect of closed-loop coaxial melt pool temperature control on thermal history and microstructure of nickel alloy 718 in directed energy deposition. *Journal of Materials Processing Technology*, 337:118725, March 2025.
[128] Youyu Su, Zhanfeng Wang, Xiang Xu, Kaiyu Luo, and Jinzhong Lu. Effect of closed-loop controlled melt pool width on microstructure and tensile property for Fe-Ni-Cr alloy in directed energy deposition. *Journal of Manufacturing Processes*, 82:708–721, October 2022.
[129] Subin Shin, Ikgeun Jeon, and Hoon Sohn. Enhanced geometric accuracy in directed energy deposition via closed-loop melt pool height control using real-time thermal imaging. *Additive Manufacturing*, 109:104846, July 2025.
[130] Almir Heralić, Anna-Karin Christiansson, and Bengt Lennartson. Height control of laser metal-wire deposition based on iterative learning control and 3D scanning. *Optics and Lasers in Engineering*, 50(9):1230–1241, September 2012.
[131] Wim Devesse, Dieter De Baere, and Patrick Guillaume. Design of a Model-based Controller with Temperature Feedback for Laser Cladding. *Physics Procedia*, 56:211–219, 2014.
[132] Mohammad H. Farshidianfar, Farzad Khodabakhshi, Amir Khajepour, and Adrian P. Gerlich. Closed-loop control of microstructure and mechanical properties in additive manufacturing by directed energy deposition. *Materials Science and Engineering: A*, 803:140483, January

2021.

[133] Mohammad H. Farshidianfar, Amir Khajepour, and Adrian Gerlich. Real-time control of microstructure in laser additive manufacturing. *The International Journal of Advanced Manufacturing Technology*, 82(5–8):1173–1186, July 2015.

[134] Meysam Akbari and Radovan Kovacevic. An investigation on mechanical and microstructural properties of 316LSi parts fabricated by a robotized laser/wire direct metal deposition system. *Additive Manufacturing*, 23:487–497, October 2018.

[135] Meysam Akbari and Radovan Kovacevic. Closed loop control of melt pool width in robotized laser powder–directed energy deposition process. *The International Journal of Advanced Manufacturing Technology*, 104(5–8):2887–2898, July 2019.

[136] Abdalla R. Nassar, Jayme S. Keist, Edward W. Reutzel, and Todd J. Spurgeon. Intra-layer closed-loop control of build plan during directed energy additive manufacturing of Ti–6Al–4V. *Additive Manufacturing*, 6:39–52, April 2015.

[137] Du-Rim Eo, Jongcheon Yoon, and Hyub Lee. Heterostructure effect at the interface of maraging steel deposited upon carbon steel via directed energy deposition. *Materials & Design*, 225:111574, January 2023.

[138] Gyeong Yun Baek, Ki Yong Lee, Sang Hu Park, and Do Sik Shim. Effects of substrate preheating during direct energy deposition on microstructure, hardness, tensile strength, and notch toughness. *Metals and Materials International*, 23(6):1204–1215, October 2017.

[139] Fabian Bieg, Clemens Maucher, and Hans-Christian Möhring. Influence of the Substrate Size on the Cooling Behavior and Properties of the DED-LB Process. *Journal of Machine Engineering*, 24(2):105–116, June 2024.

[140] Kai Zhang, Shijie Wang, Weijun Liu, and Risheng Long. Effects of substrate preheating on the thin-wall part built by laser metal deposition shaping. *Applied Surface Science*, 317:839–855, October 2014.

[141] Erik R Denlinger and Pan Michaleris. Mitigation of distortion in large additive manufacturing parts. *Proceedings of the Institution of Mechanical Engineers, Part B: Journal of Engineering Manufacture*, 231(6):983–993, April 2015.

[142] Wei Fan, Hua Tan, Fengying Zhang, Zhe Feng, Yongxia Wang, Yunlong Hu, Xin Lin, and Weidong Huang. Effect of synchronous induction heating on residual stress for laser-based directed energy deposition of thin-walled structures. *Materials Today Communications*, 35:105702, June 2023.

[143] Shiming Gao, Ojo Philip Bodunde, Mian Qin, Wei-Hsin Liao, and Ping Guo. Microstructure and phase transformation of nickel-titanium shape memory alloy fabricated by directed energy deposition with in-situ heat treatment. *Journal of Alloys and Compounds*, 898:162896, March 2022.

[144] Seung Yeong Cho, Gwang Yong Shin, and Do Sik Shim. Effect of laser remelting on the surface characteristics of 316L stainless steel fabricated via directed energy deposition. *Journal of Materials Research and Technology*, 15:5814–5832, November 2021.

[145] Wei Zhang, Kyeongsik Ha, Qing-Ye Jin, Hyunji Nam, Jiyoung Park, and Wookjin Lee. Effects of laser rescanning on microstructure and mechanical properties of Al-10Si-1Mg alloy produced by laser-directed energy deposition. *Materials Today Communications*, 37:106979, December 2023.

[146] Zhiyuan Yu, Yi Zheng, Junmei Chen, Chuanfeng Wu, Jijin Xu, Hao Lu, and Chun Yu. Effect of laser remelting processing on microstructure and mechanical properties of 17-4 PH stainless steel during laser direct metal deposition. *Journal of Materials Processing Technology*, 284:116738, October 2020.

[147] Bintao Wu, Zengxi Pan, Guangyu Chen, Donghong Ding, Lei Yuan, Dominic Cuiuri, and Huijun Li. Mitigation of thermal distortion in wire arc additively manufactured Ti-6Al-4V part using active interpass cooling. *Science and Technology of Welding and Joining*, 24(5):484–494, July 2019.

[148] Fang Li, Shujun Chen, Junbiao Shi, Yun Zhao, and Hongyu Tian. Thermoelectric Cooling-Aided Bead Geometry Regulation in Wire and Arc-Based Additive Manufacturing of Thin-Walled Structures. *Applied Sciences*, 8(2):207, January 2018.

[149] Uwe Reisgen, Rahul Sharma, Samuel Mann, and Lukas Oster. Increasing the manufacturing efficiency of WAAM by advanced cooling strategies. *Welding in the World*, 64(8):1409–1416, June 2020.

[150] Hideaki Nagamatsu, Hiroyuki Sasahara, Yuusuke Mitsutake, and Takeshi Hamamoto. Development of a cooperative system for wire and arc additive manufacturing and machining. *Additive Manufacturing*, 31:100896, January 2020.

[151] Thomas Bergs, Sebastian Kammann, Gabriel Fraga, Jan Riepe, and Kristian Arntz. Experimental investigations on the influence of temperature for Laser Metal Deposition with lateral Inconel 718 wire feeding. *Procedia CIRP*, 94:29–34, 2020.

[152] Florian Pixner, Fernando Warchomicka, Marta Lipińska, Simon Elmiger, Clemens Jechtl, Peter Auer, Florian Riedlsperger, Ricardo Buzolin, Josef Domitner, Małgorzata Lewandowska, and Norbert Enzinger. Thermal cycling effects on the local microstructure and mechanical properties in wire-based directed energy deposition of nickel-based superalloy. *Additive Manufacturing*, 83:104066, March 2024.

[153] Wenjun Zhang, Chunguang Xu, Cencheng Li, and Sha Wu. Advances in Ultrasonic-Assisted Directed Energy Deposition (DED) for Metal Additive Manufacturing. *Crystals*, 14(2):114, January 2024.

[154] Chaolin Tan, Runsheng Li, Jinlong Su, Dafan Du, Yang Du, Bonnie Attard, Youxiang Chew, Haiou Zhang, Enrique J. Lavernia, Yves Fautrelle, Jie Teng, and Anping Dong. Review on field assisted metal additive manufacturing. *International Journal of Machine Tools and Manufacture*, 189:104032, June 2023.

[155] Huachen Li, Li Cui, Dingyong He, Zhenfu Shi, Fanhui Bu, Qing Cao, and Shengjun Wan. Non-contact ultrasonic vibration-assisted laser metal deposition manufacturing Fe-based powder: Numerical simulation and experimental investigation. *Materials Today Communications*, 40:109865, August 2024.

[156] Mingxia Diao, Chunhuan Guo, Qianfei Sun, Fengchun Jiang, Liyu Li, Jifeng Li, De Xu, Chuanming Liu, and Haolun Song. Improving mechanical properties of austenitic stainless steel by the grain refinement in wire and arc additive manufacturing assisted with ultrasonic impact treatment. *Materials Science and Engineering: A*, 857:144044, November 2022.

[157] Yutai Su, Roman Savinov, Yachao Wang, Dong Lin, and Jing Shi. Microstructure and property enhancement of 7075 aluminium alloy via laser metal deposition augmented by in-situ ultrasonic vibration. *Virtual and Physical Prototyping*, 19(1), January 2024.

[158] Lin Zhou, Suiyuan Chen, Mingzhi Ma, Jing liang, Jialu Chen, and Mei Wang. The dynamic recrystallization mechanism of ultrasonic power on non-contact ultrasonic-assisted direct laser deposited alloy steel. *Materials Science and Engineering: A*, 840:142971, April 2022.

[159] Mirza Imširović, Uroš Trdan, Damjan Klobčar, Drago Bračun, Aleš Nagode, and Laurent Berthe. Mitigating defects in directed energy deposited aluminium 5356 alloy through in-situ workpiece vibration. *Journal of Materials Research and Technology*, 33:1581–1599, November 2024.

[160] Xufei Lu, Wenyou Zhang, Michele Chiumenti, Miguel Cervera, Bobby Gillham, Pengfei Yu, Shuo Yin, Xin Lin, Ramesh Padamati Babu, and Rocco Lupoi. Crack-free laser powder bed fusion by substrate design. *Additive Manufacturing*, 59:103149, November 2022.

[161] Xufei Lu, Guohao Zhang, Michele Chiumenti, Miguel Cervera, Mehdi Slimani, Liang Ma, Lei Wei, and Xin Lin. Smart-substrate: a novel structural design to avert residual stress accretion in directed energy deposition additive manufacturing. *Virtual and Physical Prototyping*, 18(1), August 2023.

[162] Hang Jing, Peng Ge, Zhao Zhang, Jun-Qi Chen, Zhong-Ming Liu, and Wei-Wei Liu. Numerical Studies of the Effects of the Substrate Structure on the Residual Stress in Laser Directed Energy Additive Manufacturing of Thin-Walled Products. *Metals*, 12(3):462, March 2022.

[163] Sergei Ivanov, Antoni Artinov, Evgenii Zemlyakov, Ivan Karpov, Sergei Rylov, and Vaycheslav Em. Spatiotemporal Evolution of Stress Field during Direct Laser Deposition of Multilayer Thin Wall of Ti-6Al-4V. *Materials*, 15(1):263, December 2021.

[164] Xuan Li, Zhiwei Zhao, Xinyu Cheng, Hui Chen, and Jun Xiong. Residual stress and distortion in arc-directed energy deposition: Formation mechanisms, analysis techniques, and mitigation strategies. *Journal of Manufacturing Processes*, 141:17–35, May 2025.

[165] J.R. Hönnige, P.A. Colegrove, S. Ganguly, E. Eimer, S. Kabra, and S. Williams. Control of residual stress and distortion in aluminium wire + arc additive manufacture with rolling. *Additive Manufacturing*, 22:775–783, August 2018.

[166] Francisco Werley Cipriano Farias, Telmo Jorge Gomes dos Santos, and João Pedro Oliveira. Directed energy deposition + mechanical interlayer deformation additive manufacturing: a state-of-the-art literature review. *The International Journal of Advanced Manufacturing Technology*, 131(3–4):999–1038, February 2024.

[167] Haiou Zhang, Xiangping Wang, Guilan Wang, and Yang Zhang. Hybrid direct manufacturing method of metallic parts using deposition and micro continuous rolling. *Rapid Prototyping Journal*, 19(6):387–394, September 2013.

[168] Paul A. Colegrove, Harry E. Coules, Julian Fairman, Filomeno Martina, Tariq Kashoob, Hani Mamash, and Luis D. Cozzolino. Microstructure and residual stress improvement in wire and arc additively manufactured parts through high-pressure rolling. *Journal of Materials Processing Technology*, 213(10):1782–1791, October 2013.

[169] Paul A. Colegrove, Filomeno Martina, Matthew J. Roy, Blanka A. Szost, Sofiane Terzi, Stewart W. Williams, Philip J. Withers, and David Jarvis. High Pressure Interpass Rolling of Wire + Arc Additively Manufactured Titanium Components. *Advanced Materials Research*, 996:694–700, August 2014.

[170] F. Martina, M. J. Roy, B. A. Szost, S. Terzi, P. A. Colegrove, S. W. Williams, P. J. Withers, J. Meyer, and M. Hofmann. Residual stress of as-deposited and rolled wire+arc additive manufacturing Ti–6Al–4V components. *Materials Science and Technology*, 32(14):1439–1448, September 2016.

[171] J.R. Hönnige, P.A. Colegrove, B. Ahmad, M.E. Fitzpatrick, S. Ganguly, T.L. Lee, and S.W. Williams. Residual stress and texture control in Ti-6Al-4V wire + arc additively manufactured intersections by stress relief and rolling. *Materials & Design*, 150:193–205, July 2018.

[172] Jan Hönnige, Cui Er Seow, Supriyo Ganguly, Xiangfang Xu, Sandra Cabeza, Harry Coules, and Stewart Williams. Study of residual stress and microstructural evolution in as-deposited and inter-pass rolled wire plus arc additively manufactured Inconel 718 alloy after ageing treatment. *Materials Science and Engineering: A*, 801:140368, January 2021.

[173] Xinni Tian, Yuman Zhu, Chao Voon Samuel Lim, James Williams, Rod Boyer, Xinhua Wu, Kai Zhang, and Aijun Huang. Isotropic and improved tensile properties of Ti-6Al-4V achieved by in-situ rolling in direct energy deposition. *Additive Manufacturing*, 46:102151, October 2021.

[174] Wen Hao Kan, Derui Jiang, Matthew Humbert, Xiang Gao, Vijay Kumar Bhatia, Gwénaëlle Proust, Yuman Zhu, Peter Hodgson, and Aijun Huang. Effect of in-situ layer-by-layer rolling on the microstructure, mechanical properties, and corrosion resistance of a directed energy deposited 316L stainless steel. *Additive Manufacturing*, 55:102863, July 2022.

[175] Shi-Hao Li, Yakai Zhao, Punit Kumar, and Upadrasta Ramamurty. Effect of initial dislocation density on the plastic deformation response of 316L stainless steel manufactured by directed energy deposition. *Materials Science and Engineering: A*, 851:143591, August 2022.

[176] V Paranthaman, Dhivakar Poosapadi, Ashwin Sailesh, Vipin Sharma, Rahul Singh, Rajasekhara Babu L, K.K. Arun, M. Ravichandran, and T.S. Senthil. Role of heat treatment in enhancing microstructure and properties of Inconel 625 manufactured by directed energy deposition using wire arc. *Journal of Alloys and Metallurgical Systems*, 9:100147, March 2025.

[177] Jon L. Dossett and Howard E. Boyer. *Practical Heat Treating*. ASM International, 2 edition, March 2006.

[178] Francesco Careri, Stano Imbrogno, Domenico Umbrello, Moataz M. Attallah, José Outeiro, and António C. Batista. Machining and heat treatment as post-processing strategies for Ni-superalloys structures fabricated using direct energy deposition. *Journal of Manufacturing Processes*, 61:236–244, January 2021.

[179] A.N. Jinoop, J. Denny, C.P. Paul, J. Ganesh Kumar, and K.S. Bindra. Effect of post heat-treatment on the microstructure and mechanical properties of Hastelloy-X structures manufactured by laser based Directed Energy Deposition. *Journal of Alloys and Compounds*, 797:399–412, August 2019.

[180] Rachel Boillat-Newport, Sriram Praneeth Isanaka, Jonathan Kelley, and Frank Liou. Heat Treatments for Minimization of Residual Stresses and Maximization of Tensile Strengths of Scalmalloy® Processed via Directed Energy Deposition. *Materials*, 17(6):1333, March 2024.

[181] Anna Ermakova, Nima Razavi, Sandra Cabeza, Elzbieta Gadalinska, Mark Reid, Anna Paradowska, Supriyo Ganguly, Filippo Berto, and Ali Mehmanparast. The effect of surface treatment and orientation on fatigue crack growth rate and residual stress distribution of wire arc additively manufactured low carbon steel components. *Journal of Materials Research and Technology*, 24:2988–3004, May 2023.

[182] Seung-Yeong Cho, Gwang-Yong Shin, Ki-Yong Lee, and Do-Sik Shim. Post-building successive treatments using surface laser remelting and ultrasonic nanocrystalline surface modification for rough surface built via directed energy deposition. *Journal of Manufacturing Processes*, 84:1076–1093, December 2022.

[183] Xiaoyu Zhang, Sheng Huang, Dichen Li, Jiale Geng, Fan Yang, and Qingyu Li. An approach to improve the microstructure and mechanical properties: A hybrid manufacturing of laser directed energy deposition and shot peening. *Additive Manufacturing*, 55:102686, July 2022.

[184] Xing Peng, Lingbao Kong, Jerry Ying Hsi Fuh, and Hao Wang. A Review of Post-Processing Technologies in Additive Manufacturing. *Journal of Manufacturing and Materials Processing*, 5(2):38, April 2021.

[185] Rujian Sun, Liuhe Li, Ying Zhu, Wei Guo, Peng Peng, Baoqiang Cong, Jianfei Sun, Zhigang Che, Bo Li, Chao Guo, and Lei Liu. Microstructure, residual stress and tensile properties control of wire-arc additive manufactured 2319 aluminum alloy with laser shock peening. *Journal of Alloys and Compounds*, 747:255–265, May 2018.

[186] Wei Guo, Rujian Sun, Binwen Song, Ying Zhu, Fei Li, Zhigang Che, Bo Li, Chao Guo, Lei Liu, and Peng Peng. Laser shock peening of laser additive manufactured Ti-6Al-4V titanium alloy. *Surface and Coatings Technology*, 349:503–510, September 2018.

[187] Jiaxuan Chi, Zhongyi Cai, Hepeng Zhang, Hongqiang Zhang, Wei Guo, Zhandong Wan, Guofeng Han, Peng Peng, and Zhi Zeng. Combining manufacturing of titanium alloy through direct energy deposition and laser shock peening processes. *Materials & Design*, 203:109626, May 2021.

[188] Yongxin Zhang, Wei Guo, Jiaxin Shi, Jiaxuan Chi, Guoxing Chen, Guofeng Han, and Hongqiang Zhang. Improved rotating bending fatigue performance of laser directed energy deposited Ti-6Al-4V alloys by laser shock peening. *Journal of Alloys and Compounds*, 980:173664, April 2024.

[189] Yongxiang Hu, Mengqi Lai, Zonghao Hu, and Zhenqiang Yao. Effect of multiple laser peening on surface integrity and microstructure of laser additive manufactured Ti-6Al-4V titanium alloy. *Rapid Prototyping Journal*, 25(8):1379–1387, September 2019.

[190] Jiaxuan Chi, Zhongyi Cai, Zhandong Wan, Hongqiang Zhang, Zhenlin Chen, Liuhe Li, Ying Li, Peng Peng, and Wei Guo. Effects of heat treatment combined with laser shock peening on wire and arc additive manufactured Ti17 titanium alloy: Microstructures, residual stress and mechanical properties. *Surface and Coatings Technology*, 396:125908, August 2020.

[191] Zhibin An, Weifeng He, Xin Zhou, Liucheng Zhou, and Xiangfan Nie. On the Microstructure, Residual Stress and Fatigue Performance of Laser Metal Deposited TC17 Alloy Subjected to Laser Shock Peening. *Materials*, 15(18):6501, September 2022.

[192] Abeer Mithal, Niroj Maharjan, and Sridhar Idapalapati. Effect of Laser Peening on Surface Morphology and Deformation Level of Additively Manufactured 316L Stainless Steel. In *Proceedings of the 3rd International Conference on Advanced Surface Enhancement (INCASE) 2023*, pages 85–96. Springer Nature Singapore, 2024.

[193] Wei Dai, Wei Guo, Jun Xiao, Ying Zhu, Zewu Qi, Jiaxin Shi, Changhao Yin, Dongsheng He, Jiaxuan Chi, Zhandong Wan, Baoqiang Cong, Minggao Li, and Hongqiang Zhang. Tailoring properties of directed energy deposited Al-Mg alloy by balancing laser shock peening and heat treatment. *Journal of Materials Science & Technology*, 203:78–96, December 2024.

[194] M.P. Sealy, H. Hadidi, C.J. Kanger, X.L. Yan, B. Cui, and J.A. McGeough. Glocal integrity in 420 stainless steel by asynchronous laser processing. *CIRP Annals*, 68(1):189–192, 2019.

[195] Jiantao Zhou, Xin Zhou, Hui Li, Jiawei Hu, Xu Han, and Sheng Liu. In-situ laser shock peening for improved surface quality and mechanical properties of laser-directed energy-deposited AlSi10Mg alloy. *Additive Manufacturing*, 60:103177, December 2022.

[196] Yachao Wang, Sougata Roy, Hyunsuk Choi, and Touhid Rimon. Cracking suppression in additive manufacturing of hard-to-weld nickel-based superalloy through layer-wise ultrasonic impact peening. *Journal of Manufacturing Processes*, 80:320–327, August 2022.

[197] Yichong Yang, Xin Jin, Changmeng Liu, Muzheng Xiao, Jiping Lu, Hongli Fan, and Shuyuan Ma. Residual Stress, Mechanical Properties, and Grain Morphology of Ti-6Al-4V Alloy Produced by Ultrasonic Impact Treatment Assisted Wire and Arc Additive Manufacturing. *Metals*, 8(11):934, November 2018.

[198] Yachao Wang and Jing Shi. Microstructure and Properties of Inconel 718 Fabricated by Directed Energy Deposition with In-Situ Ultrasonic Impact Peening. *Metallurgical and Materials Transactions B*, 50(6):2815–2827, September 2019.

[199] Yang Zhang, Lianyong Xu, Kangda Hao, Yongdian Han, and Lei Zhao. Effect of ultrasonic micro-forging on the microstructure and properties of GH4169 superalloy deposited by laser direct energy deposition. *Materials Science and Engineering: A*, 914:147177, November 2024.

[200] Sheng Huang, Zhenjia Qi, Anfeng Zhang, Xiaoyu Zhang, Qingyu Li, and Dichen Li. Reducing the anisotropy of the mechanical properties of directed energy deposited Ti-6Al-4V alloy with inter-layer ultrasonic impact peening and heat treatment. *Materials Science and Engineering: A*, 857:144123, November 2022.